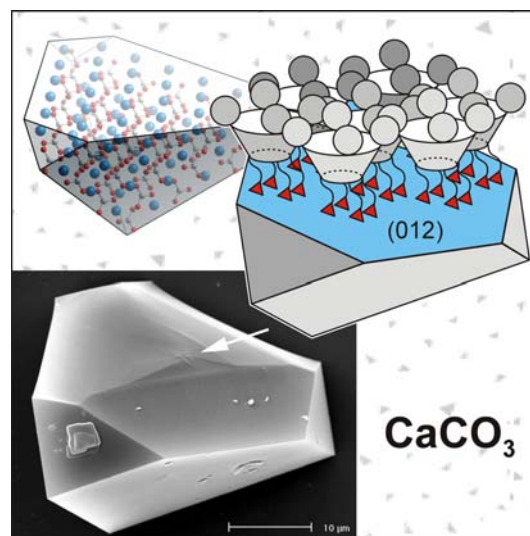


Modellstudien zur Funktion saurer Matrixproteine in der Biomineralisation

– kumulative Dissertation –

von

Marc Fricke



vorgelegt

der Fakultät für Chemie

der Universität Bielefeld

zur Erlangung

des naturwissenschaftlichen Doktorgrades

Bielefeld

April 2004

Gedruckt auf alterungsbeständigem Papier

1. Gutachter: Priv. Doz. Dr. D. Volkmer

2. Gutachter: Prof. Dr. J. Mattay

Tag der mündlichen Prüfung: 14. 05. 2004

Die vorliegende Arbeit entstand im Zeitraum von Dezember 2000 bis April 2004 in der Arbeitsgruppe Anorganische Chemie I der Fakultät für Chemie an der Universität Bielefeld unter der wissenschaftlichen Anleitung von Herrn Priv. Doz. Dr. Dirk Volkmer.

Mein besonderer Dank gilt Herrn Priv. Doz. Dr. Dirk Volkmer für die gute Zusammenarbeit, die zuverlässige Unterstützung, die uneingeschränkten Entfaltungsmöglichkeiten und die große Freiheit, mit der ich das Thema bearbeiten konnte.

Herrn Prof. Dr. Jochen Mattay danke ich für die Anfertigung des Zweitgutachtens.

Dem Arbeitsgruppenleiter, Herrn Prof. Dr. Dr. h.c. mult. Achim Müller, danke ich für die Bereitstellung der Infrastruktur und das Vertrauen in unsere Arbeit.

Für die Durchführung folgender Analysen bzw. spektroskopischer Messungen danke ich Frau B. Michel (C,H,N-Analysen), Herrn K.-P. Mester (NMR-Spektroskopie), Herrn Dr. M. Letzel (Massenspektrometrie), Herrn T. Tak bzw. Frau G. Heinze-Bruckner (IR-, Raman-Spektroskopie sowie SEM), Herrn M. Schmidtman und Herrn Dr. H. Bögge (Röntgenstrukturanalysen).

Den Arbeitsgruppen von Prof. Dr. Jochen Mattay und Prof. Dr. Norbert Sewald in Bielefeld, Prof. Dr. Dieter Vollhardt in Potsdam, Priv. Doz. Dr. Lifeng Chi in Münster, Priv. Doz. Dr. Andreas Ziegler in Ulm, Prof. Laurie Gower in Gainesville (Florida) und Prof. Willi Jahnen-Dechent in Aachen danke ich für die konstruktive Zusammenarbeit.

Mein besonderer Dank gilt der gesamten Arbeitsgruppe AC1 für die ständige Hilfsbereitschaft und die freundliche Arbeitsatmosphäre.

Ich möchte meinen engen Freunden für die wichtige moralische Unterstützung danken.

Meiner Familie und insbesondere meinen Eltern, die mir dieses Studium ermöglicht haben, danke ich von ganzem Herzen für Ihr Vertrauen, Ihre Geduld und ihre Unterstützung während der gesamten Ausbildung.

Diese Arbeit widme ich meiner lieben Freundin Andrea, die als großer Rückhalt vor und während der Promotion alle Höhen und Tiefen mitgetragen hat. Durch ihre positive Ausstrahlung aber auch realistische Einschätzung hat sie einen besonderen Anteil an dieser Arbeit.

Inhaltsverzeichnis

	Seite
1. Vorwort	1
2. Einleitung	2
2.1 Kristallkeimbildung in Mollusken	2
2.2 Biologisch inspiriertes Kristall-Engineering von CaCO ₃	4
2.3 Kristallisation von CaCO ₃ unter Monoschichten amphiphiler Oligosäuren	7
2.3.1 Kristallstrukturen von Oligocarbonsäuren und deren Ca-Komplexen	8
2.3.2 Kristallisation von CaCO ₃ an Modellgrenzflächen	9
2.4 Kristallisation von CaCO ₃ in Gegenwart saurer Oligopeptide	18
3. Zusammenfassung und Ausblick	19
4. Summary	
5. Anhang Publikationen	
A1 <i>Oriented crystallization of calcite single crystals grown underneath monolayers of tetracarboxyresorc[4]arenes</i> D. Volkmer, M. Fricke, C. Agena, J. Mattay, <i>CrystEngComm.</i> 2002 , 4, 288–295.	
A2 <i>Crystallization of (012) oriented calcite single crystals underneath monolayers of tetra(carboxymethoxy)calix[4]arenes</i> D. Volkmer, M. Fricke, S. Siegel, D. Vollhardt, <i>J. Chem. Soc., Dalton Trans.</i> 2002 , 4547–4554.	
A3 <i>Growth of calcite single crystals underneath monolayers of 5,11,17,23-tetra-t-butyl-25,26,27,28-tetrakis(carboxymethoxy)calix[4]arenes</i> D. Volkmer, M. Fricke, <i>Z. Anorg. Allg. Chem.</i> 2003 , 626, 2381–2390.	
A4 <i>Elucidating the role of charge density on the growth of CaCO₃ crystal underneath calix[4]arene monolayers</i> D. Volkmer, M. Fricke, M. Gleiche, L. Chi, <i>Mater Sci. Eng. C</i> , im Druck.	
A5 <i>Interfacial electrostatics guiding the crystallization of CaCO₃ underneath monolayers of calixarenes and resorcurenes</i> D. Volkmer, M. Fricke, C. Agena, J. Mattay, <i>J. Mater. Chem.</i> 2004 , 14, 2249–2259.	
A6 <i>Acidic peptides acting as growth modifiers of calcite crystals</i> D. Volkmer, M. Fricke, T. Huber, N. Sewald, <i>Chem. Commun.</i> 2004 , 1872–1873.	
6. Publikationen, Auszeichnungen, Vorträge und Posterbeiträge	
7. Lebenslauf	

1. Vorwort

Das Studium der Biomineralisation beschäftigt sich mit der Bildung, den Strukturen und den Eigenschaften anorganischer Festkörper in biologischen Systemen. In den letzten zwei Jahrzehnten haben sich Studien zur Biomineralisation zunehmend auf die physikalisch-chemischen Prinzipien konzentriert. Aus den Erkenntnissen hat sich eine Quelle der Inspiration für die Materialwissenschaften¹ und aus einem Zweig der Bioanorganischen Chemie eine Biomimetische Materialchemie entwickelt.² Mittlerweile gilt die Biomineralisation, neben anderen Arbeitsgebieten wie der Supramolekularen Chemie, als eine der Schlüsseldisziplinen der modernen Chemie.³ In diesem Zusammenhang wird das gestiegene Interesse an der Funktionalität chemischer Systeme deutlich, welches sowohl potenzielle technologische Anwendungen als auch grundlegende Aspekte der Selbstorganisation beinhaltet. Chemikern eröffnet sich damit ein viel versprechender Ansatz, in einem interdisziplinären Umfeld verbesserte Strategien für die Lösung (nano-) technologischer, ökologischer und medizinischer Fragestellungen zu erarbeiten. Nicht zuletzt könnte der Chemie ein wichtiger Schritt zur Steigerung ihrer gesellschaftlichen Akzeptanz gelingen.

¹ P. Ball, *Made to Measure: New Materials for the 21st Century*, Princeton University Press, **1999**.

² S. Mann, *Biomimetic Materials Chemistry*, VCH, Weinheim, **1996**.

³ S. Mann, *Biomineralization. Principles and Concepts in Bioinorganic Materials Chemistry*, Oxford University Press, Oxford, **2001**.

2. Einleitung

Die kontrollierte Kristallisation anorganischer Festkörper an selbstorganisierten Grenzflächen ist ein bedeutender Prozess in der Biomineralisation⁴ und im Kristall-Engineering.⁵ Durch die Wechselwirkung mit geeigneten Additiven können Form und Funktion anorganischer Festkörper gezielt eingestellt werden. Zu den natürlichen Vorbildern organisch-anorganischer Hybridmaterialien gehören Biomineralien wie z. B. Knochen, Zähne oder Muschelschalen. Diese zeichnen sich häufig durch perfekt angepasste, funktionsoptimierte Materialeigenschaften aus. Die biologischen Prozesse, aus denen der hierarchische Aufbau und die Strukturvielfalt von Biomineralien resultieren, sind noch weitgehend unbekannt. Gemäß einer weit verbreiteten Modellvorstellung enthält die organische Matrix Calciumhaltiger Biomineralien spezifische Makromoleküle, die die Kristallkeimbildung ortsselektiv induzieren oder inhibieren und die Orientierung der aufwachsenden Kristallschicht determinieren.⁶ Da vollständige Strukturinformationen zu den natürlichen Matrixproteinen zur Zeit fehlen, wurden im Rahmen der Doktorarbeit amphiphile Makromoleküle entwickelt, die in geeigneten Modellsystemen entscheidende strukturelle und funktionelle Aspekte der natürlichen Systeme imitieren. Einen Schwerpunkt bilden Untersuchungen zur molekularen Erkennung und zum gerichteten Aufwuchs von CaCO_3 an biomimetisch strukturierten Grenzflächen.

2.1 Kristallkeimbildung in Mollusken

Die Exo- und Endoskelette der meisten Organismen bestehen aus calciumhaltigen Biomineralien. Während Knochen überwiegend Apatit ($\text{Ca}_5(\text{PO}_4)_3\text{OH}$) enthalten, werden Molluskenschalen hauptsächlich aus Calciumcarbonat (CaCO_3) aufgebaut. Da in den massiven Schalen vieler Mollusken (Weichtiere) unterschiedliche CaCO_3 -Polymorphe (Calcit, Aragonit und Vaterit) in räumlich streng voneinander getrennten Bereichen auftreten, wurden die Biomineralisationsvorgänge dieser Organismen besonders intensiv untersucht. Die biologische Selektion zwischen Polymorphen ist von fundamentaler Bedeutung in der Biomineralisation. Der Aufbau der Schale wird als Mikrolaminat bezeichnet, in dem die äußere prismatische Schicht aus groben, säulenförmigen Calcitkristallen besteht, während die

⁴ A. P. Wheeler, C. S. Sikes in: *Biomineralization*, (Hrsg.: S. Mann, J. Webb, R. J. P. Williams), VCH, Weinheim, **1989**, 95–131.

⁵ S. Mann, D. D. Archibald, J. M. Didymus, T. Douglas, B. R. Heywood, F. C. Meldrum, N. J. Reeves, *Science* **1993**, *261*, 1286–1292.

⁶ H. A. Lowenstam, *Science* **1981**, *211*, 1126–1131.

innere Perlmuttertschicht aus gleichförmigen Aragonitkristallplättchen aufgebaut ist. Der Mauerwerk-ähnliche Aufbau der Perlmuttertschicht ist von einer dünnen Protein-Polysaccharid-Matrix durchsetzt, die die Aragonitkristalle umschließt. Die organische Matrix limitiert das Wachstum der Kristalle und sorgt insgesamt für den strukturellen Zusammenhalt, wodurch eine im Vergleich zu reinem Aragonit vielfach höhere mechanische Stabilität erreicht wird.

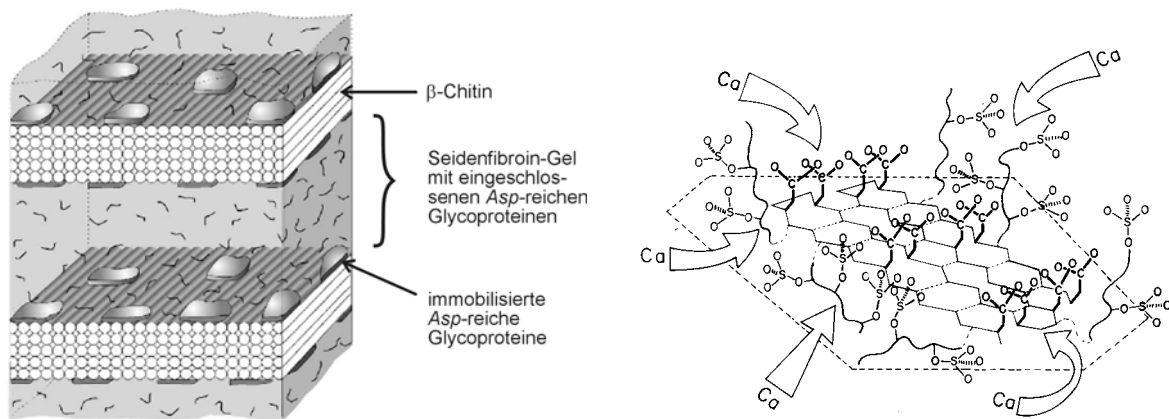


Abb. 1. Links: Schematische Darstellung des Aufbaus der organischen Matrix in der Perlmuttertschicht der Muschel *Atrina*. Die fibrösen Schichten aus β -Chitin sind in ein Gel aus Seidenfibroin eingebettet. Das Gel enthält Asp-reiche Glycoproteine, die auf die unlöslichen Chitinlamellen adsorbiert werden. Rechts: Schematische Darstellung der postulierten Nukleationszentren in der Molluskenschale. Hochgeladene, sulfatisierte Oligosaccharid-Seitenketten konzentrieren Ca-Ionen. Die Asp-reichen Domänen des adsorbierten Glycoproteins liegen in einer hochgeordneten β -Faltblattstruktur vor. Die Carbonsäurereste binden eine erste, geordnete Schicht von Ca-Ionen, auf der schließlich ein CaCO_3 -Kristallkeim gerichtet aufwächst (aus Ref. 7 und 8).

Auf Basis der identifizierten Primärstrukturen isolierter Makromoleküle aus Molluskenschalen sind frühzeitig vereinfachende Modellvorstellungen entwickelt worden. Gemäß dem aktuell diskutierten Modell dienen strukturell prä-organisierte Proteindomänen als supramolekulares Templat für die Kristallkeimbildung von CaCO_3 (Abb. 1).⁷ Demnach falten sich Asp-reiche Proteine in eine β -Faltblattstruktur und werden auf ein starres Gerüst aus wasserunlöslichen Chitinlamellen adsorbiert. Die lösliche organische Matrix besteht aus einem hydratisierten Seidenfibroin-Gelnetzwerk (Abb. 1, links).⁸ Das Gel enthält Asp-reiche Glycoproteine, die die spontane homogene Nukleation inhibieren. Ein Teil der Asp-reichen Glycoproteine wird an der Oberfläche der Chitinlamellen adsorbiert, wobei angenommen wird, dass die Proteine eine rigide Faltblattstruktur einnehmen. Durch die Faltung werden die Asp-Aminosäurereste auf einer Seite des β -Faltblattes positioniert, so dass ein selbstorganisiertes zweidimensionales Netzwerk aus koordinationsfähigen Carboxylatliganden aufgespannt würde (Abb. 1, rechts).

⁷ L. Addadi, S. Weiner in: *Biomineralization*, (Hrsg.: S. Mann, J. Webb, R. J. P. Williams), Weinheim, VCH, 1989, 133–156.

⁸ Y. Levi-Kalishman, G. Falini, L. Addadi, S. Weiner, *J. Struct. Biol.* 2001, 135, 8–17.

2.2 Biologisch inspiriertes Kristall-Engineering von CaCO_3

Die weite Verbreitung von Biomineralien aus CaCO_3 hat zu zahlreichen Modellstudien geführt, die im wesentlichen zwei experimentellen Ansätzen folgen: (I) Templat-induzierte Kristallisation an selbstorganisierten Grenzflächen, wie z. B. Langmuir-Monoschichten,⁹ selbstassemblierten Monoschichten (SAMs)¹⁰ oder Polymeren¹¹ und (II) Präzipitation von CaCO_3 aus Lösung in Gegenwart von löslichen Additiven, wie z. B. anorganischen Ionen,¹² Proteinen,¹³ Peptiden¹⁴ oder Polymeren.¹⁵

Insbesondere Langmuir-Monoschichten haben den experimentellen Vorteil, dass sich eine saubere, glatte und einheitliche Modellgrenzfläche reproduzierbar herstellen lässt. Da sich über eine gezielte Synthese die Positionen, Anzahl und chemische Natur der koordinationsfähigen Kopfgruppen der Amphiphile systematisch variieren lassen, kann deren Einfluss auf die Kristallisation von CaCO_3 untersucht werden.

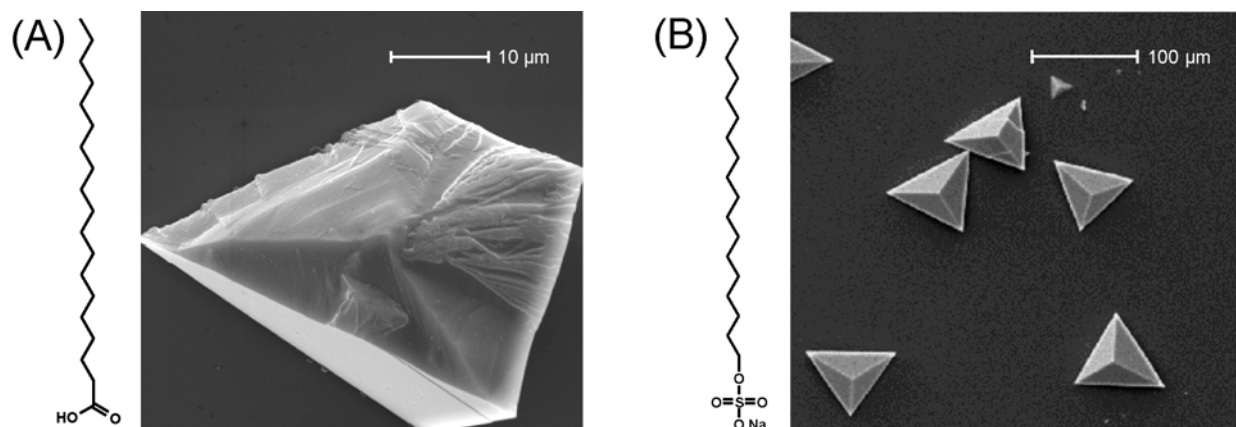


Abb. 2. Elektronenmikroskopische Aufnahmen von Calciteinkristallen, die unter Monoschichten aus Eicosansäure (A, $\pi = 25$ mN/m) und Octadecylsulfat (B, $\pi = 10$ mN/m) gewachsen sind.

In ersten Modellstudien zeigten Calcit-Einkristalle, die unter Langmuir-Monoschichten aus monofunktionellen Alkylcarbonsäuren, -sulfaten und -phosphaten wuchsen, eine enge Größenverteilung und eine stark verkürzte Keimbildungsgeschwindigkeit im Vergleich zu Kristallen, die durch spontane Kristallisation aus einer übersättigten Lösung von

⁹ S. Mann, B. R. Heywood, S. Rajam, J. D. Birchall, *Nature* **1988**, 334, 692–695.

¹⁰ (a) D. D. Archibald, S. B. Qadri, B. P. Gaber, *Langmuir* **1996**, 12, 538–546; (b) J. Küther, G. Nelles, R. Seshadri, M. Schaub, H. J. Butt, W. Tremel, *Chem. Eur. J.* **1998**, 4, 1834–1842; (c) J. Aizenberg, A. J. Black, G. M. Whitesides, *J. Am. Chem. Soc.* **1999**, 121, 4500–4509.

¹¹ A. Berman, D. J. Ahn, A. Lio, M. Salmeron, A. Reichert, D. Charych, *Science* **1995**, 269, 515–518.

¹² (a) P. M. Dove, K. J. Davis, J. J. DeYoreo, *Science* **2000**, 290, 1134–1137; (b) J. M. Didymus, P. Oliver, S. Mann, A. L. DeVries, P. V. Hauschka, P. Westbroek, *J. Chem. Soc. Faraday Trans.* **1993**, 98, 2891–2900.

¹³ G. Falini, S. Albeck, S. Weiner, L. Addadi, *Science* **1996**, 271, 67–69.

¹⁴ B. DeOliveira, R. A. Laursen, *J. Am. Chem. Soc.* **1997**, 119, 10627–10631.

¹⁵ H. Cölfen, M. Antonietti, *Langmuir* **1998**, 14, 582–589.

Calciumhydrogencarbonat erhalten wurden.¹⁶ Unter Monoschichten aus Alkylcarbonsäuren wachsen Calcit-Einkristalle vorzugsweise mit der {1-10}-Kristallfläche auf,¹⁷ während Monoschichten aus Alkylsulfaten und -phosphaten zu einer Orientierung parallel zu der {001}-Fläche des Calcitkristallgitters führen¹⁸ (Abb. 2). Zur Erklärung der unterschiedlichen Ausrichtung der Calcit-Einkristalle wurden detaillierte Bindungsmodelle ausgearbeitet, die auf die spezifischen Wechselwirkungen der Amphiphile mit den entsprechenden Kristallaufwuchsflächen eingehen.¹⁹ Eine epitaktische Beziehung zwischen der Packung der Moleküle in der Monoschicht und der Anordnung der Ca-Ionen in der Aufwuchsfläche lässt sich für einkettige Amphiphile leicht ableiten. Die Modellvorstellungen beruhen auf der stark vereinfachenden Annahme, dass die Anordnung der Ionen im ursprünglichen Kristallkeim mit den Atomlagen des makroskopischen Kristalls übereinstimmt, und somit die Grenzschicht zwischen dem Kristallkeim, bzw. dem Kristall und der Templatmatrix weitgehend identisch strukturiert ist. Bei einer geometrischen Übereinstimmung müssten sich 1:1- oder 2:1-Komplexe aus geladenen Kopfgruppen und Ca-Ionen bilden. Neuere Daten aus Synchrotron-Röntgenbeugungsstudien (GIXD, grazing incidence X-ray diffraction) an Eicosansäuremonoschichten haben allerdings gezeigt, dass die röntgenographische Dichte aus Ca-Ionen eher gering ist. Unter vier bis acht Eicosansäuremolekülen wurde nur ein Ca-Ion gefunden, das von Wassermolekülen umgeben ist.²⁰ Die bisherigen Arbeiten zur Epitaxie an organisierten Grenzflächen konzentrieren sich auf das orientierte Wachstum von Calcit oder Aragonit und liefern keine Informationen über frühe Stadien (Nukleation) der Kristallisationsprozesse. Da die zweidimensionale Ausdehnung der Molekülaggregate in kristallinen Monoschichtdomänen die Größe eines Kristallkeimes um einige Größenordnungen übertrifft, lassen sich keine Aussagen über die minimalen strukturellen Faktoren, d. h. über die Frühstadien der Templat-induzierten Nukleation ableiten.

Auch lösliche Makromoleküle und kleine Ionen können einen ausgeprägten Effekt auf die Selektion eines Polymorphes und die Morphologie der CaCO₃-Kristalle ausüben. So induzieren Proteine, die aus Aragonit- und Calcit-haltigen Schichten der Abalone-Muschelschale isoliert wurden, die gezielte Mineralisation des jeweiligen Polymorphes *in vitro*.²¹ Die Kristallisation von CaCO₃ in Gegenwart saurer Proteine, die aus calcifizierten

¹⁶ B. R. Heywood, S. Mann, *Adv. Mater.* **1994**, *6*, 9–20.

¹⁷ S. Rajam, B. R. Heywood, J. B. A. Walker, S. Mann, R. J. Davey, J. D. Birchall, *J. Chem. Soc., Faraday Trans.* **1991**, *87*, 727–734.

¹⁸ B. R. Heywood, S. Mann., *Chem. Mater.* **1994**, *6*, 311–318.

¹⁹ B. R. Heywood in: *Biomimetic Materials Chemistry*, (Hrsg.: S. Mann), Weinheim, VCH, **1996**, 143–173.

²⁰ E. DiMasi, M. J. Oltsza, V. M. Patel, L. Gower, *CrystEngComm.* **2003**, *5*, 346–350.

²¹ A. M. Belcher, X. H. Wu, R. J. Christensen, P. K. Hansma, G. D. Stucky, D. E. Morse, *Nature* **1996**, *381*, 56–58.

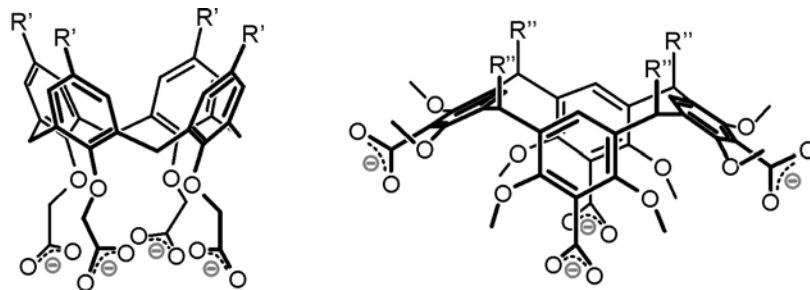
Gewebe (phylogenetisch) unterschiedlicher Organismen isoliert wurden, führte in den meisten Fällen zu Calciteinkristallen mit ausgeprägten $\{01l\}$ -Flächen mit $l = 1-1.5$ ²²

Die Ergebnisse aus den Modellstudien liefern wichtige Informationen über die möglichen Wechselwirkungen zwischen den organischen Molekülen und der daran angrenzenden anorganischen Festkörperoberfläche.

²² (a) J. Aizenberg, S. Albeck, L. Addadi, S. Weiner, *J. Cryst. Growth* **1994**, *142*, 156–164; (b) J. Aizenberg, J. Hanson, T. F. Koetzle, S. Weiner, L. Addadi, *J. Am. Chem. Soc.* **1997**, *119*, 881–886; (c) J. Aizenberg, G. Lambert, S. Weiner, L. Addadi, *J. Am. Chem. Soc.* **2002**, *124*, 32–38.

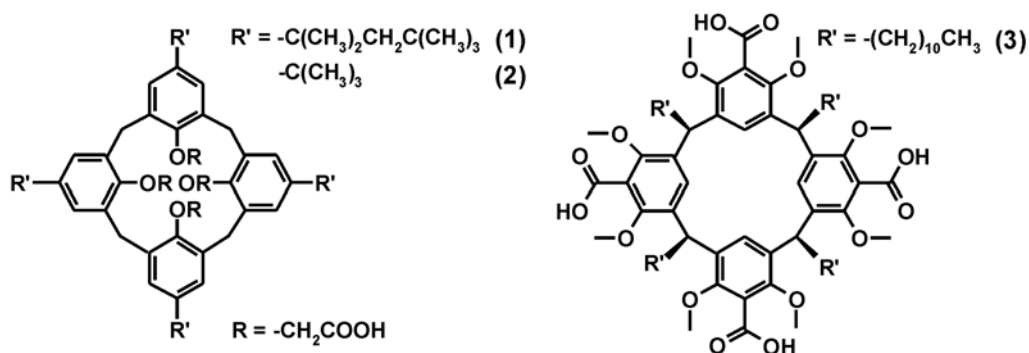
2.3 Kristallisation von CaCO_3 unter Monoschichten amphiphiler Oligosäuren

Die Erforschung der spezifischen Wechselwirkungen an der Grenzfläche zwischen anorganischem Mineral und der makromolekularen organischen Matrix gehört für den Chemiker zu den größten Herausforderung in der Biomineralisation. Um die Wechselwirkungen saurer Matrixproteine mit CaCO_3 -Mineralien in den hypothetischen Nukleationszentren von Mollusken zu imitieren, wurde im Rahmen der Doktorarbeit die Kristallisation von CaCO_3 unter Langmuir-Monoschichten aus amphiphilen, makrozyklischen Oligocarbonsäuren untersucht (Schema 1).



Schema 1. Perspektivische Strukturformeln der in Modellstudien eingesetzten makrozyklischen Oligocarbonsäuren

Da die Primärstrukturen der natürlichen sauren Matrixproteine vergleichsweise kurze Sequenzmotive mit *Asp*- und/oder *Glu*-Resten aufweisen, wurden Oligosäuren auf Basis von Calix[*n*]arenen und Resorc[*n*]arenen als supramolekulare Kristallisationstemplate in Modellstudien eingesetzt. Die gezielte Synthese erlaubt es, über die Größe und Konformation der Makromoleküle die Anzahl und räumliche Anordnung der Carboxylatgruppen systematisch zu variieren. Damit steht erstmalig eine Substanzklasse zur Verfügung, mit der die minimalen strukturellen Voraussetzungen für die gerichtete heterogene CaCO_3 -Nukleation (Frühstadium des Kristallwachstums) experimentell untersucht werden können.



Schema 2. Strukturformeln der in Modellstudien eingesetzten amphiphilen Calix[4]aren- und Resorc[4]aren-tetracarbonsäuren.

Die in Modellstudien eingesetzten Oligosäuren **1–3** (Schema 2) bilden stabile Monoschichten auf der Oberfläche wässriger Lösungen. Mit Hilfe einer Langmuir-Filmwaage lässt sich der Oberflächendruck und damit die Packungsdichte der Amphiphile reproduzierbar einstellen. Aus den Langmuir-Isothermen (π/A -Isothermen) wird die molekulare Bedeckung der Amphiphile als wichtige Stoffkonstante ermittelt und mit Werten aus Einkristallröntgenstrukturanalysen verglichen. Die Kristallstrukturen der Oligosäuren und deren Ca-Komplexen liefern Modelle für die Aggregation der Amphiphile in den Monoschichten. Aus den Strukturdaten werden supramolekulare Packungs- und Ca-Koordinationsmotive der Oligosäuren abgeleitet.

2.3.1 Kristallstrukturanalysen von Oligocarbonsäuren und deren Ca-Komplexen

Die Verbindungen kristallisieren in lamellaren Doppelschichtstrukturen, bei denen die hydrophoben Reste R' und die hydrophilen Kopfgruppen R in verschiedene Lagen segregieren (vgl. Lipidmembran). Die entsprechenden Ca-Komplexe bilden eindimensionale Koordinationspolymere (Abb. 3).

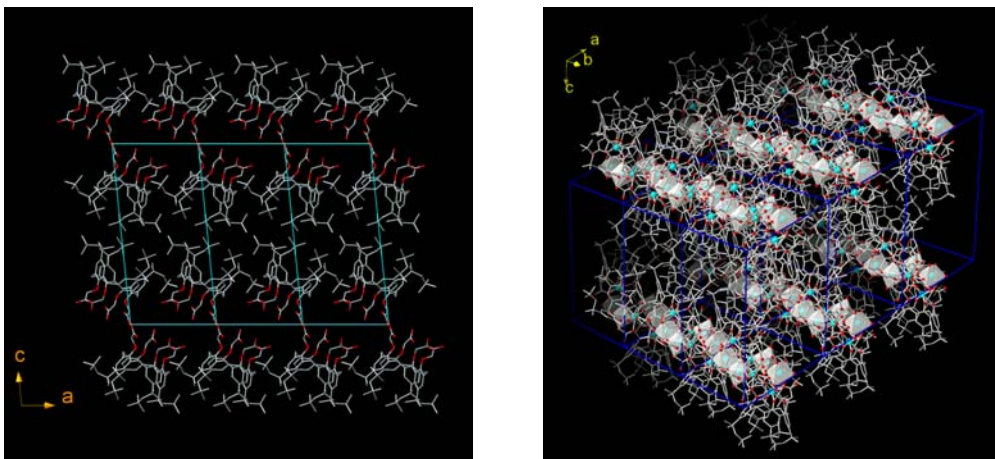


Abb. 3. Links: Drahtpackungsmodell von **1**. Rechts: Kombiniertes Draht-/Polyederpackungsmodell eines Ca-Komplexes von **1**.

Die durchschnittliche Fläche pro Molekül aus den Langmuir-Isothermen stimmt ausgezeichnet mit den Röntgenstrukturdaten überein, was darauf hindeutet, dass die Packung der Moleküle in der Monoschicht und im Kristallgitter sehr ähnlich ist (Tab. 1).

Tabelle 1: Packungsparameter der Oligosäuren 1–3

Verbindung	Fläche/Molekül [nm ²]		Literatur
	Monoschicht	Kristallstruktur	
1	1.45–1.50 ^a	1.51	23
	1.70–1.75 ^b	1.70	23
2	1.15–1.20 ^a	n.b.	24
	1.30–1.40 ^b	1.33	24
3	1.65–1.70 ^a	1.70	25
	1.75–1.80 ^b	1.83	25

^a H₂O: Millipore, R = 18.2 MΩ·cm; ^b Ca(HCO₃)₂: wässrige CaCl₂/NaHCO₃ (c = 9/18 mM); n.b.: nicht bestimmt

2.3.2 Kristallisation von CaCO₃ an Modellgrenzflächen

(A) Einfluss der Molekülgröße

Die Kristallisation von CaCO₃ unter Monoschichten aus 5,11,17,23-Tetrakis-(1,1,3,3-tetramethylbutyl)-25,26,27,28-tetrakis(carboxymethoxy)calix[4]aren (**1**)²³ und 5,11,17,23-Tetra-*t*-butyl-25,26,27,28-tetrakis(carboxymethoxy)calix[4]aren (**2**)²⁴ führt bei niedrigem Oberflächendruck ($\pi = 0.1\text{--}0.5$ mN/m) zu einheitlich orientierten Calciteinkristallen (Abb. 4. links (A)). Bei höheren Drücken findet man eine deutlich reduzierte Anzahl von Kristallen. Die Kristalle weisen unterschiedliche Kristallmorphologien und -orientierungen auf (Abb. 4. links (B)).

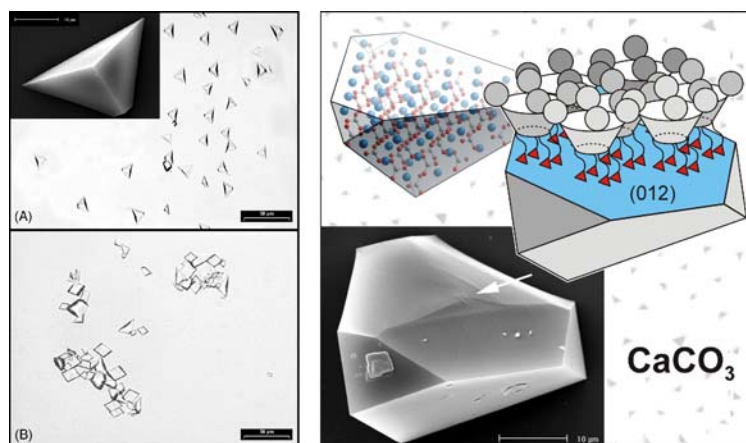


Abb. 4. Links: Hellfeld-Mikroskopieaufnahmen von (012)-orientierten Calciteinkristallen, die unter Monoschichten aus **2** wachsen, (A) $\pi = 0.1$ mN/m (Innenbild: elektronenmikroskopische Aufnahme eines (012)-orientierten Calciteinkristalls, der unter den gleichen Bedingungen wächst), (B) $\pi = 6$ mN/m (Blick von unten auf die Monoschicht); Rechts: Schematische Darstellungen der Aufwuchsfläche und elektronenmikroskopische Aufnahme eines (012)-orientierten Calciteinkristalls, der unter Monoschichten aus **1** wächst (Blick von oben auf die Monoschicht).

²³ D. Volkmer, M. Fricke, D. Vollhardt, S. Siegel, *J. Chem. Soc., Dalton Trans.* **2002**, 4547–4554 (A1).

²⁴ D. Volkmer, M. Fricke, *Z. Anorg. Allg. Chem.* **2003**, 626, 2381–2390 (A3).

²⁵ D. Volkmer, M. Fricke, C. Agena, J. Mattay, *CrystEngComm.* **2002**, 4, 288–295 (A2).

Eine Zuordnung der Aufwuchsfläche(n) der CaCO_3 -Einkristalle erfolgt durch geometrische Analyse der Kristallmorphologie (Abb. 5) und durch Röntgenbeugungsmethoden. Bei den erhaltenen CaCO_3 -Einkristallen handelt es sich um Calcitrhomboeder, die entlang der spezifischen Aufwuchsfläche trunkiert sind. Die Röntgenbeugungsdiagramme von Calcitkristallen, die unter Monoschichten aus **1** wachsen, haben die kristallgeometrischen Auswertungen bestätigt. Es treten hauptsächlich (012)- und (024)-Reflexe auf, was auf eine bevorzugte Kristallorientierung parallel zu (012) schließen lässt.²³

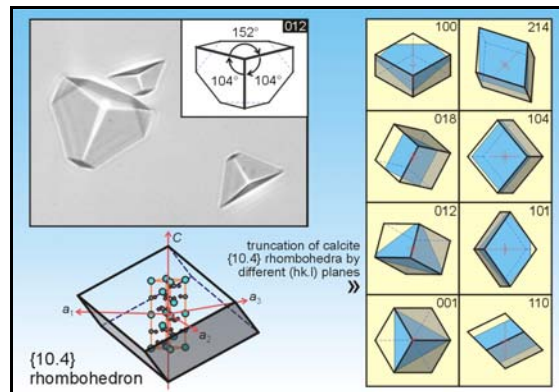


Abb. 5. Kristallgeometrisches Verfahren zur Auswertung der Aufwuchsorientierung von Calciteinkristallen (Innenbild: Hellfeld-Mikroskopieaufnahmen von Calciteinkristallen, die unter Monoschichten aus **1** wachsen mit Zuordnung der (012)-Aufwuchsfläche.)

Die {012}-Kristallflächen von Calcit sind polare Grenzflächen, in denen Ca-Ionen, bzw. Carbonationen in abwechselnden Schichten liegen (Abb. 4, rechts). Da polare Grenzflächen von Ionenverbindungen energetisch ungünstig sind und in der Regel eine hohe Wachstumsgeschwindigkeit aufweisen, treten sie im Kristallhabitus einer Verbindung normalerweise nicht in Erscheinung. Hochgeladene Carboxylat-haltige Liganden wie **1** und **2** können die elektrostatische Aufladung der polaren Kristallfläche neutralisieren und das Wachstum des Kristalles senkrecht zur Flächennormalen verzögern bzw. inhibieren.

Die Langmuir-Isothermen zeigen, dass **1** und **2** stabile Monoschichten auf wässrigen Subphasen bilden. Die durchschnittliche molekulare Fläche der beiden Verbindungen unterscheidet sich um mehr als 20% (Abb. 6).

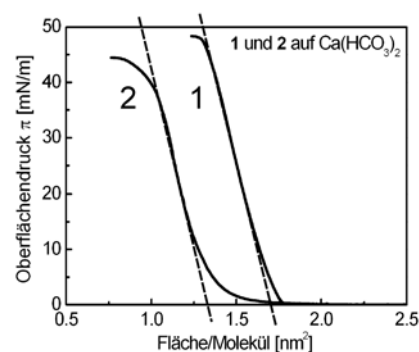


Abb. 6. Langmuir-Isothermen von **1** und **2** auf wässriger $\text{CaCl}_2/\text{NaHCO}_3$ ($c = 9/18 \text{ mM}$).

Da sich die Flächenwerte der Verbindungen erheblich unterscheiden, sollte ein direkter Vergleich des CaCO_3 -Kristallwachstums unter Monoschichten aus **1** und **2** Rückschlüsse auf mögliche Epitaxiebeziehungen zwischen der Monoschicht und der angrenzenden Kristallfläche erlauben. Überraschenderweise treten einheitlich orientierte Kristalle unter Monoschichten aus **1** und **2** bei niedrigem Druck und vergleichbarem Flächenbedarf auf ($\pi = 0.1\text{--}0.5$ mN/m, $A = 1.70\text{--}1.80$ nm²). Bei stark komprimierten Filmen ($\pi = 6\text{--}25$ mN/m, $A = 1.50\text{--}1.60$ nm² für **1**, $A = 1.20\text{--}1.30$ nm² für **2**), in denen die Amphiphile dicht gepackt sind, werden dagegen regellos orientierte Kristalle mit geringerer Nukleationsdichte erhalten. Eine Epitaxiebeziehung ist demnach bei niedrigem Druck und vergleichbarem Flächenbedarf durchaus möglich.

Um den Aggregationszustand der Amphiphile zu Beginn der Kristallisationsexperimente zu bestimmen, wurden Monoschichten aus **1** mittels Brewster-Angle-Mikroskopie (BAM) untersucht.²³ Bei niedrigem Oberflächendruck ($\pi = 0.1$ mN/m) liegen Monoschichten aus **1** sowohl auf reinem Wasser als auch auf Ca-haltiger Subphase in einer flüssig-kondensierten Phase vor (Abb. 7). Synchrotron-Röntgenbeugungsstudien an komprimierten Monoschichten haben ergeben, dass Monoschichten aus **1** auf reinem Wasser keine Reflexintensität im Druckbereich von $\pi = 0.1\text{--}20$ mN/m zeigen, die auf das Vorliegen kristalliner Filmdomänen hindeuteten.²³

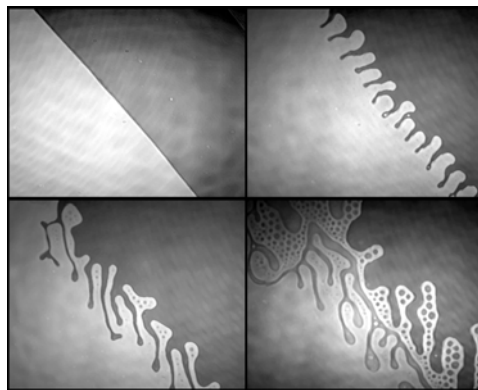


Abb. 7. BAM-Aufnahmen von Monoschichten aus **1** auf wässriger CaCl_2 ($c = 10$ mM) bei einem Druck von $\pi = 0.1$ mN/m. Zeitliche Entwicklung der Monoschichtmorphologie. Die Monoschicht erscheint hell abgesetzt gegenüber der nicht-bedeckten Wasseroberfläche.

Die Kristallisation von einheitlich (012)-orientierten Calcitkristallen erfolgt ausschließlich bei niedrigem Oberflächendruck, bei dem die Amphiphile in einem flüssig-kondensierten Aggregatzustand vorliegen und die Ca-Ionen unter der Monoschicht diffus verteilt sind. Epitaxiebeziehungen, also eine geometrische Übereinstimmung zwischen der Packung der Moleküle in der Grenzschicht und der Anordnung der Ca-Ionen in der Aufwuchsfläche des CaCO_3 -Keimkristalles spielen bei dem beobachteten Wachstum (012)-orientierter Calcitkristalle vermutlich keine Rolle.

Dagegen ist nicht auszuschließen, dass spezifische Wechselwirkungen der Calixarenliganden **1** und **2** mit Ca-Ionen eine wichtige Rolle spielen. Die Kristallstrukturen der Ca-Komplexe von **1** und **2** dienen als Modelle für die Aggregation der Moleküle in Monoschichten auf Ca-haltiger Subphase und geben Einblicke in die Koordination von Ca-Ionen bei niedrigem und bei hohem Oberflächendruck (Abb. 8).²⁴

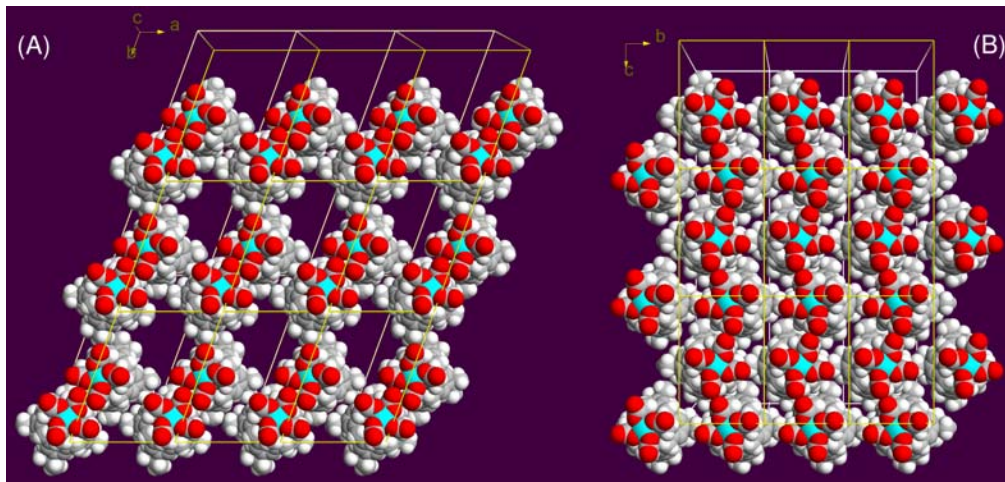


Abb. 8. CPK-Packungsmodelle zweier Ca-Komplexe von **2**. Dargestellt sind Monoschichten, die als Modelle für die Molekülpackungen auf Ca-haltiger Subphase bei niedrigem (A) und bei hohem Oberflächendruck (B) dienen.

(B) Einfluss der Koordinationsgeometrie

Der Einfluß der Amphiphilstruktur bei unveränderter Ladungsdichte wurde mit dem Resorc[4]aren *rccc*-5,11,17,23-Tetracarboxy-4,6,10,12,18,22,24-octa-*O*-methyl-2,8,14,20-tetra(*n*-undecyl)resorc[4]aren (**3**) untersucht. Da Resorc[4]arensäuren wie **3** strukturell komplementär zu Calix[4]arensäuren wie **1** und **2** sind (Schema 1), zeigen sie unterschiedliche Packungsmotive und Koordinationseigenschaften (Abb. 9). Dennoch wachsen unter Monoschichten aus **3**, ebenfalls bei geringem Oberflächendruck, (012)-orientierte Calciteinkristalle.²⁵

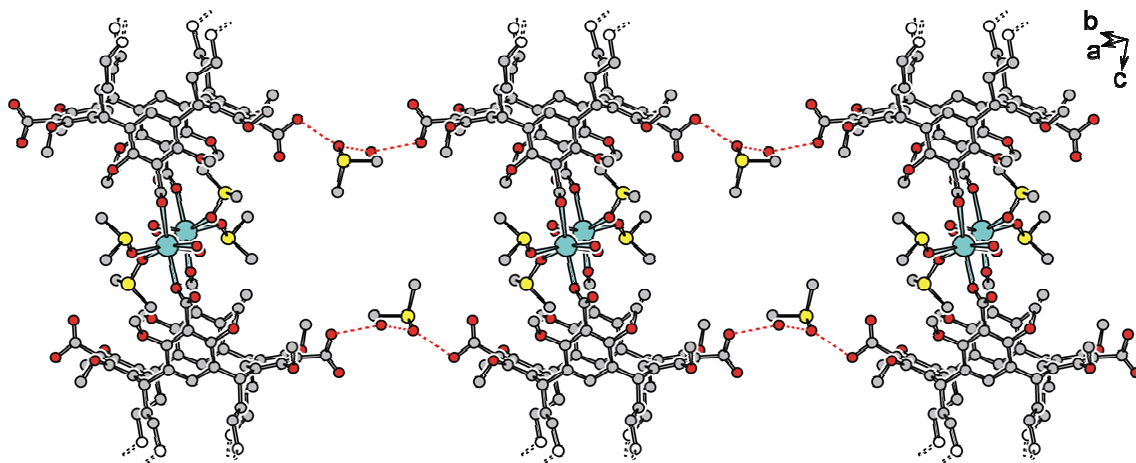


Abb. 9. Kugel-Stab-Modell der intermolekularen Wasserstoffbrückenbindungen in der Kristallstruktur des Ca-Komplexes von **3**.

Die orientierte Kristallisation von CaCO_3 an selbstorganisierten Templatoberflächen (Monoschichten, SAMs) wurde in der Literatur überwiegend mit Faktoren wie geometrischer Kommensurabilität¹⁶ und stereochemischer Komplementarität²⁶ der gegenüberliegenden Grenzflächen diskutiert. Wichtige Parameter wie elektrostatische Wechselwirkungen²⁷ und Dipolmomente²⁸ wurden in diesem Zusammenhang eher vernachlässigt. In den bisher vorgestellten Systemen kann von starken elektrostatischen und koordinativen Wechselwirkungen zwischen den Carboxylat-Kopfgruppen der Amphiphile und den Ca-Ionen in der Subphase ausgegangen werden. Da diese Wechselwirkungen von entscheidender Bedeutung für die Kristallisation unter Monoschichten sind, wurde als zusätzlicher physikalischer Parameter der druckabhängige Verlauf des Grenzflächenpotenzials ΔV der Monoschichten bestimmt. Aus den entsprechenden $\Delta V/A$ -Isothermen können Informationen über die Orientierung der molekularen Dipole, die Aggregation der Amphiphile und die Wechselwirkungen zwischen gelösten Ionen und Molekülen mit der Monoschicht abgeleitet werden.²⁹

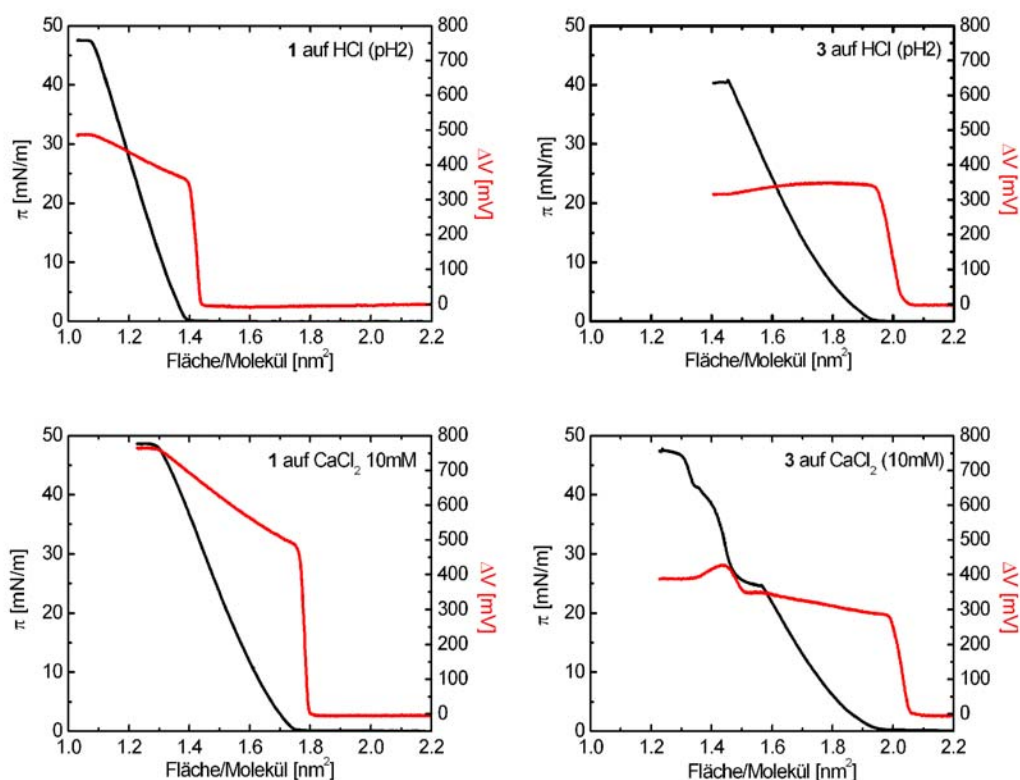


Abb. 10. π/A -Isothermen (schwarz) und $\Delta V/A$ -Isothermen (rot) von **1** und **3** auf wässriger HCl (pH2) und CaCl_2 (10mM).

²⁶ (a) L. Addadi, S. Weiner, *Proc. Natl. Acad. Sci. U.S.A.* **1985**, 82, 4110–4114; (b) Y.-J. Han, J. Aizenberg, *Angew. Chem. Int. Ed.* **2003**, 42, 3668–3670.

²⁷ S. R. Letellier, M. J. Lochhead, A. A. Campbell, V. Vogel, *Biochim. Biophys. Acta* **1998**, 1380, 31–45.

²⁸ M. J. Lochhead, S. R. Letellier, V. Vogel, *J. Phys. Chem. B* **1997**, 101, 10821–10827.

²⁹ P. Dynarowicz-Latka, A. Dhanabalan, O. N. Oliveira, Jr., *Adv. Colloid Interface Sci.* **2001**, 91, 221–293.

Die Potenzialverläufe von Monoschichten aus **1** und **3** auf Ca-haltiger Subphase zeigen deutlich unterschiedliches Verhalten (Abb. 10). Die vergleichsweise einfache Potenzialkurve von **1** deutet auf eine druckabhängige Re-Orientierung der molekularen Dipole an der Wasser/Luft-Grenzfläche hin. Der steile Anstieg in der Potenzialkurve von **1** spricht für eine Konzentration von Ca-Ionen unterhalb der Monoschicht und somit für eine stärkere Ca-Affinität von **1** im Vergleich zu **3**.³⁰ Hinweise dafür ergeben sich unmittelbar aus den Kristallstrukturen der Ca-Komplexe. Demnach bildet der achtzählige Chelatligand **1** unmittelbar nach dem Spreiten auf der Ca-haltigen Subphase einen mononuklearen Ca-Komplex. Bei der anschließenden Kompression werden die überschüssigen negativen Ladungen der Liganden von einer diffusen Schicht aus Ca-Ionen kompensiert. Unter Monoschichten aus **3** bildet sich unmittelbar nach dem Spreiten vermutlich zunächst ebenfalls ein 1:1-Komplex. Röntgenstrukturdaten legen nahe, dass diese Komplexe bereits bei niedrigem Druck assoziieren, z. B. indem Salz- oder Wasserstoffbrückenbindungen zwischen benachbarten Molekülen gebildet werden, wofür der flache Anstieg im Potenzialverlauf spricht. Der Knick in der Isothermen bei 25 mN/m deutet auf einen Phasenübergang hin.³¹ Möglicherweise findet hier eine Änderung von der *boat*- in die *crown*-Konformation statt, was in den Kristallstrukturen der freien Säure und des entsprechenden Ca-Komplexes angedeutet wird.²⁵

(C) Einfluss der Ladungsträgerdichte

Um weitere Einblicke in die Wechselwirkungen zwischen polaren Monoschichten und hydratisierten Ca- bzw. Carbonat-Ionen zu erhalten, wurde der ungeladene Alkohol 5,11,17,23-Tetrakis-(1,1,3,3-tetramethylbutyl)-25,26,27,28-tetra(2-hydroxyethoxy)-calix[4]aren (**4**) eingesetzt. Monoschichten aus **4** inhibieren die Kristallisation von CaCO₃ (Abb. 11a).³² Die unterschiedlichen Templateigenschaften von **1** und **4** sind in Abbildung 11 zusammengefasst.

³⁰ Ca-Ionen leisten einen positiven Beitrag zum Grenzflächenpotential: M. Eddaoudi, H. Parrot-Lopez, M. M. Boissonnade, A. W. Coleman, *Langmuir* **1995**, *11*, 13–15.

³¹ D. Volkmer, M. Fricke, C. Agena, J. Mattay, Manuskript in Vorbereitung.

³² D. Volkmer, M. Fricke, M. Gleiche, L. Chi, *Mater. Sci. Eng. C*, im Druck (A4).

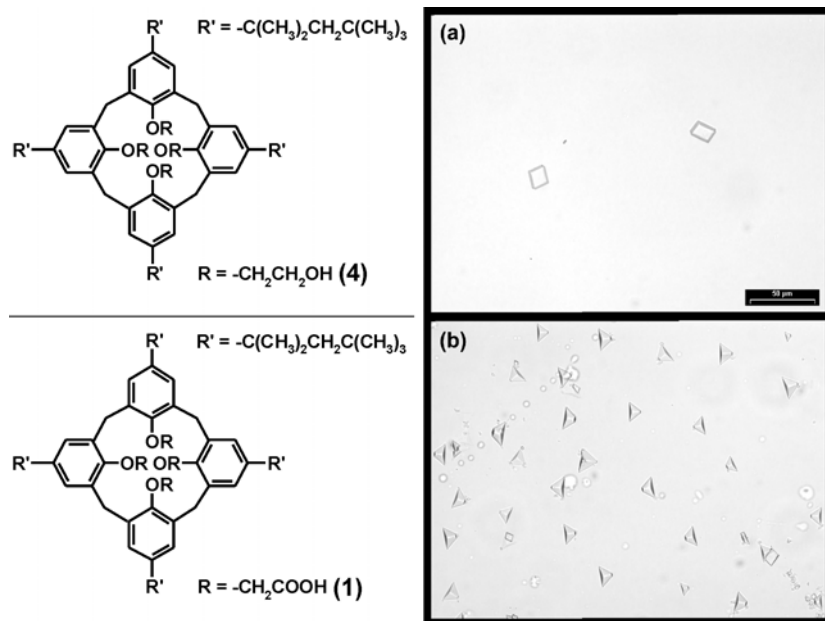


Abb. 11. Links: Strukturformeln des Calix[4]arenalkohols **4** und der Calix[4]arensäure **1**. Rechts: Hellfeldmikroskopie-Aufnahmen von Calciteinkristallen, die unter Monoschichten aus **4** und aus **1** wachsen ($\pi = 0.1$ mN/m).

Die Potenzialisothermen von **4** auf reinem Wasser und Ca-haltiger Subphase sind im niedrigen Druckbereich nahezu identisch mit der Isothermen von **1** auf reinem Wasser (Abb. 12). Auf Ca-haltiger Subphase ist der Potenzialanstieg im Druckbereich von $\pi = 0$ –30 mN/m für **4** sehr viel flacher als für **1** (Abb. 10), was auf schwächere Wechselwirkungen zwischen den ungeladenen Kopfgruppen von **4** und den Ca-Ionen der Subphase hindeutet.

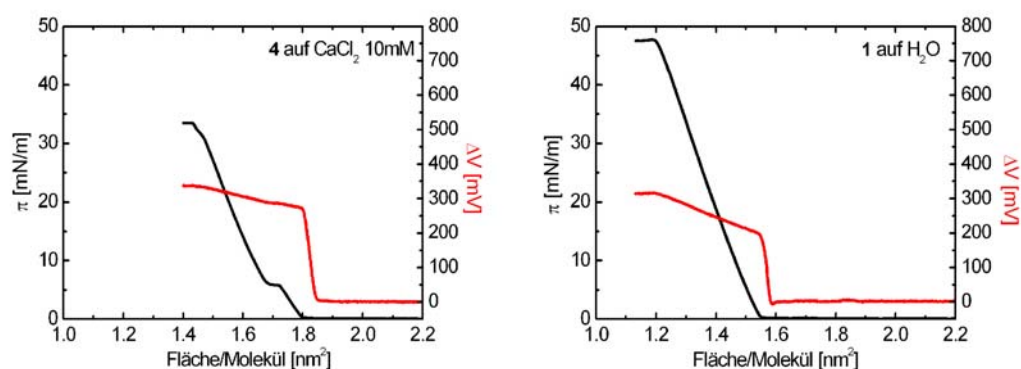
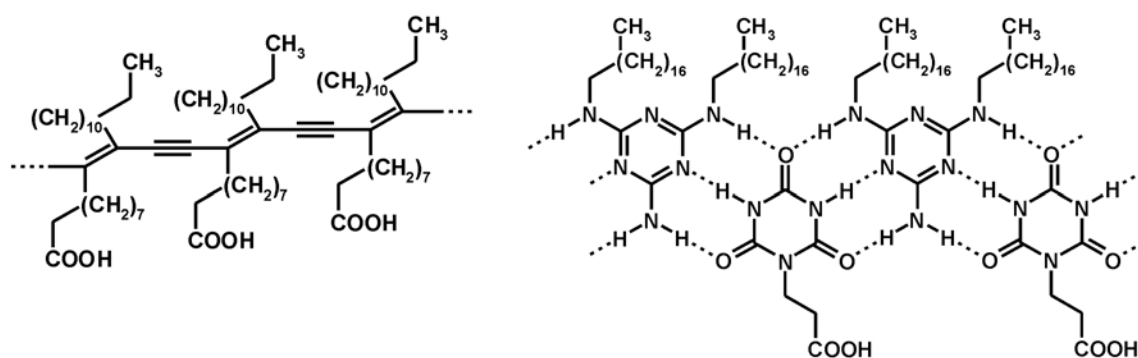


Abb. 12. π/A -Isothermen (schwarz) und $\Delta V/A$ -Isothermen (rot) von **4** auf CaCl_2 (10mM) und **1** auf reinem Wasser.

Die Ergebnisse der Potenzialmessungen demonstrieren, dass ungerichtete elektrostatische Wechselwirkungen die bestimmenden Faktoren für das Kristallwachstum von CaCO_3 an supramolekular organisierten Grenzflächen sind.

In den bisher vorgestellten Untersuchungen wurden amphiphile Calix[4]arene und Resorc[4]arene eingesetzt, die sich in ihren Strukturen und Konformationen unterscheiden. Die Kristallisation von (012)-orientierten Calciteinkristallen wurde in der Literatur auch für andere Monoschichten mit strukturell unterschiedlichen Amphiphilen beschrieben (Schema 3).^{11,33} Demnach spielen Faktoren wie Molekülstruktur und Koordinationsverhalten gegenüber Ca-Ionen eher eine untergeordnete Rolle bei der orientierten Kristallisation von Calcit unter Monoschichten.



Schema 3. Strukturformeln von polymeren Amphiphilen unter denen (012)-orientierte Calciteinkristalle wachsen.

Zur Ermittlung des Einflusses der durchschnittlichen Ladungsträgerdichte wurden Untersuchungen mit zwei Octacarbonsäuren durchgeführt, die einen unterschiedlichen Flächenbedarf und damit unterschiedliche Ladungsdichten in Monoschichten haben. Unter Monoschichten aus 5,11,17,23,29,35,41,47-Octakis-(1,1,3,3-tetramethylbutyl)-49,50,51,52,53,54,55,56-octa(carboxymethoxy)calix[8]aren (**5**) wachsen bei niedrigem Oberflächendruck und einer Ladungsdichte von 2.3–2.4 COO⁻/nm² erneut (012)-orientierte Calciteinkristalle (Tab. 2). Dieses Ergebnis stimmt ausgezeichnet mit dem Verhalten der Tetracarbonsäuren **1–3** überein, die bei vergleichbarer Kompression eine Ladungsdichte von 2.0–2.4 haben.

Mit dem Resorc[4]aren *rccc*-4,6,10,12,18,22,24-Octakis-*O*-(carboxymethyl)-2,8,14,20-tetra-(*n*-undecyl)resorc[4]aren (**6**) wird dagegen eine Erhöhung der Ladungsdichte erreicht (Abb. 13, links). Die Kristallisation von CaCO₃ führt in einem höheren Druckbereich ($\pi = 20\text{--}25$ mN/m) bei einer Ladungsdichte von 4.7–5.0 COO⁻/nm² zur Bildung der metastabilen Kristallphasen Aragonit und Vaterit (Abb. 13, rechts).³⁴ Bislang gibt es nur wenige Beispiele, in denen Aragonit ohne wasserlösliche Additive stabilisiert werden konnte. Unter Langmuir-

³³ S. Champ, J. A. Dickinson, P. S. Fallon, B. R. Heywood, M. Mascall, *Angew. Chem. Int. Ed. Engl.* **2000**, *39*, 2716–2719.

³⁴ D. Volkmer, M. Fricke, C. Agena, J. Mattay, *J. Mater. Chem.* **2004**, *14*, 2249–2259 (A5).

Monoschichten ist es zuvor nur mit der 5-Hexadecyloxyisophtalsäure gelungen,³⁵ die eine ähnliche Ladungsträgerdichte von ca. $4.65 \text{ COO}^-/\text{nm}^2$ aufweist (Tab. 2).³⁶

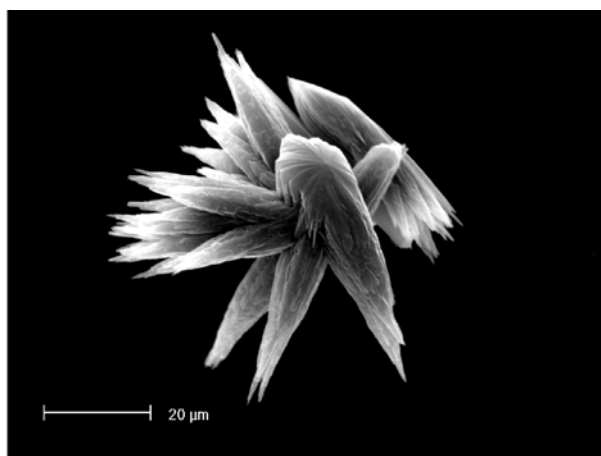
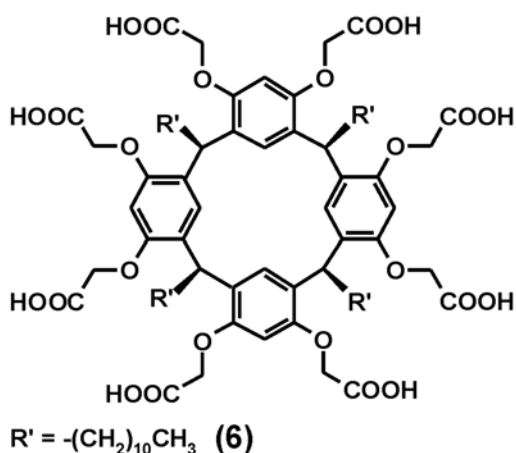


Abb. 13. Links: Strukturformel des Octacarboxyresorcärens (**6**). Rechts: Elektronenmikroskopische Aufnahme eines Kristallaggregats aus Aragonit, das unter einer Monoschicht aus **6** wächst ($\pi = 20 \text{ mN/m}$).

Die Ergebnisse untermauern eindeutig die Hypothese, dass ungerichtete elektrostatische Effekte bei der Templat-induzierten Kristallisation von CaCO_3 unter Monoschichten bestimmend sind. Epitaktisches Kristallwachstum, wie in der Literatur häufig beschrieben, kann für die vorgestellten Beispiele ausgeschlossen werden.

Tabelle 2. Korrelation zwischen der molekularen Fläche einiger ausgewählter Templatmoleküle und der induzierten CaCO_3 -Kristallorientierung

Verbindung	Fläche/Molekül [nm^2]		bei der CaCO_3 Kristalle wachsen	COO^-/nm^2	Polymorph (Vorzugsorientierung)	Lit.
	Monoschicht	Kristallstruktur				
1	1.70–1.75 ^a	1.70	1.75–1.80	2.22–2.29	Calcit (012)	23
2	1.30–1.40 ^a	1.70	1.70–1.80	2.22–2.42	Calcit (012)	24
		1.33	1.25–1.35	2.96–3.20	Inhibierung	24
3	1.75–1.80 ^b	1.83	2.00–2.10	1.90–2.00	Calcit (012)	25
5	2.75–2.80 ^b	n.b.	3.30–3.50	2.29–2.44	Calcit (012)	34
6	1.65–1.70 ^a	1.71				34
	1.80–1.85 ^b	n.b.	1.60–1.70	4.71–5.00	Aragonit, Vaterit	34
$\text{C}_{44}\text{H}_{85}\text{N}_9\text{O}_5$	0.50 ^a	n.b.	0.43–0.50	2.00–2.33	Calcit (012)	33
$\text{C}_{24}\text{H}_{38}\text{O}_5$	n.p.	0.43	$\pi=10 \text{ mN/m}$	4.65	Aragonit, Vaterit	35,36

^a H_2O : Millipore, $R = 18.2 \text{ M}\Omega\cdot\text{cm}$; ^b $\text{Ca}(\text{HCO}_3)_2$: wässrige $\text{CaCl}_2/\text{NaHCO}_3$ ($c = 9/18 \text{ mM}$)

n.b. = nicht bestimmt; n.p. = nicht publiziert

$\text{C}_{44}\text{H}_{85}\text{N}_9\text{O}_5$: $\text{N,N}'$ -Dioctadecyltriazin-2,4,6-triamin und derivatisierte Cyanursäure

$\text{C}_{24}\text{H}_{38}\text{O}_5$: 5-Hexadecyloxyisophtalsäure

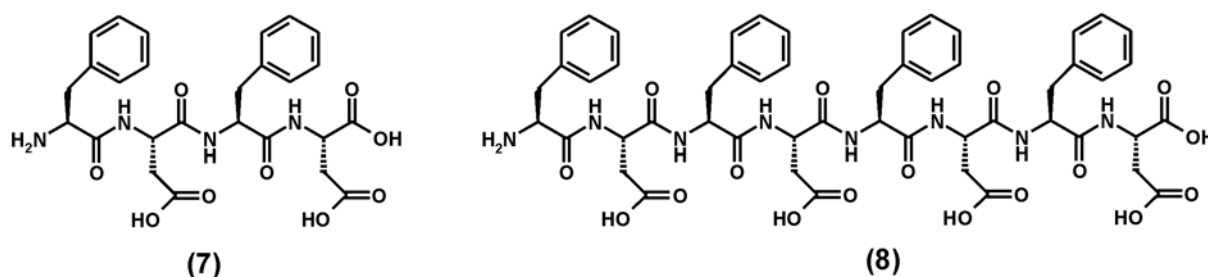
³⁵ A. L. Litvin, S. Valiyaveetil, D. L. Kaplan, S. Mann, *Adv. Mater.* **1997**, 9, 124–127.

³⁶ S. Valiyaveetil, V. Enkelmann, K. Müllen, *J. Chem. Soc., Chem. Commun.* **1994**, 2097–2098.

2.4 Kristallisation von CaCO₃ in Gegenwart saurer Oligopeptide

Mit amphiphilen Oligopeptiden soll in Zukunft ein weiterer Schritt zum biologischen Vorbild gelingen. Das rationale Design amphiphiler Peptide erlaubt es, Sekundärstrukturen wie β -Faltblattstrukturen, β -Hairpins, Helices und Peptidmakrozyklen zielgerichtet herzustellen. Zu diesem Zweck wurde die Molekülbibliothek aus amphiphilen Makrozyklen durch neuartige saure Oligopeptide mit *Asp*- und *Glu*-reichen Sequenzen erweitert, mit denen Epitope saurer Proteine in calcifiziertem Gewebe imitiert werden sollen.

Zunächst wurden amphiphile Tetra- und Octapeptide mit alternierenden hydrophilen und hydrophoben Aminosäureresten in einem neuen *bottom-up* Ansatz untersucht. Als hydrophile Aminosäuren wurden Aspartat (*Asp*), Glutamat (*Glu*), Asparagin (*Asn*), Glutamin (*Gln*) und Serin (*Ser*) eingesetzt und als hydrophobe Aminosäure stets Phenylalanin (*Phe*). Derartige Peptide tendieren dazu β -Faltblattstrukturen zu bilden, in denen die hydrophilen und die hydrophoben Reste auf gegenüberliegenden Seiten des Faltblattes liegen.³⁷



Schema 4. Strukturformeln der amphiphilen Oligopeptide *H-Phe-Asp-Phe-Asp-OH* (**7**) und *H-Phe-Asp-Phe-Asp-Phe-Asp-Phe-Asp-OH* (**8**)

Die Kristallisation von CaCO₃ in Gegenwart der amphiphilen Oligopeptide *H-Phe-Asp-Phe-Asp-OH* (**7**) und *H-Phe-Asp-Phe-Asp-Phe-Asp-Phe-Asp-OH* (**8**) als lösliche Additive, führt zu Calciteinkristallen mit spezifisch inhibierten {012}- und {110}-Flächen.³⁸ Die Ausbildung dieser Kristallflächen überrascht zunächst, da sie sich in ihrer Symmetrie und ihren elektrostatischen Eigenschaften deutlich voneinander unterscheiden. Es gibt bislang kein weiteres Beispiel, in dem ein Peptid spezifisch mit zwei verschiedenen Kristallflächen von Calcit wechselwirkt. Eine mögliche Erklärung liefern erste Ergebnisse mit 2D-NMR, wonach **7** in wässrigen, Ca-haltigen Lösungen in zwei energetisch bevorzugten Konformationen vorliegt.³⁹ In biogenen Calcitkristallen treten häufig polare Flächen indiziert als {01*l*} mit *l* = 1–2 auf. So spielt z. B. die Inhibierung von {012}-Kristallflächen eine wichtige Rolle bei der

³⁷ H. Rapaport, K. Kjaer, T.R. Jensen, L. Leiserowitz, D. A. Tirrell, *J. Am. Chem. Soc.* **2000**, *122*, 12523–12529.

³⁸ D. Volkmer, M. Fricke, T. Huber, N. Sewald, *Chem. Commun.* **2004**, 1872–1873 (A6).

³⁹ D. Volkmer, M. Fricke, T. Huber, N. Sewald, Manuskript in Vorbereitung.

Kontrolle von Kristalltextur und -morphologie in calcifizierten Schwammstacheln.⁴⁰ Proteine, die aus Seeigelstacheln, Schwammstacheln und Molluskenschalen isoliert wurden, induzieren *in vitro* die Bildung von {011}-Flächen mit $l = 1-1.5$.²² Peptide wie **7** und **8** können demnach die gleichen Effekte auf das Wachstum von Calcitkristallen ausüben wie natürliche Proteine. In der Literatur wurden häufig Modelle gezeigt, in denen organische Moleküle direkt auf bestimmten Kristallflächen adsorbieren. Da **7** und **8** in Lösung sehr flexibel sind, ist eine epitaktische Beziehung aber eher unwahrscheinlich.

Die bisherigen Ergebnisse lassen ein großes Potenzial für kurze Peptide mit repetitiven *Phe-Asp/Glu*-Einheiten in Modellstudien erkennen. Dieser Forschungsansatz sollte konsequent ausgebaut werden. Um stabile Struktur motive sowohl in Lösung als auch an der Wasser/Luft-Grenzfläche zu erhalten, sollten Peptide unterschiedlicher, zunehmender Komplexität eingesetzt werden (Abb. 14).

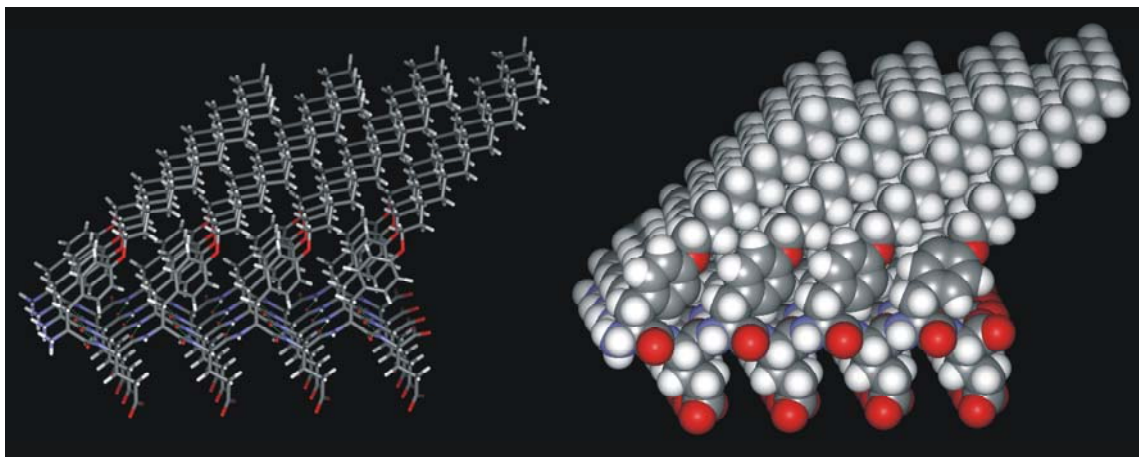


Abb. 14. Draht- und CPK-Packungsmodelle einer postulierten Aggregation des Peptids H-[Tyr(R)-Glu]₄-OH an der Wasser/Luft-Grenzfläche (R = -(CH₂)₁₁CH₃).

3. Zusammenfassung und Ausblick

Im Mittelpunkt der vorliegenden Arbeit stehen Modellstudien zum gerichteten Wachstum von CaCO₃ an biomimetisch strukturierten Grenzflächen. Die Primärstruktur saurer Proteine, die die Textur biogener Kristallphasen von CaCO₃ steuern, wurde mit Oligosäuren auf Basis von Calixarenen, Resorcarenen und Peptiden imitiert. Die Ergebnisse der Kristallisationsstudien unter Langmuir-Monoschichten haben gezeigt, dass die makrozyklischen Oligosäuren eine Templatwirkung auf das Wachstum von CaCO₃ ausüben. Über das Moleküldesign wurden die molekularen Eigenschaften so angepasst, dass der Einfluss der Molekülgröße, der

⁴⁰ J. Aizenberg, J. Hanson, T. F. Koetzle, L. Leiserowitz, S. Weiner, L. Addadi, *Chem. Eur. J.* **1995**, *1*, 414–422.

Koordinationsgeometrie und der Ladungsträgerdichte auf die Templat-induzierte Kristallisation von CaCO_3 bestimmt werden konnte. Die mittlere Ladungsträgerdichte in der Monoschicht kontrolliert sowohl das orientierte Kristallwachstum von CaCO_3 als auch die Polymorphselektion. In Gegenwart saurer Oligopeptide führte die Kristallisation von CaCO_3 zu trunkierten Calcitrhoedern mit spezifisch inhibierten Kristallflächen, die zuvor ausschließlich von natürlichen Proteinen induziert wurden. Da zwei energetisch unterschiedliche Kristallflächen von konformativ flexiblen Peptiden stabilisiert wurden, deuten die Ergebnisse erneut auf den Einfluss ungerichteter elektrostatischer Effekte hin. Eine epitaktische Beziehung wurde daher für alle vorgestellten Beispiele ausgeschlossen.

Die Ergebnisse lassen vermuten, dass auch in den Nukleationszentren von Mollusken die Ladungsdichte der Glycoproteine fein abgestimmt wird. Es sollte daher möglich sein, ein verbessertes Modellsystem zu entwickeln, indem Monoschichten aus amphiphilen Oligosäuren als Kristallisationstemplate und zusätzlich lösliche Elektrolyte eingesetzt werden, die die Kristallisation inhibieren oder verzögern. Dazu konnten vor wenigen Wochen erste Beiträge mit Monoschichten aus **3** in Gegenwart von Mg-Ionen und Polyacrylsäure (PAA) geleistet werden. In einem engen Konzentrationsbereich der wasserlöslichen Additive wachsen einheitlich dünne Aragonitplättchen, deren Abmessungen mit den charakteristischen Strukturmerkmalen im natürlichen Perlmutter vergleichbar sind (Abb. 15).

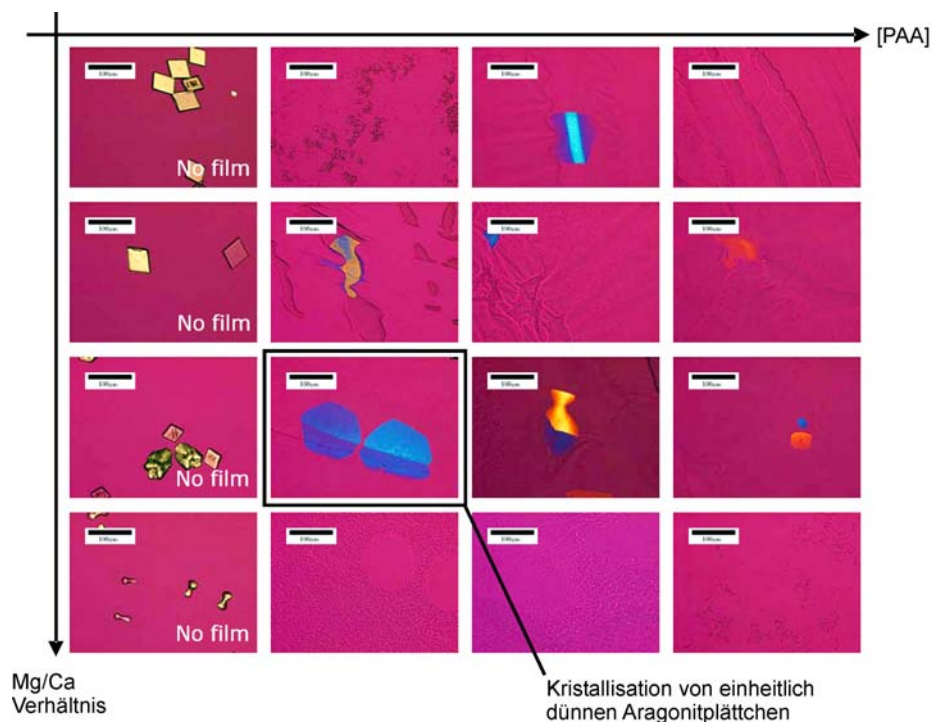
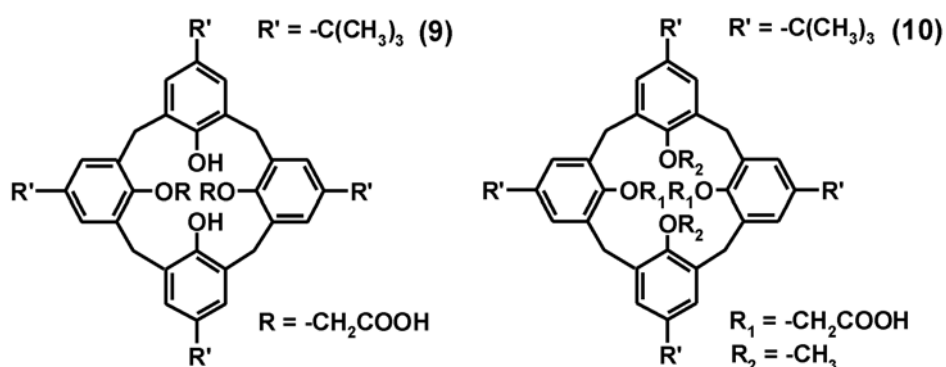


Abb. 15. Polarisationsmikroskopische Aufnahmen von CaCO_3 gewachsen unter Monoschichten aus **3** in Abhängigkeit der Mg- und Polyacrylsäure-Konzentration (PAA).

Da die Ladungsdichte als wichtiger Parameter bei der Kristallisation unter Monoschichten identifiziert wurde, sollten zukünftig Oligosäuren synthetisiert werden, die eine geringere Gesamtladung aufweisen als die bisher eingesetzten (Schema 5). Dazu wurden bereits erste Untersuchungen mit einem amphiphilen Calix[4]aren durchgeführt, welches über zwei Carbonsäurereste verfügt. Monoschichten aus 5,11,17,23-Tetra-*t*-butyl-25,27-dicarbonyl-methoxy-26,28-dihydroxycalix[4]aren (**9**) inhibieren die Kristallisation von CaCO_3 , was bisher von keiner anderen Carbonsäure-haltigen Monoschicht berichtet wurde.⁴¹



Schema 5. Strukturformeln von *tert*-Butylcalix[4]arensäuren mit unterschiedlicher Gesamtladung

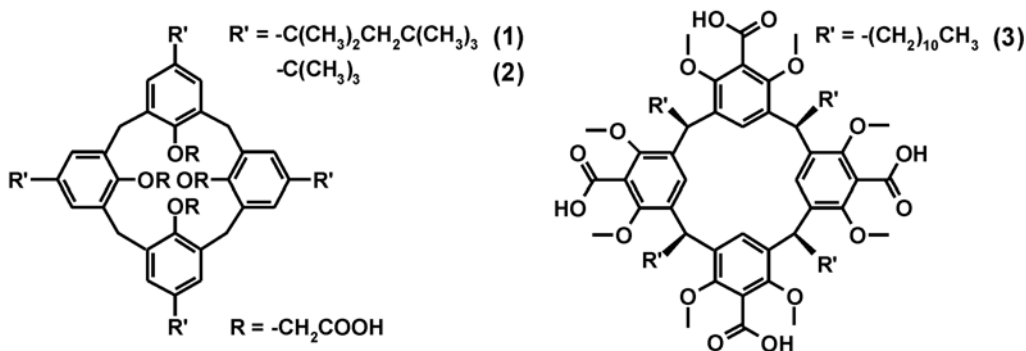
Um der fundamentalen Frage nach den minimalen strukturellen Voraussetzungen einer organischen Grenzfläche nachzugehen, die orientiertes Kristallwachstum induziert, sollten Moleküle von **1** mit einem Überschuss des entsprechenden Alkohols **4** umgeben werden. Indem nukleationsfördernde Moleküle in eine Matrix aus Molekülen eingebettet werden, die die Kristallisation inhibieren, könnte die Bildung einzelner Kristallkeime an isolierten organischen Molekülen erfolgen.

⁴¹ D. Volkmer, M. Fricke, Manuskript in Vorbereitung.

4. Summary

Crystallization of inorganic solids at self-organized surfaces is an important process in biomineralization and crystal engineering. Nucleation and growth steps taking place at the interface are often specific and result in a particular crystal morphology or polymorph. Much attention has been devoted to the characterization of mineral phases which occur in biominerals and calcified tissues. Apart from having aesthetically pleasant and intricate shapes, biominerals often possess attractive materials properties that attribute to a sophisticated internal hierarchical structure. Among the many open questions, one of the most challenging scientific goals is to gain insights into the molecular interactions that occur at the interface between the inorganic mineral and the macromolecular organic matrix. For the most widespread calcified tissues it is frequently assumed that a structurally rigid composite matrix consisting of fibrous proteins and thereon adsorbed acidic macromolecules acts as a supramolecular “blueprint” that templates nucleation of the inorganic phase. Efforts in trying to mimic aspects of these complex interactions with simple model systems will help improve the understanding of crystallization processes that are under biological control. In recent years Langmuir monolayers and self-assembled monolayers (SAMs) have been employed as 2D crystallization templates which induce epitaxial growth of highly oriented calcium carbonate crystals, the most abundant biomineral in nature. Physical parameters such as interfacial electrostatics, hydrogen bonding and interfacial molecular recognition events including geometrical lattice matching and stereochemical complementarity were discussed as crucial factors in this context. In order to mimic structural and functional aspects of the interactions between acidic proteins and biogenic calcite in calcified tissues (i. e. mollusk shells), Langmuir monolayers of macrocyclic oligoacids such as amphiphilic calix[*n*]arene or resorc[*n*]arene moieties were employed in this work.

Investigations on the amino acid composition of different natural proteins associated with biomineralisation reveal sequence motifs which are particularly rich in aspartic acid and glutamic acid residues, respectively. Unfortunately, none of the acidic proteins extracted from calcified tissues have yet been grown into single crystals suitable for X-ray crystallographic investigations and thus three-dimensional structures are currently not available. Artificial organic molecules can be designed such as to mimic the confined arrangement of acidic residues in natural proteins. Macrocyclic calix[*n*]arenes and resorc[*n*]arenes (Scheme 1) are especially suited for this purpose since they are synthetically readily available. These molecules form confined arrays of co-aligned carboxylic acid groups, the number and relative positions of which show systematic structural variations depending on the conformation and the size of the macrocyclic backbone.



Scheme 1

Monolayers of the newly synthesized macrocycles were spread at the air/water interface employing a Langmuir trough. The surface pressure–area (π -A) isotherms provide information on monolayer stability and phase behaviour. The area per molecule in the monolayers is estimated from extrapolating the Langmuir isotherms towards zero surface pressure. The determined values are in most cases in excellent agreement with the surface areas from crystal structure analysis, indicating that the packing arrangements of molecules in the monolayer and in the crystal lattice are similar. The compounds form lamellar structures in the solid state where the hydrophilic headgroups and the hydrophobic residues segregate into different layers. The corresponding Ca complexes form one-dimensional coordination polymers.

Crystallization of calcium carbonate underneath monolayers of 5,11,17,23-tetrakis-(1,1,3,3-tetramethylbutyl)-25,26,27,28-tetrakis(carboxymethoxy)calix[4]arene (**1**) and 5,11,17,23-tetra-*t*-butyl-25,26,27,28-tetrakis(carboxymethoxy)calix[4]arene (**2**) leads to uniformly oriented truncated calcite single crystals at low surface pressure ($\pi = 0.1$ – 0.5 mN/m), while randomly oriented crystals with reduced nucleation density are obtained at higher surface pressure ($\pi = 6$ – 25 mN/m). A geometrical analysis as well as X-ray diffraction measurements on polycrystalline film patches confirm that truncation occurs parallel to the {012} faces of the calcite crystal lattice. The polar {012} cleavage plane of calcite consists of separate layers of calcium and carbonate ions. Stabilization of this high-energy surface results from surface charge neutralization which most likely arises from coordination of anionic ligands, such as compound **1** and **2**, to the terminal (012) layer of Ca ions.

Langmuir isotherms indicate, that **1** and **2** form stable monolayers on aqueous subphases. The mean areas per molecule are in excellent agreement with data from crystal structure analysis, but the molecular area of **1** is 20% larger than of **2**. Surprisingly, uniform oriented crystals occur under monolayers of **1** and **2** at low surface pressure and comparable areas per molecule of 1.70 – 1.80 nm². At higher surface pressure where the molecules are close packed the nucleation density diminishes. Thus, an epitaxial correlation between the monolayer and the

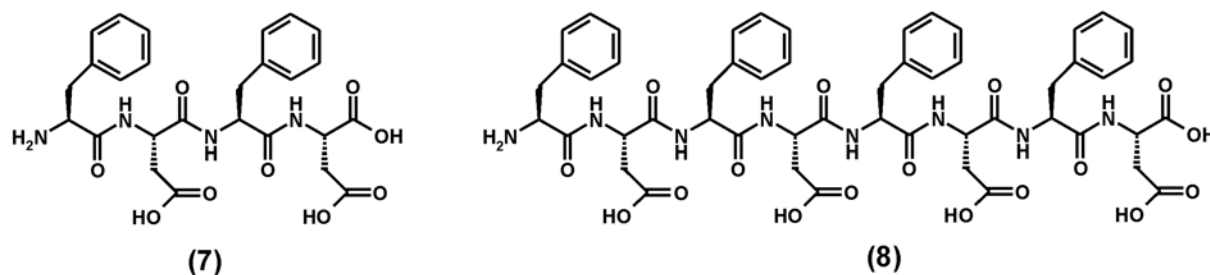
juxtaposed crystal face is possible at low surface pressure and comparable molecular areas. The dynamic macroscopic monolayer structure at the beginning of the crystallization experiments was characterized with Brewster angle microscopy (BAM). The BAM measurements indicate that already at zero surface pressure a liquid-condensed phase is formed. Grazing incidence X-ray diffraction studies, which provide information on the packing of the alkyl chains, reveal that no alkyl chain lattice exist in the condensed monolayer phase. Most likely the monolayer exists in an amorphous state lacking long range order. Since the growth of (012) oriented calcite crystals takes place exclusively at low surface pressure where the monolayer exist in a liquid-expanded state an epitaxial correlation obviously does not play a decisive role in the present case. Nevertheless, specific interactions between Ca ions from the subphase and ligands **1** and **2** are still possible. Crystal structures of Ca complexes of **1** and **2** serve as models for the putative packing arrangement of molecules in monolayers on aqueous subphases and reveal insights into the coordination of Ca ions at low and high surface pressure. The amphiphilic resorc[4]arene *rccc*-5,11,17,23-tetracarboxy-4,6,10,12,16,18,22,24-octa-*O*-methyl-2,8,14,20-tetra(*n*-undecyl)resorc[4]arene (**3**) is structurally complementary to the calix[4]arenes **1** and **2** and shows completely different packing arrangements and Ca-coordination motifs. Despite the structural and functional differences, crystallization of CaCO₃ underneath monolayers of **3** leads to (012) oriented calcite crystals at low surface pressure.

In order to characterize the pressure-dependent electrostatic properties of the monolayers, surface potential-area isotherms were recorded. The surface potential of monolayers arises from the dipole moments of the monolayer molecules, from the change in orientation of the water molecules and also from interactions between the headgroups and electrolytes which are dissolved in the subphase. These isotherms give an insight in the early stages of compression. The calixarene tetra acids **1** and **2** show an increase of the surface potential indicative of a pressure-dependent reorientation of molecular dipoles at the air-water interface. Formation of an adsorption layer of Ca ions underneath monolayers of these charged molecules leads to an increase of the surface potential. In contrast, monolayer phase behaviour of **3** is different to **1** and **2**. The increase of the surface potential of the monolayer of **3** on a Ca containing subphase is less steep and a plateau in the surface pressure-area isotherm points to a phase transition.

In order to gain more insights into the interactions between dipolar monolayers and hydrated calcium and carbonate ions, the non-charged amphiphilic alcohol 5,11,17,23-tetrakis-(1,1,3,3-tetramethylbutyl)-25,26,27,28-tetra(2-hydroxyethoxy)calix[4]arene (**4**) was employed. Monolayers of **4** strongly inhibit heterogeneous nucleation of CaCO₃ crystals. The results

indicate that non-specific electrostatic effects such as the average charge density or the mean dipole moment of the monolayer determine the orientation of crystals. In fact, growth of (012) oriented calcite crystals underneath monolayers of **1**, **2** and **3** occurs at a surface pressure where the average density of carboxylate residues at the air-water interface is about 2.0–2.4 COO⁻/nm². This hypothesis is further supported by investigations of calcium carbonate growth underneath monolayers of two different octacarboxylic acids, namely 5,11,17,23,29,35,41,47-octakis-(1,1,3,3-tetramethylbutyl)-49,50,51,52,53,54,55,56-octa-(carboxymethoxy)calix[8]arene (**5**) and *rccc*-4,6,10,12,16,18,22,24-octakis-*O*-(carboxymethyl)-2,8,14,20-tetra(*n*-undecyl)resorc[4]arene (**6**). These compounds were chosen since they differ largely in the molecular surface area and therefore in their average charge density. Crystallization of CaCO₃ under monolayers of **5** leads to (012) oriented calcite crystals at low surface pressure where the average charge density of **5** amounts to 2.3–2.4 COO⁻/nm². In contrast, a monolayer of **6** at high surface pressure ($\pi = 20\text{--}25$ mN/m) and a charge density of 4.7–5.0 COO⁻/nm² induces the formation of the metastable phases aragonite and vaterite. Crystallization of aragonite from an aqueous subphase lacking soluble (organic) additives has been achieved quite a few times. There is only one reported example in the literature for Langmuir monolayers of 5-hexadecyloxyisophtalic acid. Interestingly, the average charge density as derived from X-ray structure analysis of this compound amounts to 4.65 COO⁻/nm² which adds further support to the hypothesis that non-directional interfacial electrostatics is the dominant effect in template-directed crystal growth of CaCO₃ under Langmuir monolayers. An epitaxial correlation is ruled out for all examples.

Crystallization of CaCO₃ in the presence of the amphiphilic oligopeptides *H*-Phe-Asp-Phe-Asp-OH (**7**) and *H*-Phe-Asp-Phe-Asp-Phe-Asp-Phe-Asp-OH (**8**) (Scheme 2) as soluble additives yields truncated calcite rhombohedra with specifically inhibited {012} and {110} crystal faces.



Scheme 2

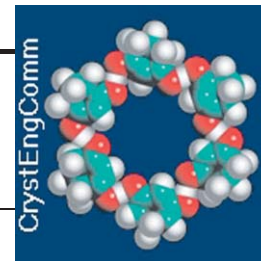
This is the first example where artificial peptides exert the same influence on the growth habit of calcite crystals as has been reported for natural acidic proteins isolated from skeletal elements of various organisms. Moreover, this is the first example where a single peptide

selectively interacts with two different faces of calcite. Conformational analysis of the short tetrapeptide **7** with 2D-NMR and MD simulations yield two distinct, energetically favourable conformations in solution which might be a possible explanation for the observed specific inhibition of two distinct crystal faces. Nevertheless, oligopeptides like **7** and **8** are still very flexible in solution. Therefore again, an epitaxial correlation is ruled out.

In summary, systematic structural variations of various organic matrices and investigations on the influence of these on the growth of CaCO₃, as presented in this work, show that the average charge density of the organic template is the dominant factor which fixes the selection of the CaCO₃ polymorphs and the growth direction of the inorganic constituents. These findings should have a profound impact on refined conceptions on the mechanisms of biomineralization processes as well as on the design of suitable organic coatings for the synthesis of novel biomimetic hybrid materials.

5. Anhang Publikationen

- A1** *Oriented crystallization of calcite single crystals grown underneath monolayers of tetracarboxyresorc[4]arenes*
D. Volkmer, M. Fricke, C. Agena, J. Mattay, *CrystEngComm*. **2002**, 4, 288–295.
- A2** *Crystallization of (012) oriented calcite single crystals underneath monolayers of tetra(carboxymethoxy)calix[4]arenes*
D. Volkmer, M. Fricke, S. Siegel, D. Vollhardt, *J. Chem. Soc., Dalton Trans.* **2002**, 4547–4554.
- A3** *Growth of calcite single crystals underneath monolayers of 5,11,17,23-tetra-*t*-butyl-25,26,27,28-tetrakis(carboxymethoxy)calix[4]arenes*
D. Volkmer, M. Fricke, *Z. Anorg. Allg. Chem.* **2003**, 626, 2381–2390.
- A4** *Elucidating the role of charge density on the growth of CaCO₃ crystal underneath calix[4]arene monolayers*
D. Volkmer, M. Fricke, M. Gleiche, L. Chi, *Mater Sci. Eng. C*, Manuskript im Druck.
- A5** *Interfacial electrostatics guiding the crystallization of CaCO₃ underneath monolayers of calixarenes and resorcarenes*
D. Volkmer, M. Fricke, C. Agena, J. Mattay, *J. Mater. Chem.* **2004**, 14, 2249–2259.
- A6** *Acidic peptides acting as growth modifiers of calcite crystals*
D. Volkmer, M. Fricke, T. Huber, N. Sewald, *Chem. Commun.* **2004**, 1872–1873.



Oriented crystallization of calcite single crystals grown underneath monolayers of tetracarboxyresorc[4]arenes†

Dirk Volkmer,^{*a} Marc Fricke,^a Ceno Agena^b and Jochen Mattay^b

^aUniversity of Bielefeld, Faculty of Chemistry (AC1), Bielefeld, Germany.
E-mail: dirk.volkmer@uni-bielefeld.de

^bUniversity of Bielefeld, Faculty of Chemistry (OC1), Bielefeld, Germany.
E-mail: mattay@uni-bielefeld.de

Paper

Received 4th March 2002, Accepted 30th April 2002

Published on the Web 16th July 2002

The crystal structures of *rccc*-5,11,17,23-tetracarboxy-4,6,10,12,16,18,22,24-octa-*O*-methyl-2,8,14,20-tetra(*n*-undecyl)resorc[4]arene, **1**, and its Ca salt, **2**, are described. Structural data were analyzed in terms of supramolecular packing motifs of the constituent amphiphilic macrocycles. Monolayer experiments indicate that a similar packing arrangement can be predicted for monolayers of **1** spread at the air–water interface. CaCO₃ (calcite) single crystals were grown underneath monolayers of **1** with highly uniform (012) orientation. This particular orientation was observed for a variety of structurally dissimilar monolayers indicating that macroscopic film properties such as average charge density or mean dipole moment have a decisive influence on templated calcite growth.

Introduction

Much attention has been devoted to the characterization of mineral phases which occur in biominerals and calcified tissues.¹ Among the many open questions, one of the most challenging scientific problems is to gain insights into the molecular interactions that occur at the interface between the inorganic mineral and the macromolecular organic matrix. For the most widespread calcified tissues it is frequently assumed that a structurally rigid composite matrix consisting of fibrous proteins and thereon adsorbed acidic macromolecules acts as a supramolecular “blueprint” that templates nucleation of the inorganic phase.²

Efforts in trying to separate and mimic aspects of these complex interactions with simple model systems will help to improve our understanding of crystallization processes that are under biological control. However, the deliberate design of interface architectures that direct crystal nucleation and growth in a predictable manner is by and large still a matter of trial and error.

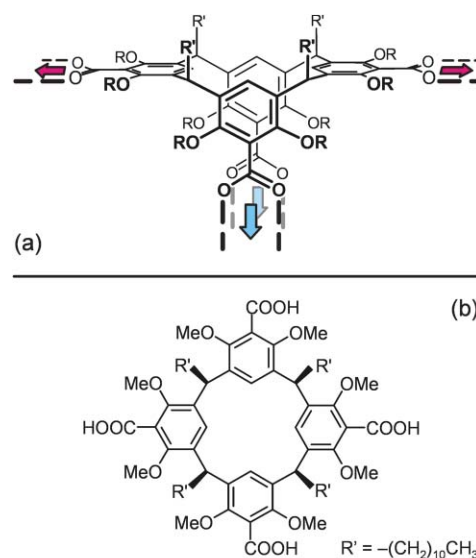
Chemists have employed different experimental set-ups to create highly-ordered template surfaces, including Langmuir monolayers,³ self-assembled monolayers (SAMs),⁴ or thin films.⁵ Especially the crystallization of inorganic compounds underneath free floating monolayers of amphiphilic molecules bears much development potential, since the surface properties may be adjusted by a suitable surfactant design as well as by simple experimental control parameters (*i.e.* subphase composition, surface area/molecule, or temperature).

We have recently initiated a research project focussing on induced crystallization underneath Langmuir monolayers of amphiphilic oligoacids.⁶ We here describe crystal structure analysis of *rccc*-5,11,17,23-tetracarboxy-4,6,10,12,16,18,22,24-octa-*O*-methyl-2,8,14,20-tetra(*n*-undecyl)resorc[4]arene, **1**, a novel surfactant bearing carboxy substituents at the resorcinol 2-positions (Scheme 1b), and its Ca salt, **2**.

Resorcinol-derived metacyclophanes have been subject of intense research since their original preparation in 1872.⁷ The

first X-ray structural characterization of a resorc[4]arene was reported in 1968.⁸ Since then, resorc[4]arene supramolecular architectures have been developed largely by the pioneering work of Cram *et al.*⁹ using conformationally immobile resorc[4]arenes (cavitands,¹⁰ carcerands¹¹) which show a rich and fascinating host–guest chemistry.

In contrast to numerous studies dealing with their complexation properties in solution,¹² resorc[4]arenes have rarely been used for the construction of infinite 2-dimensional architectures (*i.e.* monolayers, thin films)¹³ or 3-dimensional solids.¹⁴ This is surprising in light of certain molecular topological features that should render this class of macrocycles particularly attractive for crystal engineering purposes: resorc[4]arenes bearing various substituents (*e.g.* H, OH, Me) at the resorcinol 2-position are readily synthesized in gram quantities through one-pot acid catalyzed condensation with



rccc-5,11,17,23-tetracarboxy-4,6,10,12,16,18,22,24-octa-*O*-methyl-2,8,14,20-tetra-(*n*-undecyl)resorc[4]arene, (**1**)

Scheme 1

†Based on the presentation given at CrystEngComm Discussion, 29th June–1st July 2002, Bristol, UK.

aldehydes. Generally, the all-*cis* configured (*rccc*), bowl-shaped cyclic tetramer is precipitated in the course of the reaction because of its low solubility in acidic aqueous media. Under kinetic control of reaction conditions, the *cis-trans-trans* isomer (*rctt*) can also be isolated. According to X-ray structure analysis, *rccc*-resorcarenes with free hydroxy groups often yield structures in the bowl-shaped C_{4v} -symmetric *crow*n conformation,¹⁵ whereas resorcarene derivatives containing (non-bridging) *O*-alkyl substituents yield structures in the *boat* conformation.

Of special interest here is the less common C_{2v} -symmetric boat conformer where two benzene rings face each other, whereas the other ones lie in a common plane (Scheme 1a). This particular conformation results in a rectangular arrangement of functional groups (which represents a rare case for neat organic structures).

We furthermore describe our first results on induced crystallization of calcium carbonate underneath monolayers of **1**. Monolayers are spread on aqueous subphases of various compositions and the corresponding Langmuir isotherms are analyzed in terms of possible supramolecular packing arrangements. The occurrence of uniformly oriented calcite (CaCO_3) single crystals is monitored *in situ* by (polarization) optical microscopy. The orientation of epitaxially grown calcite crystals with respect to the monolayer is determined by means of X-ray diffraction, scanning electron microscopy and optical microscopy.

Results

X-Ray crystallographic investigations

Structure analysis of resorcarenes in boat conformations have so far been achieved quite a few times. A search of the Cambridge Structural Database (February 2002) yielded a subtotal of 14 X-ray structures out of 121 resorcarenes structures in all. No structures of *rccc*-resorcarenes with boat conformations containing *n*-undecyl residues have been

obtained so far. The X-ray crystallographic investigations on single crystals of *rccc*-5,11,17,23-tetracarboxy-4,6,10,12,16,18,22,24-octa-*O*-methyl-2,8,14,20-tetra(*n*-undecyl)resorc[4]arene, **1**, and its Ca salt, **2**, presented here (Table 1) are the first structural examples of a metal-free resorc[4]arene acid and its corresponding Ca complex.

Crystal structure of 1

Single crystals of the compound $\text{C}_{84}\text{H}_{128}\text{O}_{16}\cdot(\text{CH}_3\text{CN})_{1/8}$, **1**, were obtained by slow recrystallization from acetonitrile solution kept at 60 °C.

Important features of the resorcarene's molecular geometry are described by a few geometrical parameters as defined in Scheme 2.

The asymmetric unit of **1** contains two molecules which differ mainly by the arrangement of resorcarene methoxy substituents.

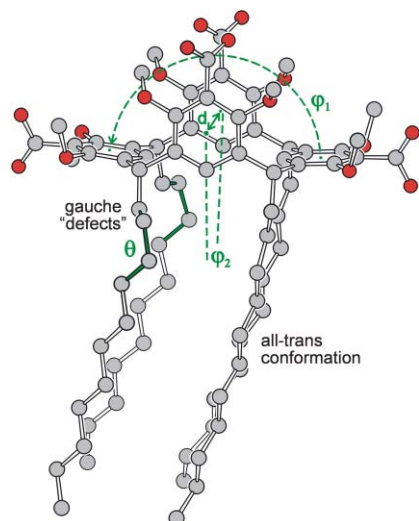
The X-ray structure analysis shows that compound **1** adopts a highly symmetrical boat conformation, which is described by the folding angle φ between least squares planes running through atomic positions of opposite benzene rings. For the first resorcarene molecule, φ_1 is 167.5°, while φ_2 amounts to 3.5°; the center-to-center spacing d between opposite benzene rings is 4.96 Å. While two out of four undecyl chains adopt an energetically favorable all-*trans* conformation (the largest deviation from the ideal torsion angle, $\theta = 180^\circ$, being 11°), the other ones display a single *gauche* "defect" (av. $\theta = 70.7^\circ$) occurring at atomic positions 1, 2, 3, and 4 of the undecyl chains. The corresponding values for the second molecule of the asymmetric unit are very similar ($\varphi_1 = 169.0^\circ$; $\varphi_2 = 6.9^\circ$; $d = 4.90$ Å; av. $\theta = 61.0^\circ$).

Compound **1** forms a lamellar structure where the hydrophilic constituents (carboxylic acid residues) and the hydrophobic residues (undecyl chains) segregate into different layers. The boat conformation of the macrocycles gives rise to formation of infinite, 2-dimensional flat strands consisting of resorcarene molecules which are interconnected through

Table 1 X-Ray crystallographic data for compounds **1** and **2**^a

Compound	1	2
Formula	$\text{C}_{84}\text{H}_{128}\text{O}_{16}\cdot(\text{CH}_3\text{CN})_{1/8}$	$[\text{Ca}(\text{C}_{84}\text{H}_{126}\text{O}_{16})](\text{DMSO})_2(\text{H}_2\text{O})_2\cdot\text{DMSO}\cdot(\text{H}_2\text{O})_4$
$M_r/\text{g mol}^{-1}$	1399.00	1774.41
T/K	183(2)	183(2)
$\lambda/\text{Å}$	0.71073	0.71073
Crystal system	monoclinic	triclinic
Space group	$P2_1/m$	$P\bar{1}$
$a/\text{Å}$	17.5950(8)	13.1315(8)
$b/\text{Å}$	58.099(3)	14.2389(8)
$c/\text{Å}$	18.2362(9)	28.243(2)
$\alpha/^\circ$	90	78.618(1)
$\beta/^\circ$	93.977(1)	86.426(1)
$\gamma/^\circ$	90	78.260(1)
$V/\text{Å}^3$	18597.0(15)	5067.3(5)
Z	8	2
$\rho_{\text{calcd}}/\text{g cm}^{-3}$	0.999	1.163
$\mu(\text{Mo-K}\alpha)/\text{mm}^{-1}$	0.068	0.191
$F(000)$	6102	1928
Crystal size/mm	0.10 × 0.25 × 0.40	0.02 × 0.40 × 0.50
θ range/°	1.12–22.52	1.47–25.01
Index ranges	$-18 \leq h \leq 18, -55 \leq k \leq 62, -19 \leq l \leq 16$	$-15 \leq h \leq 15, -16 \leq k \leq 16, -33 \leq l \leq 33$
Reflections collected	76378	45705
$R(\text{int})$	0.0425	0.0488
Independent reflections	24569	17813
Data/restraints/parameters	24569/0/1848	17813/0/1089
GoF	1.057	0.986
R values [$I > 2\sigma(I)$] ^b	$R_1 = 0.0950, wR_2 = 0.2884$	$R_1 = 0.0707, wR_2 = 0.2005$
R values (all data) ^b	$R_1 = 0.1319, wR_2 = 0.3176$	$R_1 = 0.1149, wR_2 = 0.2211$
Weighting scheme, w^{-1c}	$[\sigma^2(F_o^2) + (0.1653 \cdot P)^2 + 48.1 \cdot P]$	$[\sigma^2(F_o^2) + (0.1387 \cdot P)^2 + 0.00 \cdot P]$
Largest diff. peak/hole/e Å ⁻³	1.015/−0.384	1.179/−0.517

^aClick here for full crystallographic data (CCDC 183961 and 183962). ^b $R_1 = \Sigma||F_o| - |F_c||/\Sigma|F_o|$; $wR_2 = [\Sigma w(F_o^2 - F_c^2)^2/\Sigma w(F_o^2)^2]^{1/2}$. ^c $P = (F_o^2 + 2 \cdot F_c^2)/3$.



Scheme 2 Definition of geometrical parameters used to describe the molecular structure of resorcarene moieties in the crystal structures of **1** and **2**. $\phi_{1,2}$: folding angles between least squares planes running through atomic positions of opposite benzene rings; d : center-to-center spacing of opposite benzene rings; θ : torsion angle describing *gauche* “defects” occurring at selected atomic positions of the undecyl chains.

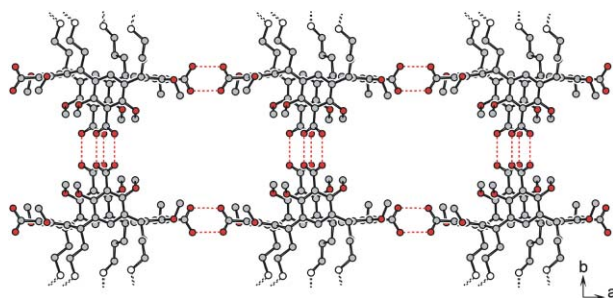


Fig. 1 Ball-and-stick model of the hydrogen bonding scheme in the crystal lattice of **1**. (Hydrogen atoms and fractions of the *n*-undecyl chains are omitted for clarity.)

hydrogen bonds between carboxylic acid residues (Fig. 1). These strands form layers in the crystallographic *ac*-plane. The average surface area occupied by a single resorcarene molecule

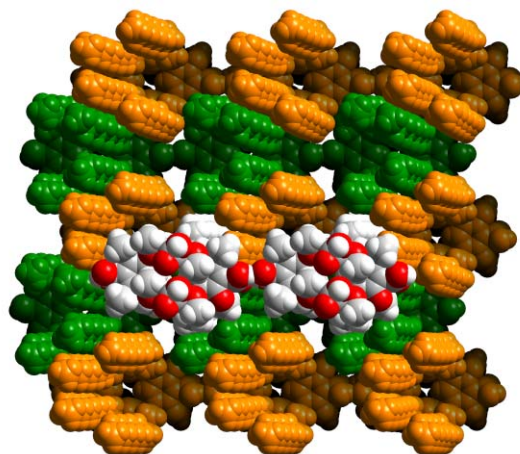


Fig. 2 Space-filling model of the supramolecular packing arrangement of **1** in the crystal lattice.

in the *ac*-plane amounts to 160 \AA^2 . The resulting packing arrangement is reminiscent of an “inverted” bilayer structure motif (Fig. 2), which is dictated by a close packing of hydrophilic head groups (as opposed to the close packing of hydrophobic alkyl chains in the bilayer structure of common surfactants or lipids).

Fig. 2 shows a space filling model of the supramolecular packing arrangement of **1** in the crystal lattice. Different strands of interconnected resorcarene molecules are highlighted in orange and green, respectively. The undecyl chains are tilted by an average angle of 20° against the *ac*-plane normal. Since the undecyl chains of an isolated bilayer are not bulky enough to fill the space completely (Fig. 2), interdigitation of successive bilayers occurs while bilayer stacking follows the *b*-direction (Fig. 3). The occurrence of *gauche* “defects” in the conformation of half of the undecyl chains may represent a further adaptation of the molecules to avoid empty spaces.

Crystal structure of **2**

Single crystals of compound $[\text{Ca}(\text{C}_{84}\text{H}_{126}\text{O}_{16})(\text{DMSO})_2 \cdot (\text{H}_2\text{O})_2] \cdot \text{DMSO} \cdot (\text{H}_2\text{O})_4$, **2**, were obtained at room temperature by slow vapor diffusion of water into a DMSO solution of **2**.

The asymmetric unit of **2** contains one half of a dinuclear Ca

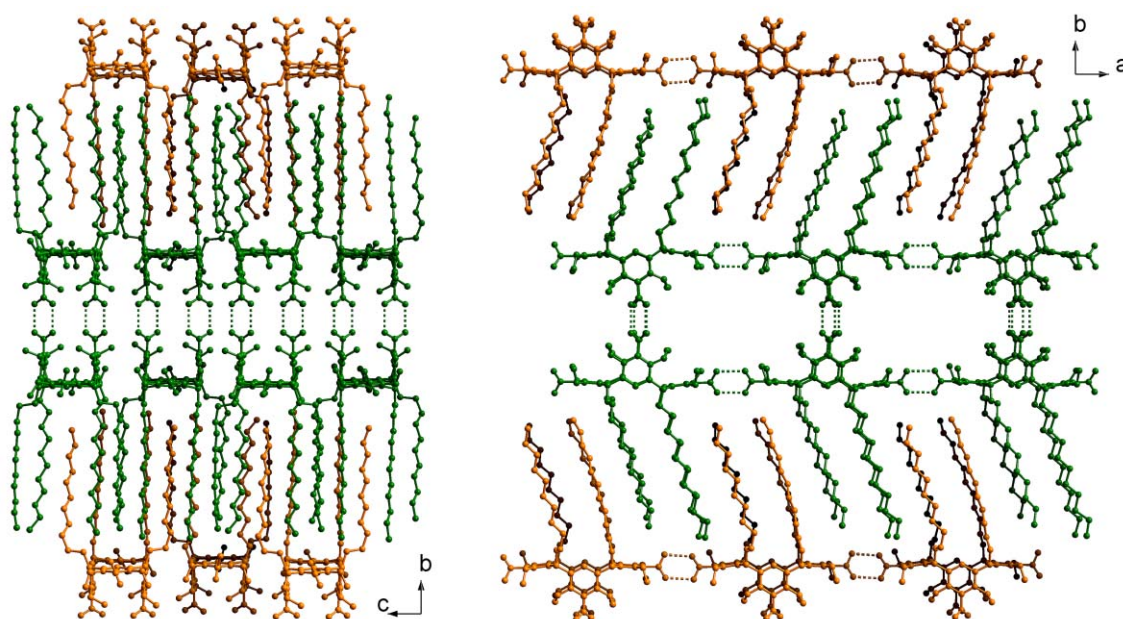


Fig. 3 Packing diagrams showing the interdigitation of bilayers of **1** in the crystal lattice. Resorcarene molecules belonging to the same “inverted” bilayer are represented with identical colors (hydrogen atoms are omitted for clarity). Click image or [here](#) to access a 3D representation.

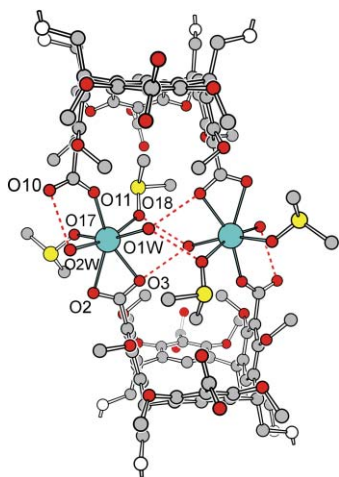


Fig. 4 Coordination scheme of the dinuclear Ca complex, **2**. Intra-molecular hydrogen bonds between different oxygen donor ligands are displayed as broken red lines. (Hydrogen atoms and fractions of the *n*-undecyl chains are omitted for clarity.)

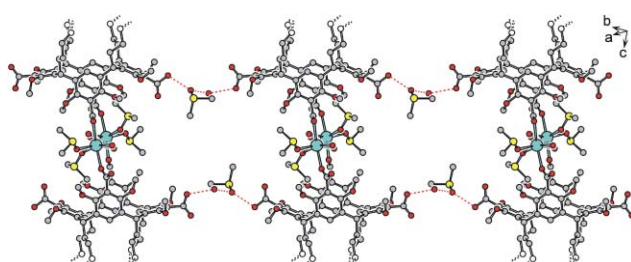


Fig. 5 Ball-and-stick model of the intermolecular hydrogen bonding scheme in the crystal lattice of **2**. (Hydrogen atoms and fractions of the *n*-undecyl chains are omitted for clarity.)

complex which is described by the molecular formula $[\text{Ca}(\text{C}_{84}\text{H}_{126}\text{O}_{16})(\text{DMSO})_2(\text{H}_2\text{O})_2]_2$. The coordination scheme of Ca ions is shown in Fig. 4. Each Ca ion is placed in a distorted pentagonal bipyramidal coordination environment consisting of different oxygen donor ligands (two DMSO molecules, two water molecules, and two carboxylate residues belonging to different resorcarene moieties, respectively). The carboxylate residues show different coordination modes, one

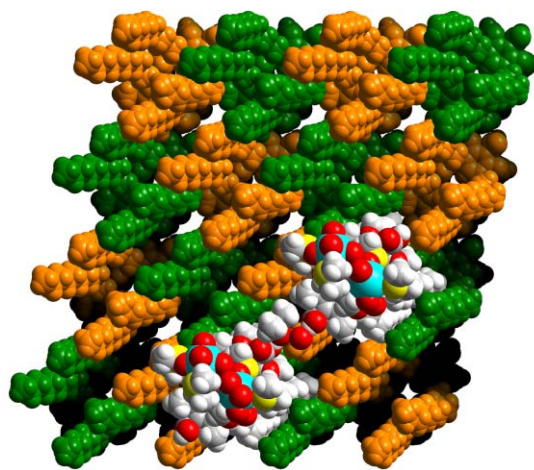


Fig. 6 Space-filling model of the supramolecular packing arrangement of **2** in the crystal lattice.

residue is coordinated in a monodentate fashion whereas the other one is coordinated in the bidentate (η^2) mode to the Ca ion. The oxygen donor ligands of the dinuclear unit are extensively interconnected by means of intra- and intermolecular hydrogen bonds which are shown in Fig. 4 and 5.

The gross structural features of the free acid **1** are likewise observed in the crystal structure of its corresponding Ca complex, **2**. Compound **2** also forms a lamellar structure where the hydrophilic constituents (carboxylate residues, oxygen donor ligands) and the hydrophobic residues (undecyl chains) segregate into different layers (Fig. 6 and 7).

The boat conformation of the macrocycles gives rise to formation of infinite, 2-dimensional flat strands consisting of the dinuclear units which are interconnected through hydrogen bonds. The *intermolecular* hydrogen bonding scheme, however, is dissimilar to that of the free acid. As shown in Fig. 5, the hydrogen bonds between non-coordinated carboxylic acid residues are intercepted by a single DMSO and a water molecule, respectively, which leads to a less dense packing of resorcarene ligands. The average surface area occupied by a single resorcarene molecule in the *ab*-plane therefore amounts to 183 \AA^2 .

X-Ray structure analysis shows that the resorcarene molecules in the crystal structure of **2** adopt a boat

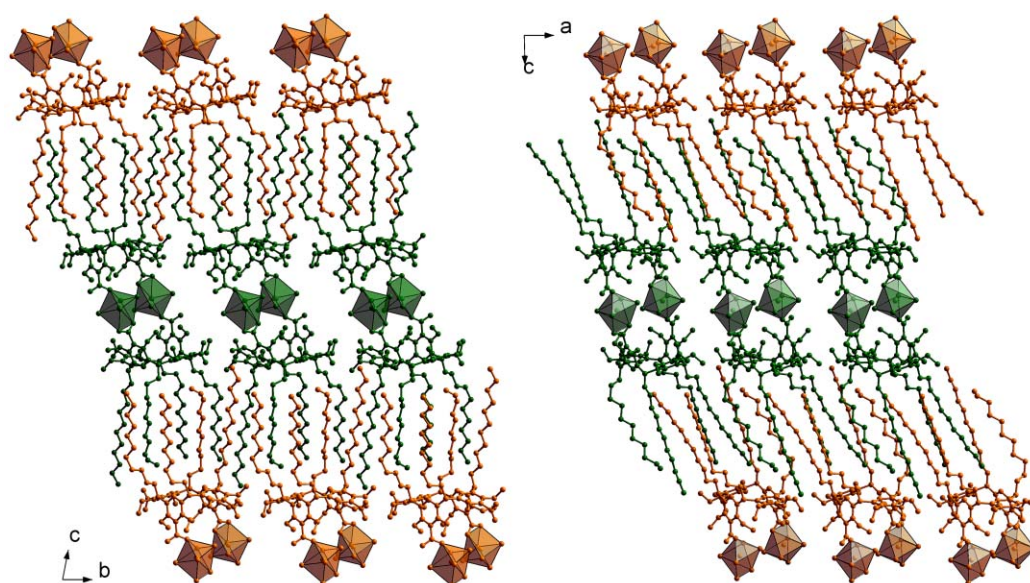


Fig. 7 Packing diagrams showing the interdigitation of bilayers of **2** in the crystal lattice. Resorcarene molecules belonging to the same “inverted” bilayer are represented with identical colors (hydrogen atoms are omitted for clarity; only the oxygen donor atoms of the Ca coordination environment are shown). Click image or here to access a 3D representation.

conformation which is distorted from ideal rectangular geometry as defined in Scheme 1a. The folding angle φ_1 is 146.4° , while φ_2 amounts to 22.4° ; the center-to-center spacing d between opposite benzene rings is 5.52 \AA . Only one of four undecyl chains adopts an energetically favorable all-*trans* conformation (the largest deviation from the ideal torsion angle $\theta = 180^\circ$ being 15°), the other ones display a single *gauche* “defect” (av. $\theta = 67.5^\circ$) occurring at atomic positions 1, 2, 3, and 4 of the undecyl chains. One of these chains shows a second *gauche* “defect” ($\theta = 88^\circ$) occurring at atomic positions 8, 9, 10, and 11.

An important question arises as to whether or not the (almost) rectangular geometry of resorcarene boat conformers in the crystal structure of **1** represents a favourable situation in terms of steric energy. In principal, it is conceivable that the gain of energy through formation of hydrogen-bonded oligomers in the structure of **2** leads to over-compensation of any steric strain which is imposed upon the macrocyclic backbone as it approaches a rectangular arrangement. Breaking the hydrogen bonds by means of solvent insertion, as observed in the crystal structure of **2**, may then lead to a more relaxed resorcarene geometry.

A close inspection of published resorcarene structural data, however, shows that in fact the rectangular arrangement seems to be favorable, at least in terms of crystal packing energy. The Cambridge Structural Database contains structural data of resorcarene derivatives 4,6,10,12,16,18,22,24-octa-*O*-methyl-2,8,14,20-tetra(isopropoxycarbonylmethyl)resorc[4]arene ($C_{56}H_{72}O_{16}$, CSD structure code: HEFKUY10),¹⁶ and of 4,6,10,12,16,18,22,24-octa-*O*-ethyl-2,8,14,20-tetramethylresorc[4]arene ($C_{48}H_{64}O_8$, CSD structure code: POBCUE).¹⁷ Both derivatives show an almost perfect rectangular boat conformation, although they do not contain any acidic substituents that are capable of forming hydrogen bonds.

Monolayer studies

Crystallographic investigations on the solid state structure of the amphiphilic resorcarene **1**, and its Ca salt, **2**, are complemented by monolayer studies.

Langmuir monolayers

An advantage of the monolayer technique using a film balance is that characteristic features of the monolayer, *e.g.* surface pressure, macroscopic texture and lattice structure, can be studied as a function of area per molecule. The surface pressure (π)-area (A) isotherms provide information on the thermodynamics and the phase behaviour of the monolayer.

Fig. 8 shows the π - A isotherms of compound **1** monolayers spread on an aqueous subphase (pure water, and 10 mM $CaCl_2$, respectively). In both cases, stable monolayers are formed which collapse upon compression at a surface pressure of $\sim 40 \text{ mN m}^{-1}$.

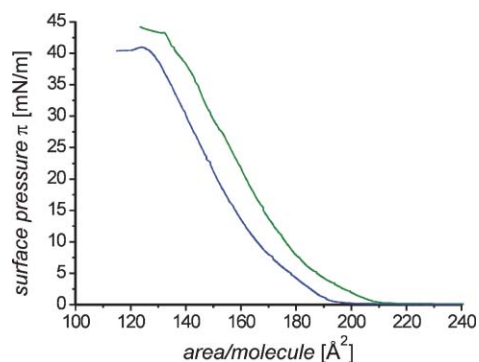


Fig. 8 π - A isotherms of monolayers of **1** at 24°C on H_2O (blue), and aqueous 10 mM $CaCl_2$ (green).

Table 2 Area per molecule of 2,8,14,20-tetra(*n*-undecyl)resorc[4]arene derivatives as determined from crystal data and Langmuir isotherms

Compound	Area per molecule/ \AA^2	Ref.
1	160; ^a 170 ^b (H_2O)	This work
2	183; ^a 180 ^b (10 mM $CaCl_2$)	This work
$C_{72}H_{112}O_8 \cdot 4EtOH$	158; ^a 170 ^b (H_2O)	19 ^c

^aCrystal structure data. ^bMonolayer data (subphase composition). ^cData estimated from Langmuir isotherms as displayed in the article.

Upon addition of $CaCl_2$, the Langmuir isotherm displays a parallel shift toward higher area-per-molecule values. The constant shape of the isotherms indicates a similar phase behaviour for both subphase compositions. The straight pressure increase over a comparatively large region of the molecular area suggests fluid properties of the condensed phase. On a pure aqueous subphase the pressure increase starts at $\sim 195 \text{ \AA}^2 \text{ molecule}^{-1}$ and on 10 mM $CaCl_2$ solution at $\sim 210 \text{ \AA}^2 \text{ molecule}^{-1}$.

The area per molecule of **1** in the monolayers is estimated from extrapolating the Langmuir isotherms toward zero pressure. The determined area values are listed in Table 2. In both cases, monolayer data are in excellent agreement with the surface area per molecule as determined from crystal structure analysis. On a subphase containing 10 mM $CaCl_2$, the molecular area of **1** shows a significant increase as compared to corresponding value of the monolayer if spread on pure water. We assume that this behaviour is due to electrostatic/coordinative interactions of Ca ions which cause the carboxylic acid residues of **1** to become deprotonated. Expansion effects of monolayers spread on metal ion-containing subphases, similar to those observed here, have been reported for several systems.¹⁸

The monolayer data obtained so far strongly indicate that the packing arrangements of molecules in the monolayer and in the crystal lattice are similar. The two-dimensional packing of the condensed monolayer phase is obviously determined by the bulky polar head group and not by the alkyl chains (for the latter case, much more complicated monolayer phase behavior should be observed).

A more refined examination of the monolayer phase diagram of **1**, including Brewster-angle microscopic investigations of film texture as a function of pH and subphase composition, is currently underway and will be presented elsewhere.²⁰

$CaCO_3$ crystallization underneath monolayers

Crystallization of calcium carbonate underneath monolayers of **1** leads to formation of uniformly oriented calcite single crystals at low compression ($\pi = 0.1$ – 0.5 mN m^{-1}), while more randomly oriented single crystals are obtained at higher surface pressure ($\pi = 5$ – 20 mN m^{-1}). Crystal growth is observed *in situ* by polarization (optical) microscopy (Fig. 9).

In order to determine the orientation of calcite crystals relative to the monolayer, X-ray powder diffraction (XRD) measurements were performed in reflection mode on polycrystalline film patches that were transferred onto glass cover slips. Film patches were examined by means of optical microscopy prior to XRD measurements, in order to ensure that the crystal orientations are preserved during film transfer.

The X-ray powder diffraction pattern (data not shown) of calcite crystals growing underneath monolayers of **1** at $\pi = 0.1 \text{ mN m}^{-1}$ is dominated by (012) reflections centered at $2\theta = 23.07^\circ$ (Cu- K_α) of the calcite crystal lattice,²¹ while (104) reflections at $2\theta = 29.42^\circ$, typical of calcite powder samples, are almost completely suppressed. This result indicates that the calcite (012) crystal planes are oriented parallel to the monolayer.

$CaCO_3$ crystals grown under monolayers of **1** show the

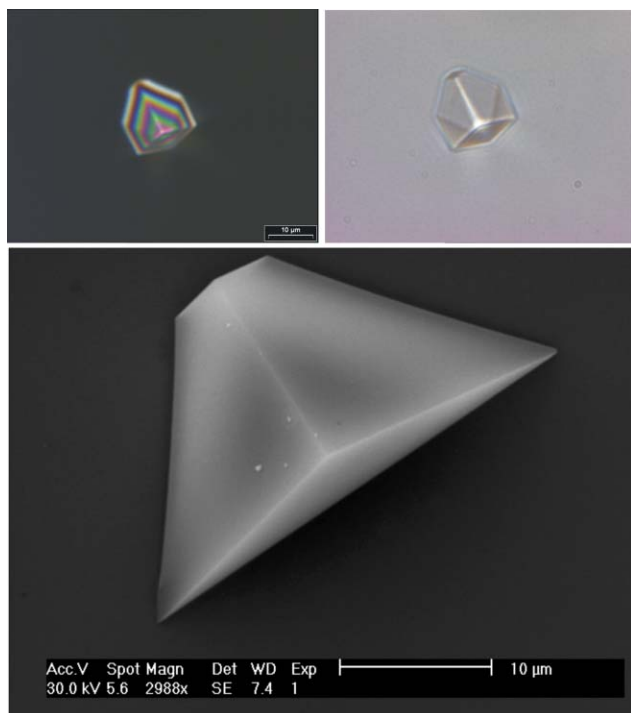


Fig. 9 Optical micrographs (crystals collected after 3 h) and scanning electron micrograph (crystals collected after 6 h) of (012) oriented calcite single crystals grown under a monolayer of **1** ($\pi = 0.1 \text{ mN m}^{-1}$, $[\text{Ca}(\text{HCO}_3)_2]_t = 0 = 9 \text{ mM}$).

characteristic shape of a (truncated) calcite {104} cleavage rhombohedron. The simple crystal morphology allows the determination of crystal orientation(s) from scanning electron micrographs (optical micrographs, respectively). A projection of rhombohedral faces onto the image plane of the micrograph yields characteristic interfacial angles, which can be assigned to the crystal's orientation. Thus, angle values determined from several micrographs such as those in Fig. 9 result in averages of about $152(2)^\circ$, $104(4)^\circ$, and $104(4)^\circ$ which are characteristic of (012) oriented calcite rhombohedra.⁵

Matrix-templated growth of calcite single crystals showing a preferential (012) orientation has been reported for other self-assembled systems, including polymeric Langmuir–Schaefer films of 10,12-pentacosadiynoic acid,^{3c} self-assembled monolayers of carboxylate-terminated alkanethiols supported on silver substrates,⁴ as well as hydrogen-bonded molecular ribbons consisting of *N,N'*-dioctadecyltriazine-2,4,6-triamine and a cyanuric acid derivative.^{3c} Much effort has been spent to correlate the periodicity of the calcite {012} cleavage plane with the putative monolayer structures. The polar {012} cleavage plane of calcite consists of separate layers of calcium and carbonate ions. Stabilization of this high-energy surface results from surface charge neutralization which most likely arises from coordination of anionic ligands, such as compound **1**, to the terminal (012) layer of Ca ions. However, the exact arrangement of ligands at the interface is hard to predict, considering the fact that the outward-bound Ca ions will become hydrated which should lead to considerable relaxation of their atomic positions.

It is hard to believe that the coincident growth of (012) oriented calcite crystals underneath monolayers of structurally dissimilar amphiphiles can be traced back to strict geometrical or even stereochemical matching of the two juxtaposed surfaces in all cases. We suggest that the epitaxy of calcite single crystals, which only occurs underneath monolayers of **1** at low surface pressure, is rather due to cooperative effects.²² According to this, the surfactant monolayer should not be regarded as a rigid template. It is more likely that macroscopic

materials properties such as average charge density or mean dipole moment of the templating monolayer determine the orientation of crystals. Our current investigations on oriented CaCO_3 crystal growth underneath monolayers of 5,11,17,23-tetrakis(1,1,3,3-tetramethylbutyl)-25,26,27,28-tetra(carboxymethoxy)calix[4]arene strongly support this hypothesis: in both cases, the (012) orientation of calcite crystals is prevailing.⁶

Summary

The crystal structures of *rccc*-5,11,17,23-tetracarboxy-4,6,10,12,16,18,22,24-octa-*O*-methyl-2,8,14,20-tetra(*n*-undecyl)-resorc[4]arene, **1**, as well as of its Ca salt, **2**, are analyzed in terms of the supramolecular packing arrangement of the constituting amphiphilic molecules. Both compounds form lamellar structures where the hydrophilic headgroups and the hydrophobic alkyl chains segregate into different layers. The packing arrangement of resorcarene moieties in both cases is governed by the sterically demanding macrocyclic headgroup. The *n*-undecyl chains of resorcarenes belonging to different layers are deeply interdigitated.

Monolayer experiments indicate that a similar packing arrangement can be predicted for monolayers of **1** spread at the air–water interface. The featureless Langmuir isotherms point to a liquid-condensed state of **1** throughout the investigated compression range.

CaCO_3 (calcite) single crystals grow underneath monolayers of **1** with highly uniform (012) orientation. This particular orientation is observed for a variety of structurally dissimilar monolayers, which leads us to conclude that macroscopic film properties such as average charge density or mean dipole moment have a decisive influence on templated calcite growth. Local supramolecular packing motifs are less important in those cases where calcite nucleation occurs at polar (highly charged) crystal faces.

Experimental

Synthesis

Melting points were determined on a Büchi B-540 apparatus and are uncorrected. IR spectra were recorded on a Perkin-Elmer 841 infrared spectrophotometer.

Synthesis of *rccc*-5,11,17,23-tetracarboxy-4,6,10,12,16,18,22,24-octa-*O*-methyl-2,8,14,20-tetra(*n*-undecyl)resorc[4]arene, **1**, will be described elsewhere.²⁰

Calcium complex of **1**:

$[\text{Ca}(\text{C}_{88}\text{H}_{126}\text{O}_{16})(\text{DMSO})_2(\text{H}_2\text{O})_2] \cdot \text{DMSO} \cdot (\text{H}_2\text{O})_4$, (**2**)

Compound **1** (34.8 mg, 0.025 mmol) was suspended in an aqueous solution of calcium acetate (8 mg, 0.05 mmol in 5 mL H_2O).

The suspension was treated ultrasonically and centrifuged. The remaining pellet was suspended with 5 mL water, treated ultrasonically and once again was centrifuged. The wet residue was dissolved in 10 mL dimethyl sulfoxide. Single crystals were grown by water vapor diffusion into the solution. Colourless plate-shaped crystals were obtained after 3 days.

Mp: 100°C . IR (KBr): $\bar{\nu} = 3431, 2922, 2852, 1726, 1577, 1469, 1423, 1381, 1275, 1236, 1188, 1096, 1009, 951, 719 \text{ cm}^{-1}$. Elemental analysis calcd. for $[\text{C}_{90}\text{H}_{156}\text{O}_{25}\text{S}_3\text{Ca}]$: C 61.82, H 8.93; found: C 62.95, H 9.99%.

Crystallography

X-Ray crystallographic data for *rccc*-5,11,17,23-tetracarboxy-4,6,10,12,16,18,22,24-octa-*O*-methyl-2,8,14,20-tetra(*n*-undecyl)-resorc[4]arene, **1.** A single crystal of **1** was removed from the mother liquor and immediately cooled to 183 K on a Bruker AXS SMART diffractometer (three circle goniometer with 1 K

CCD detector, Mo-K α radiation, graphite monochromator; hemisphere data collection in ω at 0.3° scan width in three runs with 606, 435 and 230 frames ($\Phi = 0, 88$ and 180°) at a detector distance of 5 cm). A total of 76378 reflections ($1.12 < \theta < 22.52^\circ$) were collected of which 24569 unique reflections ($R(\text{int}) = 0.0425$) were used. An empirical absorption correction using equivalent reflections was performed with the program SADABS.

Table 1 summarizes the crystallographic data and refinement parameters. The structure was solved by direct methods with the program SHELXS-97 and refined by full matrix least squares based on F^2 using SHELXL-97.²³ All hydrogen atoms were placed in calculated positions with the following parameters: $d(\text{C}_{\text{ar}}\text{-H}) = 0.95 \text{ \AA}$, $U(\text{H}) = 1.2 U_{\text{eq}}(\text{C})$; $d(\text{C}_{\text{methylene}}\text{-H}) = 0.99 \text{ \AA}$, $U(\text{H}) = 1.2 U_{\text{eq}}(\text{C})$; $d(\text{C}_{\text{methyl}}\text{-H}) = 0.98 \text{ \AA}$, $U(\text{H}) = 1.5 U_{\text{eq}}(\text{C})$; $d(\text{O-H}) = 0.84 \text{ \AA}$, $U(\text{H}) = 1.5 U_{\text{eq}}(\text{O})$.

X-Ray crystallographic data for [Ca(C₈₄H₁₂₆O₁₆)(DMSO)₂(H₂O)₂]-DMSO·(H₂O)₄, 2. Thin colourless crystal plates of **2** were grown from water vapor diffusion into a DMSO solution of **2** at room temperature.

A single crystal of **2** was removed from the mother liquor and immediately cooled to 183 K on a Bruker AXS SMART diffractometer (three circle goniometer with 1 K CCD detector, Mo-K α radiation, graphite monochromator; hemisphere data collection in ω at 0.3° scan width in four runs with 606, 500, 606 and 500 frames ($\Phi = 0, 88, 180$ and 268°) at a detector distance of 5 cm). A total of 45705 reflections ($1.47 < \theta < 25.01^\circ$) were collected of which 17813 unique reflections ($R(\text{int}) = 0.0488$) were used. An empirical absorption correction using equivalent reflections was performed with the program SADABS. Table 1 summarizes the crystallographic data and refinement parameters. The structure was solved by direct methods with the program SHELXS-97 and refined by full matrix least squares based on F^2 using SHELXL-97. All hydrogen atoms were placed in calculated positions (see above).

Monolayer experiments

Monolayer experiments were performed with a double-barrier NIMA trough using a compression speed of 15 cm² min⁻¹. The surface pressure of the monolayers was measured using a Wilhelmy plate. The surfactant was spread using a chloroform solution (10 μl , 0.6 mg mL⁻¹). Compression was started after 10 min.

CaCO₃ crystal growth experiments

Solutions of calcium bicarbonate were prepared by bubbling carbon dioxide gas through a stirred aqueous (Millipore, resistance 18.2 M Ω cm) solution of Ca(HCO₃)₂ (9 mM) for a period of 2 h. Compressed films were formed by adding known amounts of surfactant to generate a liquid- or solid-like film at the air-water interface. Crystals were studied after several times either *in situ* by optical (polarization) microscopy (Olympus IX 70) or on cover slips laid on the film. The cover slips were also mounted on scanning electron microscope (SEM) specimen tubs. A Phillips XL30 ESEM operating at 30 keV was used. Bulk samples for X-ray diffraction (XRD) were obtained by collecting the crystals on cover slips laid on the film and removed horizontally. A Philips PW 1050/70 X-ray powder diffractometer was employed (2θ scans, Bragg-Brentano para-focussing geometry) using CuK α radiation ($\lambda = 1.54 \text{ \AA}$).

Crystallographic indices are presented in three-index (hkl) notation, based on the hexagonal setting of the calcite unit cell ($R\bar{3}c$, $a = 4.96 \text{ \AA}$, $c = 17.002 \text{ \AA}$).

Acknowledgements

D. V. and M. F. thank the Deutsche Forschungsgemeinschaft (DFG) for financial support of their work (DFG grant Vo829/2-1). C. A. and J. M. are grateful to the DFG and the Fonds der Chemischen Industrie for financial support.

References

- (a) H. A. Lowenstam and S. Weiner, *On Biomineralization*, Oxford University Press, Oxford, 1989; (b) A. P. Wheeler and C. S. Sikes, in *Biomineralization*, ed. S. Mann, VCH, Weinheim, 1989, pp. 95–131; (c) S. Weiner and L. Addadi, *J. Mater. Chem.*, 1997, **7**, 689.
- S. Weiner and L. Addadi, in *Biomineralization*, ed. S. Mann, VCH, Weinheim, 1989, pp. 133–156.
- (a) S. Mann, B. R. Heywood, S. Rajam and J. D. Birchall, *Nature*, 1988, **334**, 692; (b) S. Rajam, B. R. Heywood, J. B. A. Walker, S. Mann, R. J. Davey and J. D. Birchall, *J. Chem. Soc., Faraday Trans.*, 1991, **87**, 727; (c) A. Berman, D. J. Ahn, A. Lio, M. Salmeron, A. Reichert and D. Charych, *Science*, 1995, **269**, 515; (d) G. Xu, N. Yao, I. A. Aksay and J. T. Groves, *J. Am. Chem. Soc.*, 1998, **120**, 11977; (e) S. Champ, J. A. Dickinson, P. S. Fallon, B. R. Heywood and M. Mascal, *Angew. Chem., Int. Ed.*, 2000, **39**, 2716; (f) P. J. J. A. Buijnsters, J. J. M. Donners, S. J. Hill, B. R. Heywood, R. J. M. Nolte, B. Zwanenburg and N. A. J. M. Sommerdijk, *Langmuir*, 2001, **17**, 3623.
- (a) J. Aizenberg, A. J. Black and G. M. Whitesides, *J. Am. Chem. Soc.*, 1999, **121**, 4500; (b) J. K  ther, G. Nelles, R. Seshadri, M. Schaub, H. J. Butt and W. Tremel, *Chem. Eur. J.*, 1998, **4**, 1834.
- D. D. Archibald, S. B. Qadri and B. P. Gaber, *Langmuir*, 1996, **12**, 538.
- D. Volkmer, M. Fricke, S. Siegel and D. Vollhardt, in preparation.
- (a) A. Bayer, *Ber. Dtsch. Chem. Ges.*, 1872, **5**, 25; (b) A. Bayer, *Ber. Dtsch. Chem. Ges.*, 1872, **5**, 280.
- (a) H. Erdtman, S. H  gberg, S. Abrahamsson and B. Nilsson, *Tetrahedron Lett.*, 1968, **14**, 1679; (b) B. Nilsson, *Acta Chem. Scand.*, 1968, **22**, 732.
- L. M. Tunstad, J. A. Tucker, E. Dalcanele, J. Weiser, J. A. Byrant, J. C. Sherman, R. C. Helgeson, C. B. Knobler and D. J. Cram, *J. Org. Chem.*, 1989, **54**, 1305.
- D. J. Cram, *Science*, 1983, **219**, 1177.
- (a) R. Moran, S. Karbach and D. J. Cram, *J. Am. Chem. Soc.*, 1982, **104**, 5826; (b) D. J. Cram, S. Karbach, Y. H. Kim, L. Baczynskyj and G. W. Kallemeyn, *J. Am. Chem. Soc.*, 1985, **107**, 2575; (c) D. J. Cram, S. Karbach, H. E. Kim, C. B. Knobler, E. F. Maverick, J. L. Ericson and R. C. Helgeson, *J. Am. Chem. Soc.*, 1988, **110**, 2229; (d) D. J. Cram, S. Karbach, Y. H. Kim, L. Baczynskyj, K. Marti, R. M. Sampson and G. W. Kallemeyn, *J. Am. Chem. Soc.*, 1988, **110**, 2554.
- Reviewed in: P. Timmerman, W. Verboom and D. N. Reinhoudt, *Tetrahedron*, 1996, **52**, 2663.
- (a) H. Adams, F. Davis and C. J. M. Stirling, *Chem. Commun.*, 1994, 2527; (b) F. Davis and C. J. M. Stirling, *J. Am. Chem. Soc.*, 1995, **117**, 10385.
- (a) L. R. MacGillivray and J. L. Atwood, *Nature*, 1997, **389**, 469; (b) L. R. MacGillivray and J. L. Atwood, *J. Am. Chem. Soc.*, 1997, **119**, 6931; (c) L. R. MacGillivray and J. L. Atwood, in *Crystal Engineering: From Molecules and Crystals to Materials*, NATO Science Series C: Mathematical and Physical Sciences, Vol. **538**, ed. D. Braga, F. Grepioni and A. G. Orpen, Kluwer, Dordrecht, 1999, pp. 407–419; (d) T. Gerkenmeier, W. Iwanek, C. Agena, R. Fr  hlich, S. Kotila, C. N  ther and J. Mattay, *Eur. J. Org. Chem.*, 1999, 2257; (e) T. Gerkenmeier, C. Agena, W. Iwanek, R. Fr  hlich, S. Kotila, C. N  ther and J. Mattay, *Z. Naturforsch. B Chem. Sci.*, 2001, **56**, 1063.
- H. Adams, F. Davis and C. J. M. Stirling, *Chem. Commun.*, 1994, 2527.
- HEFKUY: E. Benedetti, C. Pedone, R. Iacovino, B. Botta, G. Dellemonache, M. C. Derosa, M. Botta, F. Corelli, A. Tafi and A. Santini, *J. Chem. Res. S*, 1994, **12**, 476.
- POBCUE: S. Zahn, K. M  ller and G. Mann, *Z. Kristallogr.*, 1994, **209**, 470.
- (a) V. A. Arsentiev and J. Leja, in *Colloid and Interface Science*, Vol. **5**, ed. M. Kerker, Academic Press, New York, 1976, pp. 251–270; (b) G. T. Barnes, in *Colloid Science*, Vol. **2**, ed. D. H. Everett, Chemical Society, London, 1975, pp. 173–190.
- (a) D. E. Hibbs, M. B. Hursthouse, K. M. Abdul Malik, H. Adams, C. J. M. Stirling and F. Davis, *Acta Crystallogr., Sect. C*, 1998, **54**, 987;

- (b) Davis, A. J. Lucke, K. A. Smith and C. J. M. Stirling, *Langmuir*, 1998, **14**, 4180.
- 20 D. Volkmer, M. Fricke, C. Agena and J. Mattay, in preparation.
- 21 Joint Committee on Powder Diffraction Standards – International Center for Diffraction Data, Swarthmore, PA, USA, 1986; File No. 24-27 (calcite).
- 22 M. J. Lochhead, S. R. Letellier and V. Vogel, *J. Phys. Chem. B*, 1997, **101**, 10821–10827.
- 23 SHELXS/L/H, SADABS from G.M. Sheldrick, University of Göttingen, 1997.

DALTON

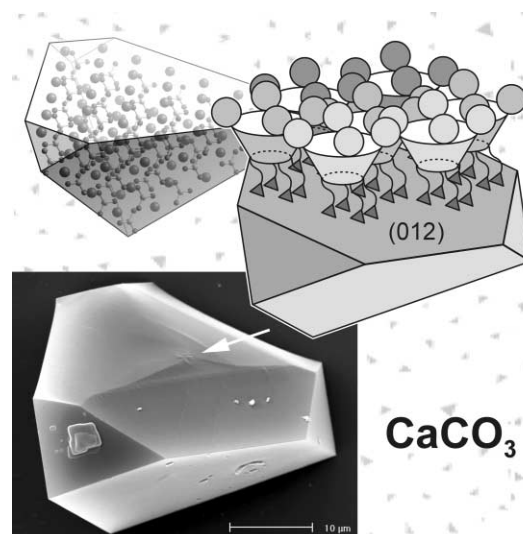
Incorporating *Acta Chemica Scandinavica*

An international journal of inorganic chemistry

CONTENTS



Chemical biology articles published in this journal also appear in the *Chemical Biology Virtual Journal*: www.rsc.org/chembiol

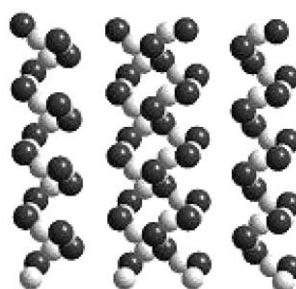


The cover picture shows different representations of a calcite (CaCO_3) single crystal which grows with uniform (012) orientation underneath the monolayer of an amphiphilic calix[4]arene derivative (Dirk Volkmer, Marc Fricke, Dieter Vollhardt and Stefan Siegel, *J. Chem. Soc., Dalton Trans.*, 2002, 4547-4554).

Dalton Communications

- 4527 **Synthesis and structure of a novel**
 ● open-framework zincophosphate with
 ■ intersecting three-dimensional helical channels

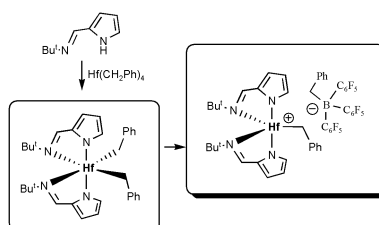
Zhi-En Lin, You-Wei Yao, Jie Zhang and Guo-Yu Yang



A new open-framework zincophosphate, $\text{Zn}_{0.5}(\text{H}_2\text{PO}_4) \cdot 0.5\text{H}_2\text{O}$, possessing intersecting three-dimensional helical channels, has been synthesized under solvothermal conditions. This is one of the least dense zincophosphates reported to date.

- 4529 **Efficient ethylene polymerisation**
 ● catalysis by a cationic benzyl hafnium
 ■ complex containing pyrrolide-imine ligands

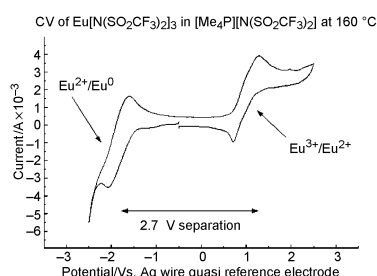
Shigekazu Matsui, Thomas P. Spaniol, Yukihiko Takagi, Yasunori Yoshida and Jun Okuda



A dibenzyl hafnium(IV) complex with pyrrolide-imine ligands and its cationic mono benzyl complex are described. The cationic complex exhibits high activity for ethylene polymerisation.

- 4532 **Group 15 quaternary alkyl bistriflimides: ionic liquids with potential application in electropositive metal deposition and as supporting electrolytes**

Anand I. Bhatt, Iain May, Vladimir A. Volkovich, Melissa E. Hetherington, Bob Lewin, Rob C. Thied and Nigar Ertok



Group 15 quaternary alkyl bistriflimide salts have very wide electrochemical windows (between +2.6 and -3.4 V) when used as supporting electrolytes in MeCN. They can also be used for the electrodeposition of very electropositive metals, including Eu, in the molten state.

Crystallization of (012) oriented calcite single crystals underneath monolayers of tetra(carboxymethoxy)calix[4]arenes †

Dirk Volkmer,^{*a} Marc Fricke,^a Dieter Vollhardt^b and Stefan Siegel^b

^a Faculty of Chemistry (AC1), University of Bielefeld, P.O. Box 100 131, D-33501 Bielefeld, Germany. E-mail: dirk.volkmer@uni-bielefeld.de

^b Max-Planck-Institute of Colloids and Interfaces, MPI-KG Golm, D-14424 Potsdam, Germany. E-mail: dieter.vollhardt@mpikg-golm.mpg.de

Received 16th July 2002, Accepted 24th October 2002

First published as an Advance Article on the web 8th November 2002

The amphiphilic 5,11,17,23-tetrakis(1,1,3,3-tetramethylbutyl)-25,26,27,28-tetra(carboxymethoxy)calix[4]arene, **1**, forms stable monolayers at the air–water interface which can be employed as supramolecular templates for induced calcite crystallization. Uniform, (012) oriented CaCO₃ (calcite) single crystals grow underneath monolayers of **1** at low compression ($\pi = 0.1\text{--}0.5\text{ mN m}^{-1}$), while more randomly oriented single crystals are obtained at higher surface pressure ($\pi = 5\text{--}20\text{ mN m}^{-1}$). The use of easy-to-synthesize calixarenes for this particular area of crystal engineering is reported here for the first time. A range of structural analysis methods is employed in order to obtain a refined picture of the structural factors that govern the growth of uniformly oriented calcite crystals underneath monolayers of **1**. Thus, the crystal structures of 5,11,17,23-tetrakis(1,1,3,3-tetramethylbutyl)-25,26,27,28-tetra(carboxymethoxy)-calix[4]arene, **1**, as well as of its Ca salt, **2**, were solved and analysed in terms of typical supramolecular packing arrangements and coordination motifs. The Langmuir isotherms point to a liquid-condensed state of the monolayers of **1** throughout the investigated compression range. Brewster angle microscopic observation of the monolayer morphology at low surface pressure reveals a highly viscous consistency, which does not change upon further compression. Grazing incidence X-ray diffraction (GIXD) investigations on the monolayer structure provide no indications for the occurrence of a two-dimensional lattice of the alkyl chains. Considering the non-crystalline, highly dynamic state of the monolayer during crystal maturation, an epitaxial correlation based on geometric matching of lattice positions between the monolayer and the overgrowing calcite crystals is ruled out. We, therefore, suggest that non-specific monolayer properties such as average charge density or mean dipole moment are the main determinants for templated calcite growth in the present and related cases.

Introduction

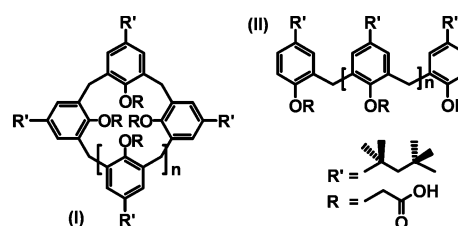
Much attention has been devoted to the characterization of mineral phases which occur in biominerals and calcified tissues.¹ Apart from aesthetically pleasant, intricate shapes, biominerals often possess attractive materials properties that attribute to a sophisticated internal hierarchical structure.² Among the many open questions, one of the most challenging scientific goals is to gain insights into the molecular interactions that occur at the interface between the inorganic mineral and the macromolecular organic matrix.

For the most widespread calcified tissues it is frequently assumed that a structurally rigid composite matrix consisting of fibrous proteins and thereon adsorbed acidic macromolecules acts as a supramolecular “blueprint” that templates nucleation of the inorganic phase.³

Efforts aimed at trying to mimic aspects of these complex interactions with simple model systems will help to improve our understanding of crystallization processes that are under biological control. However, the deliberate design of interface architectures that direct the crystal nucleation and growth of inorganic crystal phases in a predictable manner is by and large still a matter of trial and error. Chemists have employed different experimental set-ups to create highly-ordered template surfaces, including Langmuir monolayers,⁴ or self-assembled monolayers (SAMs).⁵ In particular, the crystallization of inorganic compounds underneath free floating monolayers of

amphiphilic molecules bears much development potential, since the surface properties may be adjusted by a suitable surfactant design as well as by simple experimental parameters (*i.e.* sub-phase composition, surface area per molecule, or temperature).

We have initiated a research project which focuses on induced CaCO₃ crystallization underneath Langmuir monolayers of amphiphilic oligoacids. The envisaged molecular library (Scheme 1) consists of macrocyclic oligo(2-carboxymethoxy-5-



Scheme 1

(alkyl)-1,3-phenyl)methylene derivatives (I) (“calix[*n*]arenes”) and their open-chain derivatives (II).

Employing macrocyclic amphiphiles we would like to address the rather fundamental question concerning the putative structure of crystal nucleation sites in calcified tissues. Investigations on the amino acid composition of different natural proteins associated with biomineralisation reveal sequence motifs which are particularly rich in aspartic and glutamic acid residues, respectively.⁶ Unfortunately, none of the acidic proteins extracted from calcified tissues have yet been grown into single crystals suitable for X-ray crystallographic investigations and thus three-dimensional structures are currently

† Electronic supplementary information (ESI) available: synthesis and characterization details and atom numbering schemes for **1** and **2**. See <http://www.rsc.org/suppdata/dt/b2/b206912a/>

not available. However, a representative structural model of a mineral/peptide interface architecture may be derived from the iron storage protein (ferritin) which is regarded as an archetypal biological model for the formation of a nanocrystalline mineral phase within a confined space.⁷ Here, the ferritin L-chain subunit bears four suitably aligned glutamic acid residues that are necessary for mineral formation. Artificial organic molecules can be designed so as to mimic the confined arrangement of acidic residues in natural proteins. Macrocyclic calix[*n*]arenes such as (**1**) are especially suited for this purpose since they are synthetically readily available. These molecules form confined arrays of co-aligned carboxylic acid groups, the number and relative positions of which show systematic structural variations depending on the size of the macrocyclic backbone. Previous studies on calcium carbonate crystallization underneath surfactant monolayers have not addressed the particular question of whether or not *single template molecules* can induce crystal nucleation. However, related investigations have been reported recently, focussing on the *minimum size of segregated hydroxyl domains* in mixed Langmuir films for inducing ice nucleation.⁸

Here we present the first results on induced crystallization of calcium carbonate underneath monolayers of one member of the molecular library of amphiphilic oligoacids (Scheme 1), namely 5,11,17,23-tetrakis(1,1,3,3-tetramethylbutyl)-25,26,27,28-tetra(carboxymethoxy)calix[4]arene, **1**. The crystal structures of the free acid and its Ca salt **2** are investigated by means of single crystal X-ray crystallography. Monolayers of **1** are spread on aqueous subphases and the resulting isotherms are analysed in terms of possible supramolecular packing arrangements. The dynamic macroscopic monolayer structure is characterized by means of Brewster angle microscopy (BAM) and grazing incidence X-ray diffraction (GIXD). The growth of uniformly (012) oriented calcite (CaCO₃) single crystals underneath monolayers of **1** is monitored *in situ* by (polarization) optical microscopy. The orientation of calcite crystals relative to the monolayer is determined by means of X-ray diffraction, scanning electron microscopy and optical microscopy.

Results and discussion

NMR spectroscopy

The ¹H-NMR spectra of **1** in CDCl₃ solution show the characteristic doublet splitting of the CH₂ resonance signal ($\delta = 4.59$ and 3.25, ²*J* = 7.1 Hz) of the macrocyclic methylene protons, which shows that there is no interconversion between the main four calix[4]arene conformers.⁹ The 1,1,3,3-tetramethylbutyl resonance signals (and the carboxymethoxy substituents, respectively) on the other hand display sharp singlet signals indicating a high rotational flexibility of the pendant calixarene substituents.

The ¹H- and ¹³C-NMR spectra of **2** in CDCl₃ solution show characteristic chemical shifts which are indicative of metal complex formation.¹⁰ In the ¹H-NMR spectrum of **2**, the aromatic protons display a downfield shift as compared to the resonance signal of the non-coordinated calixarene ligand **1**. The separation of the CH₂ resonance signal ($\delta = 4.27$ and 3.35, ²*J* = 12.3 Hz) of the macrocyclic methylene protons decreases while the CH₂ resonance signal of the carboxymethoxy substituents splits into a doublet of doublets ($\delta = 5.10$ and 3.96, ²*J* = 14.3 Hz).

X-Ray crystallographic investigations

Structural analyses of calixarenes comprising the sterically demanding 1,1,3,3-tetramethylbutyl group are rare. A search of the Cambridge structural database (October 2002) yielded a total of four X-ray structures.¹¹ The X-ray crystallographic investigations on single crystals of 5,11,17,23-tetrakis(1,1,3,3-tetramethylbutyl)-25,26,27,28-tetra(carboxymethoxy)calix[4]-

arene and its Ca salt presented here are the first examples of a metal-free calix[*n*]arene acid and its corresponding Ca complex.

Crystal structure of 1. Single crystals of the compound C₆₈H₉₆O₁₂·4.75CH₃OH·0.25H₂O (**1**) were obtained from a methanol solution containing 10% of water. The X-ray structure analysis shows that the calix[4]arene molecules adapt a highly symmetrical cone-conformation where the hydrophobic *para*-substituents are placed at stereochemically equivalent positions (Fig. 1a). Due to crystal packing effects the

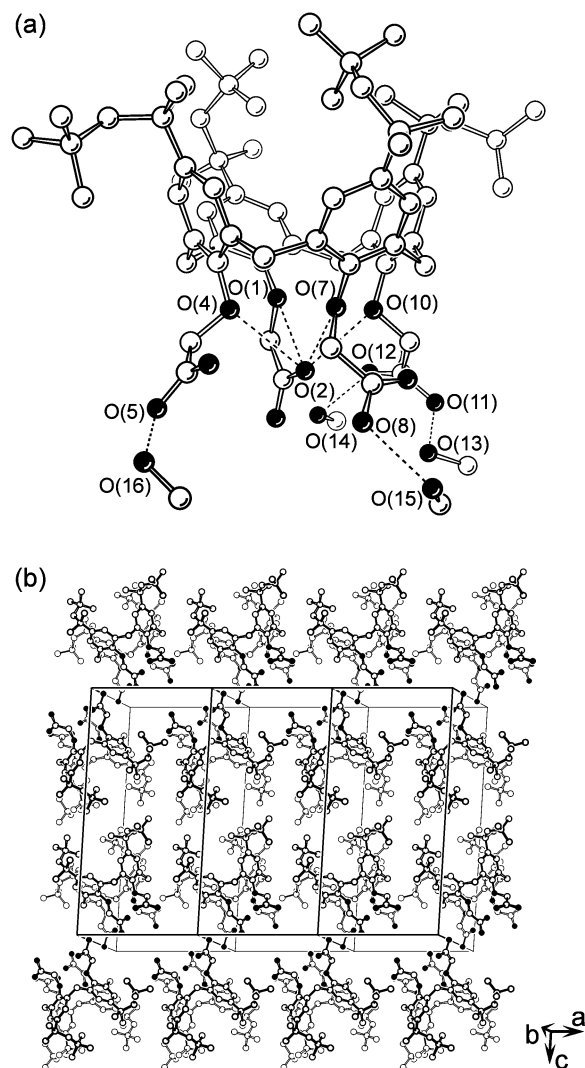


Fig. 1 (a) Ball-and-stick model of the molecular structure of **1** (hydrogen atoms are omitted for clarity). The atomic numbering scheme indicates those oxygen pairs which form strong hydrogen bonds. Non-bonding (intramolecular) oxygen–oxygen distances: O(2) ··· O(1) 2.638(1), O(2) ··· O(4) 3.060(2), O(2) ··· O(7) 2.811(2), O(2) ··· O(10) 2.845(1) Å. Closest (intermolecular) oxygen–oxygen distances between carboxylic acid groups and crystal methanol molecules: O(5) ··· O(16) 2.622(1), O(8) ··· O(15) 2.589(1), O(11) ··· O(13) 2.553(2), O(12) ··· O(14) 2.767(1) Å. (b) Ball-and-stick model of the supramolecular packing arrangement of **1** in the crystal lattice (methanol molecules and hydrogen atoms are omitted for clarity).

calixarene moiety differs significantly from idealized *C*_{4v} point symmetry. First, the 1,1,3,3-tetramethylbutyl groups become irregularly placed such that two of them point inside the calixarene cavity, while the neighbouring hydrophobic residues are bent outwards. As a consequence, no further molecular guests are located within the internal cavities of **1** or **2**, in contrast to host–guest inclusion phenomena frequently observed in conjunction with structurally similar *tert*-butylcalix[4]arene hosts.¹² This structural behaviour seems rather typical for

calix[4]arene molecules containing the sterically demanding 1,1,3,3-tetramethylbutyl substituent, since similar arrangements are found in the crystal structures of 5,11,17,23-tetrakis(1,1,3,3-tetramethylbutyl)-25,26,27,28-tetrahydroxycalix(4)arene,¹³ and of *exo-endo*-25,26,27,28-bis(*n*-butoxyphosphoryl)-5,11,17,23-tetrakis(1,1,3,3-tetramethylbutyl)calix(4)arene, respectively.¹⁴

As a second distinctive feature, the molecular structure of **1** shows four intramolecular hydrogen bonds of the acidic proton bound to O(2) and the phenolic oxygens O(1), O(4), O(7) and O(10) (Fig. 1a). The residual acidic protons form strong intermolecular hydrogen bonds with solvent (methanol) molecules occluded in the crystal lattice. There are no direct intermolecular hydrogen bonds between neighbouring calixarene acids, in contrast to the frequently observed formation of carboxylic acid dimers.¹⁵

Compound **1** forms a lamellar structure where the hydrophilic constituents (carboxylic acid residues, crystal methanol solvate) and the hydrophobic residues segregate into different layers. This supramolecular packing arrangement is reminiscent of the bilayer structural motif of membrane forming biogenic lipids and likewise amphiphilic molecules.¹⁶ The bilayers run parallel to the crystallographic *ab*-plane and layer stacking follows the *c*-direction (Fig. 1b). Within the layer, calixarene molecules are close packed with their pseudo C_{4v} symmetry axis being tilted by 24° against the *ab*-plane normal. The average surface area occupied by a single calixarene molecule in the crystal structure of **1** amounts to 1.51 nm².

The formation of a planar bilayer is surprising at first, since a close packing of conically shaped amphiphilic molecules should introduce a certain degree of curvature into the interfacial region. However, a calculation of the packing parameter according to Israelachvili *et al.*¹⁷ yields a value close to unity taking the spatial requirements of the methanol molecules into account, which form intermolecular hydrogen bonds with the carboxylic acid headgroups.

Crystal structure of 2. Single crystals of the Ca complex **2** were obtained by slow recrystallization of the crude product from DMSO–H₂O mixtures (5 : 1) held at 98 °C. The X-ray structure analysis once again confirms that the calixarene ligands possess a cone conformation (Fig. 2). The Ca complex may be formally described as a coordination polymer with the sum formula $1/n[\text{Ca}(\text{C}_{68}\text{H}_{92}\text{O}_{12}\text{Ca})(\text{H}_2\text{O})_2(\text{DMSO})\text{Ca}(\text{C}_{68}\text{H}_{92}\text{O}_{12}\text{Ca})(\text{DMSO})_3]_n \cdot 5\text{DMSO}$. Apparently, a 1 : 1 complex of a single Ca ion and the octadentate calixarene ligand forms at the beginning, which possesses a two-fold net negative charge under the chosen reaction conditions (excess of Ca(OH)₂). The non-coordinated carboxylic acid oxygen donors of each mononuclear $[\text{C}_{68}\text{H}_{92}\text{O}_{12}\text{Ca}]^{2-}$ building block can then bind to excess “free” calcium ions in solution to build up a coordination polymer.

The coordination environments of Ca ions in the crystal structure of **2** are quite different: The Ca ions (Ca(1), Ca(2), Fig. 2) sequestered by the calixarene ligand **2** are eight-fold coordinated. The square planes spanned by the phenolic and the carboxylate oxygen donors, respectively, are rotated by 35° against each other. Therefore, the Ca coordination polyhedron may be described as an intermediate form between a square antiprism and a cube. In contrast, the bridging Ca ions (Ca(3), Ca(4)) are in distorted octahedral coordination environments where each Ca ion is coordinated by three monodentate oxygen donors of different calixarene ligands. The coordination environment of Ca(3) is completed by two water ligands and a further oxygen donor of a monodentate DMSO ligand, whereas Ca(4) is further coordinated by three oxygen donors stemming from distinct DMSO ligands.

Due to the stoichiometric (2 : 1) ratio of Ca ions and (deprotonated) calixarene ligands, electrostatically neutral, one-dimensional coordination polymers form which have a dumb-bell shape in cross-sectional view (Fig. 3, left). The

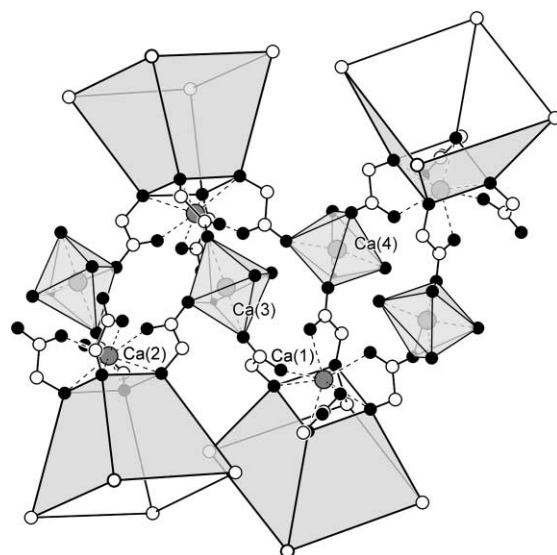


Fig. 2 Simplified representation of the coordination scheme of **2** (coordination polyhedrons are displayed for interconnecting Ca ions only). Selected Ca–O bond lengths and closest Ca ⋯ Ca non-bonding distances: Ca(1)–O(1) 2.487(2), Ca(1)–O(2) 2.367(2), Ca(1)–O(4) 2.510(2), Ca(1)–O(5) 2.394(3), Ca(1)–O(7) 2.530(2), Ca(1)–O(8) 2.371(2), Ca(1)–O(10) 2.549(2), Ca(1)–O(11) 2.349(2), Ca(2)–O(13) 2.522(2), Ca(2)–O(14) 2.370(2), Ca(2)–O(16) 2.579(2), Ca(2)–O(17) 2.386(2), Ca(2)–O(19) 2.575(2), Ca(2)–O(20) 2.364(2), Ca(2)–O(22) 2.532(2), Ca(2)–O(23) 2.347(2), Ca(3)–O(12) 2.341(2), Ca(3)–O(15) 2.283(2), Ca(3)–O(18) 2.401(2), Ca(3)–O(25) 2.395(3), Ca(3)–O(26) 2.397(3), Ca(3)–O(27) 2.277(3), Ca(4)–O(6) 2.311(3), Ca(4)–O(9) 2.264(3), Ca(4)–O(21) 2.297(3), Ca(4)–O(28) 2.351(3), Ca(4)–O(29) 2.409(6), Ca(4)–O(31) 2.338(6); Ca(1) ⋯ Ca(3) 6.051(2), Ca(1) ⋯ Ca(4) 6.511(2), Ca(2) ⋯ Ca(3) 5.425(2), Ca(2) ⋯ Ca(4) 6.496(2), Ca(3) ⋯ Ca(4) 6.542(2) Å.

coordination strands run in the *b* direction of the crystal lattice. There are no coordinative bonds between coordination strands next to each other, which may explain the high solubility of the complex in non-polar aprotic solvents (*e.g.* trichloromethane). The voids in the packing of coordination strands are filled with (non-coordinated) DMSO molecules. In analogy to the lamellar arrangement of the calixarene moieties in the crystal structure of **1**, compound **2** forms a bilayer structure where the polar functional groups and the hydrophobic residues segregate into different layers. Each bilayer runs parallel to the *ab* crystal plane while distinct bilayers are stacked along the *c* direction (Fig. 3, right). Within the layer, calixarene molecules are close packed with their pseudo C_4 symmetry axis tilted by 24° (34°, respectively) against the *ab*-plane normal. The average surface area occupied by a single calixarene molecule in **2** amounts to 1.70 nm².

From the crystal structure analysis important packing parameters can be extracted and compared to the results from Langmuir monolayer investigations.

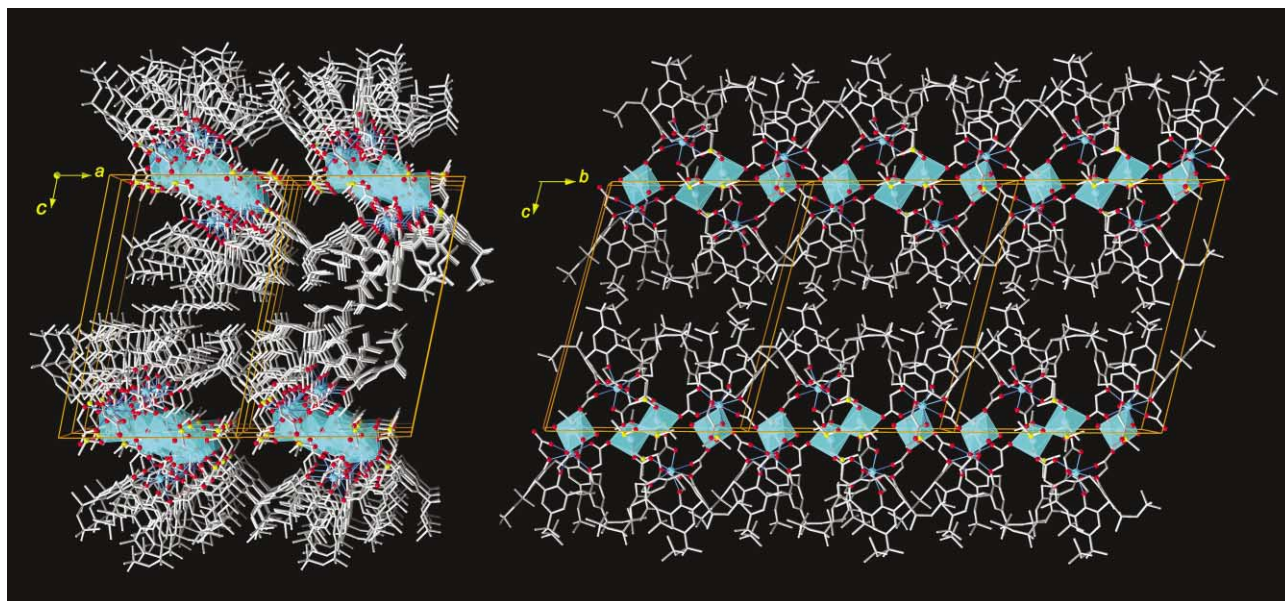
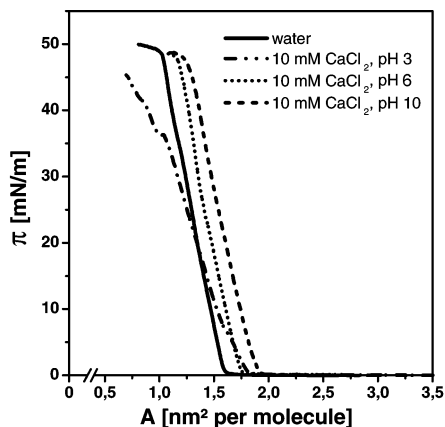
Monolayer studies

Crystallographic investigations on the solid state structure of the amphiphilic calixarene **1**, and its Ca salt, **2**, were complemented by monolayer studies. An advantage of the monolayer technique using a film balance is that characteristic features of the monolayer, *e.g.* surface pressure, macroscopic texture and lattice structure, can be studied as a function of area per molecule. The surface pressure–area (π –*A*) isotherms provide information on the thermodynamics and the phase behaviour of the monolayer. Fig. 4 shows the π –*A* isotherms of compound **1** monolayers spread on aqueous subphases of different compositions (pure water, and 10 mM CaCl₂ at different pH values). In all cases, stable monolayers form which collapse upon compression at a surface pressure of ~50 mN m⁻¹. Upon addition of CaCl₂, the Langmuir isotherm displays a parallel shift toward higher areas per molecule which is more

Table 1 Area per molecule of (1,1,3,3-tetramethylbutyl)calix[4]arene derivatives as determined from crystal data and Langmuir isotherms

Compound	Area per molecule/nm ²		Inclination angle ^a /°	Ref.
	Crystal structure	Monolayer		
1	1.51	1.45–1.50 (H ₂ O)	24	This work
2	1.70	1.55–1.60 (10 mM CaCl ₂)	34, 24 ^b	This work
C ₆₀ H ₈₈ O ₄ ·C ₇ H ₈	2.25	n.d.	0	11

^a Angle between the pseudo C₄ symmetry axis of the calixarene molecule and the plane normal of the crystallographic *ab* plane. ^b Two symmetry-independent calixarene molecules per asymmetric unit.

**Fig. 3** Wire models of the coordination polymer **2** showing the packing arrangement of the one-dimensional polymeric strands in the crystal lattice. (Solvent DMSO molecules occluded in the crystal lattice and hydrogen atoms are omitted for clarity. Coordination polyhedrons are displayed for interconnecting Ca ions only).**Fig. 4** Surface pressure–area (π – A) isotherms of monolayers of **1** at 24 °C on H₂O, and aqueous 10 mM CaCl₂ at different pH values.

pronounced at high pH values. The constant shape of the isotherms indicates a similar phase behaviour for all subphase compositions. The straight pressure increase over a comparatively large region of the molecular area suggests fluid properties for the condensed phase. On a pure aqueous subphase the pressure increase starts at ~ 1.65 nm² molecule⁻¹ and on a 10 mM CaCl₂ solution at ~ 1.75 nm² molecule⁻¹.

The area per molecule of **1** in the monolayers is estimated from extrapolating the Langmuir isotherms toward zero pressure. The determined area values are listed in Table 1. In both cases, monolayer data are in excellent agreement with the surface area per molecule as determined from crystal structure analysis. On a subphase containing 10 mM CaCl₂ at pH 10, the molecular area of **1** shows a significant increase as compared to the corresponding value of the monolayer if spread on pure

water. We assume that this behaviour is due to electrostatic/coordinative interactions of Ca ions which cause the carboxylic acid residues of **1** to become deprotonated. Expansion effects of monolayers spread on metal ion-containing subphases, similar to those observed here, have been reported for several systems.¹⁸ The expansion effect is still seen to some extent at pH 3, where deprotonation of the carboxylic acid residues and coordination of Ca ions is expected to be minimal. This observation suggests that formation of a diffuse adsorption layer of Ca ions beneath the monolayer adds to this effect, since adsorption in the interfacial region could lead to a surface pressure rise in accordance with the Gibbs and Langmuir adsorption equation.¹⁹

The monolayer data show that the packing density of molecules in the monolayer is similar to the density of molecules in the *ab* crystallographic planes of the crystal lattices of **1** and **2**, respectively. However, the featureless compression isotherms point to the fact that the arrangement of molecules in the monolayer is lacking long-range order. The two-dimensional packing of the condensed monolayer phase is obviously determined by the polar head group and not by the alkyl chains (for the latter case, a much more complicated monolayer phase behaviour should be observed). This is in agreement with preliminary results of grazing incidence X-ray diffraction (GIXD) studies which provide information on the packing of the alkyl chains. The measurements revealed that no alkyl chain lattice exists in the condensed monolayer phase.

BAM images of the monolayer of **1** spread on pure water and on a CaCl₂ containing aqueous subphase (pH 10), respectively, show that already at zero pressure the fluid-like condensed phase is formed. Both monolayer systems show special features if compared to other amphiphilic monolayers,²⁰ namely at the beginning, the condensed and gaseous phase are separated by

straight interfaces. A slight compression to a low surface pressure (0.1 mN m^{-1}) causes the condensed phase to grow into the gaseous phase in the form of irregular out-turnings which branch increasingly and transform into foam-like textures (Fig. 5). Upon further compression, a homogeneous condensed

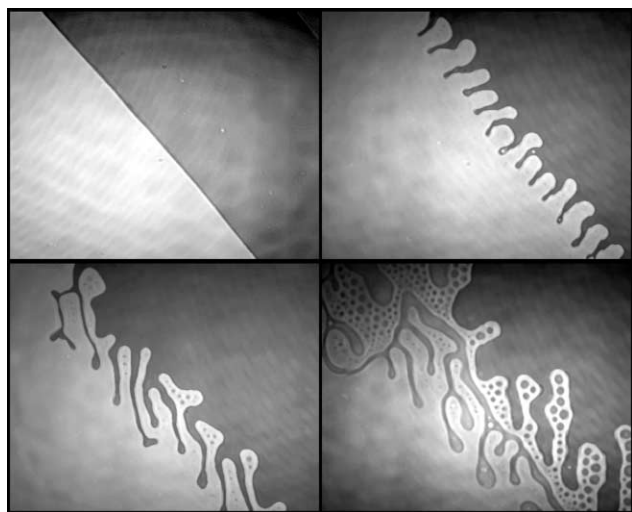


Fig. 5 BAM micrographs of monolayers of **1** at $24 \text{ }^\circ\text{C}$ on 10 mM CaCl_2 . Monolayer domains appear as light regions. All micrographs were recorded at identical surface pressure ($\pi = 0.1 \text{ mN m}^{-1}$) within a period of 5 minutes. (Scanned image area: $450 \times 400 \text{ }\mu\text{m}$).

phase immediately forms at low surface pressure ($>1 \text{ mN m}^{-1}$) which does not show optical anisotropic changes during further pressure increases (BAM image not shown). The phase region which displays the irregular coexistence of the fluid condensed and the gaseous monolayer phase ($\pi \approx 0.1 \text{ mN m}^{-1}$) provides optimal conditions for the growth of uniformly oriented calcite single-crystals. The area per molecule at $\pi \approx 0.1 \text{ mN m}^{-1}$ amounts to $1.70\text{--}1.80 \text{ nm}^2 \text{ molecule}^{-1}$ which is in good agreement with the cross-sectional molecular area of compound **2** ($1.70 \text{ nm}^2 \text{ molecule}^{-1}$) as calculated from the crystal data.

CaCO₃ crystallization underneath monolayers

Crystallization of calcium carbonate underneath monolayers of **1** leads to formation of uniformly oriented calcite single crystals at low compression ($\pi = 0.1\text{--}0.5 \text{ mN m}^{-1}$), while more randomly oriented single crystals with comparable nucleation density are obtained at higher surface pressure ($\pi = 5\text{--}20 \text{ mN m}^{-1}$).²¹ Crystal growth is observed *in situ* by (polarization) optical microscopy (Fig. 6).

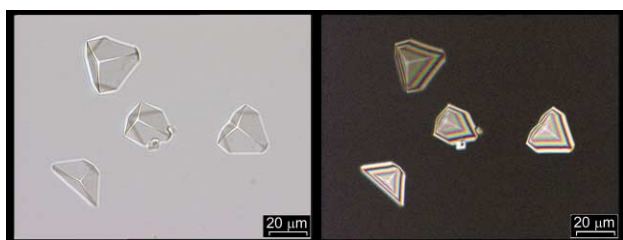


Fig. 6 Left: optical micrograph (brightfield) of (012) oriented calcite single crystals grown under a monolayer of **1** after 3 h. ($\pi = 0.1 \text{ mN m}^{-1}$, $[\text{Ca}(\text{HCO}_3)_2]_0 = 9 \text{ mM}$). Right: Same crystal specimen observed in plane polarized light. (The viewing direction is parallel to the monolayer surface normal, crystals are observed from below the aqueous subphase).

CaCO₃ crystals grown under monolayers of **1** show the characteristic shape of a (truncated) calcite {104} cleavage rhombohedron. The simple crystal morphology allows determination of crystal orientation(s) from scanning electron micrographs (optical micrographs, respectively). A projection

of rhombohedral faces onto the image plane of the micrograph yields characteristic interfacial angles, which can be assigned to the crystal's orientation. Thus, angle values determined from several micrographs such as those in Figs. 6 or 7 (left) result in

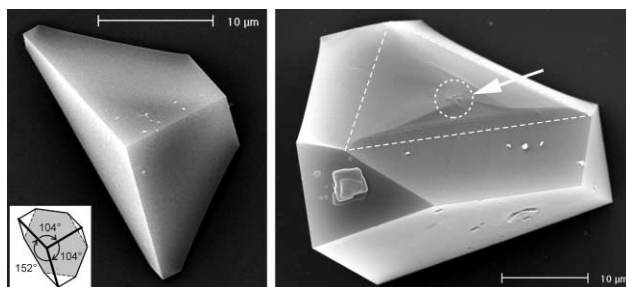


Fig. 7 Left: Scanning electron micrograph (crystals collected after 6 h) of (012) oriented calcite single crystals grown under a monolayer of **1**. ($\pi = 0.1 \text{ mN m}^{-1}$, $[\text{Ca}(\text{HCO}_3)_2]_0 = 9 \text{ mM}$). The inset shows the scheme of characteristic interfacial angles gleaned from the projection of {104} rhombohedral faces of a (012) oriented calcite single crystal onto the image plane of the micrograph. Right: Same crystal specimen observed from the opposite direction. The intercepted line in the micrograph indicates the region of the calcite (012) growth plane which attaches to the monolayer. The white arrow and the circle highlight a central elevated feature in the (012) growth plane, which is common to all crystals that were grown beneath the monolayer.

averages of about $152(\pm 2)$, $104(\pm 4)$, and $104(\pm 4)^\circ$ which are characteristic of (012) oriented calcite rhombohedra.^{5c} The (012) plane of calcite single crystals grown underneath monolayers of **1** show distinctive morphological features as presented in Fig. 7 (right side). The white arrow in the electron micrograph indicates the region of the calcite (012) growth plane which attaches to the monolayer during the initial stage of crystal growth. It is seen that the growth plane contains a central elevated feature of irregular morphology (Fig. 7, white circle), which develops into a rough crystal face (Fig. 7, white intercepted line) upon crystal maturation. The fact that the growth plane shows terraces and (microscopic) growth steps which are clearly distinguishable is presumably due to the fact that the crystals become detached from the monolayer due to gravitational forces. Unfortunately, investigations concentrating on the early steps of crystal nucleation, that might help to explain the appearance of the central elevated feature, are less than straightforward. Investigations are underway to examine the morphologically distinguishable regions of the calcite crystal growth planes by means of atomic force microscopy. Clearly, more experimental evidence is needed to characterize the likely mechanisms of crystal nucleation and growth that are operative underneath surfactant monolayers.

Further assignment of the preferential growth direction is gleaned from X-ray powder diffraction (XRPD) measurements in reflection mode on polycrystalline film patches that were transferred onto glass cover slips. Film patches were examined by means of optical microscopy prior to XRPD measurements, in order to ensure that the crystal orientations were preserved during film transfer.

The X-ray powder diffraction pattern of calcite crystals grown underneath monolayers of **1** at $\pi = 0.1 \text{ mN m}^{-1}$ is dominated by (012) reflections centered at $2\theta = 23.07^\circ$ (Cu-K α) of the calcite crystal lattice,²² while (104) reflections at $2\theta = 29.42^\circ$, typical of calcite powder samples, are almost completely suppressed (Fig. 8, line (a)). The residual diffraction intensity corresponding to (104) reflections presumably arises from calcite single crystals which have grown spontaneously at the air–water interface. For comparison, crystal growth experiments were repeated under identical experimental conditions but in the absence of a surface monolayer and the resulting film of calcite crystals floating at the air–water interface was transferred onto a glass cover slip. The corresponding diffrac-

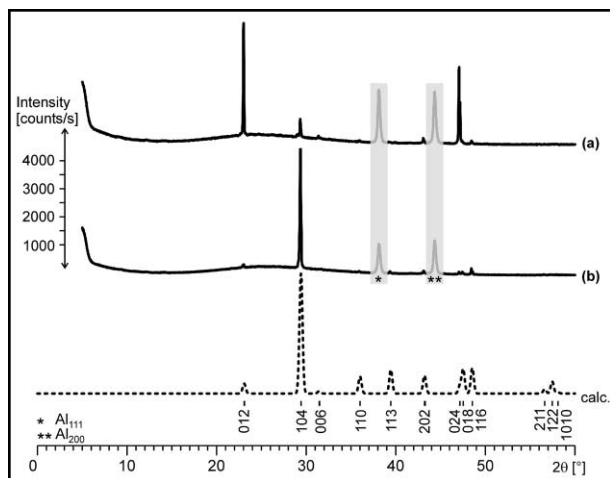


Fig. 8 X-Ray powder diffraction pattern of calcite crystals grown underneath a monolayer of **1** (a, $\pi = 0.1 \text{ mN m}^{-1}$), and at the air–water interface without monolayer (b). The dashed line represents the calculated diffraction pattern of randomly oriented calcite crystals. (Peaks marked with an asterisk correspond to the (111) and (200) Al reflections of the aluminium supports).

tion pattern reveals exclusive (104) orientation of calcite single crystals (Fig. 8, line (b)), which is expected for a loose collection of calcite single crystals being deposited onto one of the symmetry equivalent {104} faces during film transfer.

The crystal morphology and the diffraction data unequivocally demonstrate that monolayers of **1** exert a pronounced template effect on the growth of calcite single crystals. The crystals show a uniform (012) orientation with the corresponding {012} crystal faces being juxtaposed to the monolayer. The polar {012} cleavage plane of calcite consists of separate layers of Ca and carbonate ions. Stabilization of this high-energy surface results from surface charge neutralization which most likely arises from coordination of anionic ligands, such as compound **1**, to the terminal (012) layer of Ca ions.

In order to examine a possible geometric correlation between the monolayer of **1** and the calcite {012} cleavage plane, the *ab* lattice plane of Ca complex **2** is considered here as a model of the average packing arrangement of calixarene molecules in the monolayer, since the calculated packing density of calixarene molecules in this particular lattice plane (Fig. 3) equals the experimentally determined density of the monolayer (Table 1). In Fig. 9, the crystallographic positions of interconnecting Ca ions (Ca(3), Ca(4), Fig. 2) in the crystal structure of **2** are drawn as an overlay of the Ca ion position in the calcite {012} cleavage plane. Apparently, a loose geometric correlation exists between the basis vectors of the two different lattice planes (Fig. 9(a)), while the individual matching of Ca lattice positions further improves if unidirectional lattice rows of **2** are projected onto the calcite lattice (Fig. 9(b)). However, in both cases the exact arrangement of calixarene ligands at the interface is hard to predict, considering the fact that the outward-bound Ca ions of the calcite {012} cleavage plane will become hydrated which should lead to considerable relaxation of their atomic positions. The basis vectors of the calcite {012} cleavage plane span a primitive cell ($a = b = 4.048 \text{ \AA}$, $\gamma = 76.07^\circ$) with an area $A = 15.904 \text{ \AA}^2$. The surface charge density thus amounts to $\sigma = +0.1258 \text{ \AA}^{-2}$ which is about an order of magnitude higher than the surface charge density calculated for the *ab* crystallographic plane of **2** ($\sigma = -0.0235 \text{ \AA}^{-2}$).²³ This calculation immediately demonstrates that the interface between the calixarene monolayer and the overgrown calcite {012} cleavage plane must contain additional anionic species in order to balance the total amount of charges between the two juxtaposed surfaces. Taking into account that the density of surface hydroxyl and carbonate groups on calcite crystals increases with pH,²⁴ we have to consider hydroxide and carbonate ions being

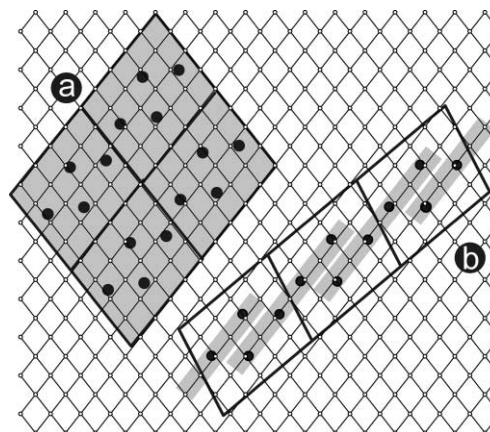


Fig. 9 Schematic representation of geometric correlations between the *ab* plane of the crystal lattice of **2** and the calcite {012} cleavage plane. (a): geometric correlation between the basis vectors of the two different lattice planes; (b): matching of Ca lattice positions at unidirectional lattice rows. (Ca ion positions in the lattice of **2** are represented by black circles while those of the calcite lattice are indicated by smaller white circles).

coordinated to Ca ions of the calcite {012} cleavage plane. Unfortunately, there are no empirical or theoretical studies currently available that focus on the equilibrium structure of this particular calcite cleavage plane,²⁵ which could serve as a starting point for the construction of atomically refined interface models.

With the crystallographic information presented here on amphiphilic calixarene **1** and its corresponding Ca salt **2**, respectively, molecular dynamics simulations of surfactant monolayer patches attaching to particular (reconstructed) crystal surfaces should become feasible and efforts in this direction are currently underway.

Matrix-templated growth of calcite single crystals showing a preferential (012) orientation has been reported for other self-assembled systems, including polymeric Langmuir–Schaefer films of 10,12-pentacosadiynoic acid,^{46,26} self-assembled monolayers of carboxylate-terminated alkanethiols supported on Ag^{5a} or Au substrates,²⁷ as well as hydrogen-bonded molecular ribbons consisting of *N,N'*-dioctadecyltriazine-2,4,6-triamine and a cyanuric acid derivative.⁴⁶ Much effort has been spent on correlating the periodicity of the calcite {012} cleavage plane with the proposed monolayer structures (although experimental evidence such as crystallographic investigations on principal surfactant packing arrangements and Ca ion coordination motifs were not presented). However, it is hard to believe that the coincident growth of (012) oriented calcite crystals underneath monolayers of structurally dissimilar amphiphiles, including those reported here, can be traced back to strict geometrical or even stereochemical matching of the two juxtaposed surfaces in all cases. Since oriented growth of calcite single crystals under monolayers of **1** preferentially occurs at low surface pressure, where the monolayer displays a liquid-condensed phase, an epitaxial correlation of the monolayer (host) lattice and the overgrown calcite {012} crystal face might in fact be ruled out. It is more likely that non-specific film properties such as average charge density or mean dipole moment of the templating monolayer determine the orientation of crystals.²⁸ Our recent investigations on oriented crystal growth underneath monolayers of *rccc*-5,11,17,23-tetracarboxy-4,6,10,12,16,18,22,24-octa-*O*-methyl-2,8,14,20-tetra(*n*-undecyl)resorc[4]arene strongly support this hypothesis: in both cases, the (012) orientation of calcite crystals prevailed.²⁹ While the complementary molecular structures of the calix[4]arene and resorc[4]arene tetraacids lead to completely different packing arrangements and coordination motifs, the average surface area per molecule in the monolayers and thus the average charge density is of comparable size.

Summary

Amphiphilic calixarene derivatives, such as 5,11,17,23-tetrakis-(1,1,3,3-tetramethylbutyl)-25,26,27,28-tetra(carboxymethoxy)-calix[4]arene, **1**, form stable monolayers which can be employed as supramolecular templates for induced calcite crystallization. The use of easy-to-synthesize calixarenes for this particular area of crystal engineering is reported here for the first time.³⁰ A range of analytical methods are employed to obtain a clear picture of structural factors that govern the occurrence of uniformly oriented calcite crystals growing underneath monolayers of **1**. Thus, the crystal structures of 5,11,17,23-tetrakis-(1,1,3,3-tetramethylbutyl)-25,26,27,28-tetra(carboxymethoxy)-calix[4]arene, **1**, as well as of its Ca salt, **2**, were solved in order to obtain information on typical supramolecular packing arrangements of the macrocyclic surfactants. The free acid **1** forms a lamellar structure where the hydrophilic headgroups and the hydrophobic alkyl chains segregate into different layers. The corresponding Ca salt **2** comprises a structurally rigid Ca complex of the octadentate calixarene ligand. These structural building blocks are interconnected by Ca ions leading to a sandwich type one-dimensional coordination polymer.

Monolayer compression isotherms indicate that the packing density of amphiphilic calixarenes in the monolayers is almost identical to the corresponding arrangement of molecules in the crystal structures. The featureless Langmuir isotherms, however, point to a liquid-condensed state of **1** throughout the investigated compression range. Brewster angle microscopic observations of the monolayer morphology at low surface pressure reveal a highly viscous consistency, which does not change upon further compression. No indications for the occurrence of a liquid-crystalline phase behavior of **1** were found. Uniform, (012) oriented CaCO₃ (calcite) single crystals grow underneath monolayers of **1** at low compression ($\pi = 0.1\text{--}0.5\text{ mN m}^{-1}$), while more randomly oriented single crystals are obtained at higher surface pressure ($\pi = 5\text{--}20\text{ mN m}^{-1}$). Considering the liquid-like state of the monolayer during crystal maturation, an epitaxial correlation between the templating monolayer and the overgrowing calcite crystals is ruled out (although a geometrical match between the putative packing arrangement of calixarene molecules in the monolayer and the arrangement of Ca ions in the calcite {012} cleavage plane can be easily constructed). We, therefore, suggest that non-specific monolayer properties such as average charge density or mean dipole moment are the main determinants for templated calcite growth in the present case.³¹

In summary we have to conclude that the rules which govern the selection of a particular calcite crystal growth plane underneath free-floating surfactant monolayers are not well understood. This (necessarily unsatisfying) statement can be extended to biological systems: Examination of the common crystal orientations in a variety of calcifying organisms reveal that aragonite and calcite single crystals most frequently nucleate from the polar *ab* planes. The arrangement of Ca ions in this plane (the shortest distance between Ca²⁺ ions is 4.99 Å in calcite, and 4.69 Å in aragonite, respectively) is geometrically *not* commensurate with the period of amino acid residues in a protein β -strand (approx. 6.9 Å). Moreover—on pointing more or less perpendicular towards the Ca²⁺ ions in the crystal (001) face—the carboxylate residues of the β -pleated sheet cannot continue the parallel arrangement of planar carbonate anions in the underlying layer(s). The current nucleation model thus does not support the picture of a calcite or aragonite single crystal being nucleated from (001) crystal faces by virtue of stereochemical or geometric matching selection principles.

Future investigations using amphiphilic calix[*n*]arenes of larger ring sizes ($n = 6, 8$) will help to improve our understanding on different mechanisms of induced crystallization underneath structurally non-rigid monolayers. A particularly interesting scientific goal is the quest for the minimum size of

an array of pre-organized acidic residues which could still act as a template for heteroepitaxial crystal nucleation. Structurally confined macrocycles such as **1** might be ideal candidates to study this challenging problem as long as the three-dimensional structures of naturally occurring macromolecules fulfilling this task remain to be solved.

Experimental

Synthetic procedures and analytical data for 5,11,17,23-tetrakis(1,1,3,3-tetramethylbutyl)-25,26,27,28-tetra(carboxymethoxy)calix[4]arene, **1**, and its Ca salt **2** are available as ESI.

X-Ray crystallographic data for

C₆₈H₉₆O₁₂·4.75CH₃OH·0.25H₂O (**1**)

Colourless crystals of **1** were obtained by recrystallization from methanol–water mixtures (10 : 1 vol.%). A single crystal of **1** was removed from the mother liquor, mounted in inert oil and transferred to the cold gas stream of a Bruker AXS SMART diffractometer.

Crystal data. C₆₈H₉₆O₁₂·4.75CH₃OH·0.25H₂O (**1**): $M = 1262.15$, triclinic, $a = 12.2924(5)$, $b = 12.8365(5)$, $c = 25.2557(11)$ Å, $\alpha = 97.251(1)$, $\beta = 93.337(1)$, $\gamma = 107.202(1)^\circ$, $U = 3757.2(3)$ Å³, $T = 183(2)$ K, space group $P\bar{1}$ (no. 2), $Z = 2$, $\mu(\text{Mo-K}\alpha) = 1.9\text{ mm}^{-1}$, 38412 reflections measured, 16065 unique ($R_{\text{int}} = 0.0341$) which were used in all calculations. The final $wR(F^2)$ was 0.2007 (all data).

CCDC reference number 190054.

X-Ray crystallographic data for

[Ca(C₆₈H₉₂O₁₂Ca)(DMSO)₂(H₂O)]·2.5DMSO (**2**)

Block-shaped colourless crystals of **2** grew slowly from a powder suspension of **2** in DMSO–H₂O (5 : 1 vol.%) mixture held at constant temperature ($T = 98^\circ\text{C}$, 3 d). A single crystal of **2** was removed from the mother liquor, mounted in inert oil and transferred to the cold gas stream of a Bruker AXS SMART diffractometer.

Crystal data. [Ca(C₆₈H₉₂O₁₂Ca)(DMSO)₂(H₂O)]·2.5DMSO (**2**): $M = 1551.17$, triclinic, $a = 17.0762(5)$, $b = 20.4361(7)$, $c = 25.9349(8)$ Å, $\alpha = 102.671(1)$, $\beta = 98.326(1)$, $\gamma = 102.872(1)^\circ$, $U = 8427.9(5)$ Å³, $T = 183(2)$ K, space group $P\bar{1}$ (no. 2), $Z = 4$, $\mu(\text{Mo-K}\alpha) = 1.9\text{ mm}^{-1}$, 56343 reflections measured, 35273 unique ($R_{\text{int}} = 0.0174$) which were used in all calculations. The final $wR(F^2)$ was 0.2306 (all data).

CCDC reference number 190055.

See <http://www.rsc.org/suppdata/dt/b2/b206912a/> for crystallographic data in CIF or other electronic format.

Brewster angle microscopy (BAM)

A Brewster angle microscope (BAM-2, NFT, Göttingen) mounted on the Langmuir trough, was used to observe the morphology of the monolayers dependent on the state of the spread calixarene monolayer. Therefore, the surface pressure–area (π – A) isotherms of the monolayers were recorded with a computer-interfaced film balance with a surface area of approximately 300 cm². The surface pressure was measured to within 0.1 mN m⁻¹ by the Wilhelmy method using a roughened glass plate. All isotherms were obtained with a compression rate of 1.5 Å² molecule⁻¹ min⁻¹. A 0.42 mM solution of the monolayer-forming calixarene in chloroform was spread on the aqueous surface by means of a microsyringe. The monolayer was left to equilibrate for a period of 15 min prior to compression. Brewster angle microscopy (BAM) uses the zero reflectance of the air/water surface for parallel (p) polarised light at the incident Brewster angle. The condensed phase of a monolayer leads to a measurable change in reflectivity, thus allowing visualisation of the monolayer morphology without

affecting the monolayer with probes. Optical anisotropy in the monolayer is detected by introducing an analyser into the reflected beam path. The reflected light was detected by means of a CCD camera and recorded on a videotape. The morphological features of the monolayer were monitored with a spatial resolution of $\sim 3 \mu\text{m}$. BAM images were recorded at continuous compression or after compression of the monolayer.

Grazing incidence X-ray diffraction (GIXD)

GIXD experiments were performed using the liquid-surface diffractometer on the undulator beamline BW1 at HASYLAB, DESY, Hamburg, Germany to obtain information on the two-dimensional lattice structure of the spread monolayer. Details of the method have been described elsewhere.³²

CaCO₃ crystal growth experiments

Solutions of calcium bicarbonate were prepared by bubbling carbon dioxide gas through a stirred aqueous (Millipore, resistance 18.2 M Ω cm) solution of Ca(HCO₃)₂ (9 mM) for a period of 2 h. Compressed films were formed by spreading trichloromethane solutions of the surfactant in order to generate a liquid- or solid-like film at the air–water interface. Crystals were studied at several times either *in situ* by optical (polarization) microscopy (Olympus IX 70) or on cover slips laid on the film. The cover slips were also mounted on scanning electron microscope (SEM) specimen tubs. A Phillips XL30 ESEM operating at 30 keV was used. The calcite crystals were sputtered with Au prior to examination.

Bulk samples for X-ray powder diffraction (XRPD) were obtained by collecting the crystals on cover slips laid on the film and removed horizontally. A Philips PW 1050/70 X-ray powder diffractometer was employed (2θ scans, Bragg–Brentano para-focussing geometry) using Cu-K α radiation ($\lambda = 1.54 \text{ \AA}$). Crystallographic indices are presented in three-index (*hkl*) notation, based on the hexagonal setting of the calcite unit cell ($R\bar{3}c$, $a = 4.96 \text{ \AA}$, $c = 17.002 \text{ \AA}$).

Acknowledgements

D. V. thanks the Minerva foundation for a Minerva fellowship. The research was supported by the Deutsche Forschungsgemeinschaft (DFG Schwerpunktprogramm 1117, ‘‘Prinzipien der Biomineralisation’’; DFG grant Vo829/2–1). Donation of the starting material *p*-1,1,3,3-tetramethylbutylphenol by CONDEA Chemie GmbH (Marl, Germany) is gratefully acknowledged. The authors would also like to thank Prof. Lia Addadi and Prof. Steve Weiner (The Weizmann Institute of Science, Israel) for fruitful discussions.

References and notes

- (a) H. A. Lowenstam and S. Weiner, *On Biomineralization*, Oxford University Press, Oxford, 1989; (b) A. P. Wheeler and C. S. Sikes, in *Biomineralization*, S. Mann, ed., VCH, Weinheim, 1989, pp. 95–131.
- S. Weiner and L. Addadi, *J. Mater. Chem.*, 1997, **7**, 689–702.
- S. Weiner and L. Addadi, in *Biomineralization*, S. Mann, ed., VCH, Weinheim, 1989, pp. 133–156.
- (a) S. Mann, B. R. Heywood, S. Rajam and J. D. Birchall, *Nature*, 1988, **334**, 692–695; (b) S. Rajam, B. R. Heywood, J. B. A. Walker, S. Mann, R. J. Davey and J. D. Birchall, *J. Chem. Soc., Faraday Trans.*, 1991, **87**, 727–734; (c) A. Berman, D. J. Ahn, A. Lio, M. Salmeron, A. Reichert and D. Charych, *Science*, 1995, **269**, 515–518; (d) G. Xu, N. Yao, I. A. Aksay and J. T. Groves, *J. Am. Chem. Soc.*, 1998, **120**, 11977–11985; (e) S. Champ, J. A. Dickinson, P. S. Fallon, B. R. Heywood and M. Mascal, *Angew. Chem., Int. Ed.*, 2000, **39**, 2716–2719; (f) P. J. J. A. Buijnsters, J. J. M. Donners, S. J. Hill, B. R. Heywood, R. J. M. Nolte, B. Zwaneburg and N. A. J. M. Sommerdijk, *Langmuir*, 2001, **17**, 3623–3628.
- (a) J. Aizenberg, A. J. Black and G. M. Whitesides, *J. Am. Chem. Soc.*, 1999, **121**, 4500–4509; (b) J. Köther, G. Nelles, R. Seshadri,

- M. Schaub, H. J. Butt and W. Tremel, *Chem. Eur. J.*, 1998, **4**, 1834–1842; (c) D. D. Archibald, S. B. Qadri and B. P. Gaber, *Langmuir*, 1996, **12**, 538–546.
- As reviewed in D. Volkmer, *Biomineralization in Encyclopedia of Separation Science*, (M. Cooke, C. F. Poole, eds.), Vol. 2 (Crystallization), Academic Press, 2000, pp. 940–950.
- P. M. Harrison and P. Arosio, *Biochim. Biophys. Acta*, 1996, **1275**, 161–203.
- (a) M. Arbel-Haddad, M. Lahav and L. Leiserowitz, *J. Phys. Chem. B*, 1998, **102**, 1543; (b) J. Majewski, R. Popovitz-Biro, R. Edgar, M. Arbel-Haddad, K. Kjaer, W. Bouwman, J. Als-Nielsen, M. Lahav and L. Leiserowitz, *J. Phys. Chem. B*, 1997, **101**, 8874.
- A. Arduini, A. Pochini, S. Reverberi and R. Ungano, *J. Chem. Soc., Chem. Commun.*, 1984, 981–982.
- A. Arduini, A. Pochini, S. Reverberi and R. Ungaro, *Tetrahedron*, 1986, **42**, 2089–2100.
- CSD codes: CARJAG, CARJEK, ZUVFOL, and SOVJAO.
- Early examples of numerous crystallographic investigations on host–guest properties of *tert*-butylcalix[4]arene derivatives include: (a) G. D. Andreetti, R. Ungaro and A. Pochini, *J. Chem. Soc., Chem. Commun.*, 1979, 1005–1007; (b) C. D. Gutsche, B. Dhawan, K. H. No and R. Muthukrishnan, *J. Am. Chem. Soc.*, 1981, **103**, 3782–3792; (c) M. Coruzzi, G. D. Andreetti, V. Bocchi, A. Pochini and R. Ungaro, *J. Chem. Soc., Perkin Trans. 2*, 1982, 1133–1138.
- CSD codes: CARJAG, CARJEK. G. D. Andreetti, A. Pochini and R. Ungaro, *J. Chem. Soc., Perkin Trans. 2*, 1983, 1773–1779.
- CSD code: ZUVFOL. J. M. Harrowfield, M. Mocerino, B. J. Peachey, B. W. Skelton and A. H. White, *J. Chem. Soc., Dalton Trans.*, 1996, 1687–1699.
- G. R. Desiraju, *Angew. Chem., Int. Ed. Engl.*, 1995, **34**, 2311–2327.
- H. Ti Tien, in *Thin Liquid Films*, I. B. Ivanov, ed., Surfactant Science Series, vol. 29, 1988, pp. 927–1057.
- J. Israelachvili, D. J. Mitchel and B. W. Ninham, *J. Chem. Soc., Faraday Trans.*, 1976, **72**, 1525–1568.
- (a) V. A. Arsentiev and J. Leja, in *Colloid and Interface Science*, vol. 5, M. Kerker, ed., Academic Press, New York, 1976, pp. 251–270; (b) G. T. Barnes, in *Colloid Science*, vol. 2, D. H. Everett, ed., Chemical Society, London, 1975, pp. 173–190.
- S. J. Cooper, R. B. Sessions and S. D. Lubetkin, *Langmuir*, 1997, **13**, 7165–7172.
- D. Vollhardt, *Adv. Colloid Interface Sci.*, 1996, **64**, 143–171.
- Crystallization experiments at even higher surface pressure ($\pi > 20 \text{ mN/m}$) were impossible due to the insufficient long-term stability of the monolayer.
- Joint Committee on Powder Diffraction Standards – International Center for Diffraction Data, Swarthmore, UK, 1986; File No. 24–27 (Calcite).
- The calculated σ values represent the surface charge density of a calcite (012) cleavage plane consisting of Ca²⁺ ions, and the surface charge density of a close-packed *ab* layer of [C₆₈H₉₂O₁₂Ca]²⁻ units, respectively.
- O. S. Pokrovsky, J. A. Mielczarski, O. Barres and J. Schott, *Langmuir*, 2000, **16**, 2677–2688.
- N. H. de Leeuw and S. C. Parker, *J. Phys. Chem. B*, 1998, **102**, 2914–2922.
- D. J. Ahn, A. Berman and D. Charych, *J. Phys. Chem.*, 1996, **100**, 12455–12461.
- A. M. Travaille, J. J. M. Donners, J. W. Gerritsen, N. A. J. M. Sommerdijk, R. J. M. Nolte and H. van Kempen, *Adv. Mater.*, 2002, **14**, 492–495.
- (a) M. J. Lochhead, S. R. Letellier and V. Vogel, *J. Phys. Chem. B*, 1997, **101**, 10821–10827; (b) S. J. Cooper, R. B. Sessions and S. D. Lubetkin, *J. Am. Chem. Soc.*, 1998, **120**, 2090–2098.
- D. Volkmer, M. Fricke, C. Agena and J. Mattay, *CrystEngComm*, 2002, **4**, 288–295.
- Monolayers and Langmuir–Blodgett thin films of amphiphilic calixarenes have been reported: (a) M. A. Markowitz, V. Janout, D. G. Castner and S. L. Regen, *J. Am. Chem. Soc.*, 1989, **111**, 8192–8200; (b) W. Lee, R. A. Hendel, P. Dedek, V. Janout and S. L. Regen, *J. Am. Chem. Soc.*, 1995, **117**, 6793–6794; (c) F. Davis, L. O’Toole, R. Short and C. J. M. Stirling, *Langmuir*, 1996, **12**, 1892–1894; (d) A. V. Nabok, T. Richardson, F. Davis and C. J. M. Stirling, *Langmuir*, 1997, **13**, 3198–3201; (e) R. A. Hendel, E. Nomura, V. Janout and S. L. Regen, *J. Am. Chem. Soc.*, 1997, **119**, 6909–6918; (f) W. He, F. Liu, Z. Ye, Y. Zhang, Z. Guo, L. Zhu, X. Zhai and J. Li, *Langmuir*, 2001, **17**, 1143–1149; (g) E. Houel, A. Lazar, E. Da Silva, A. W. Coleman, A. Solovoyov, S. Cherenok and V. I. Kalchenko, *Langmuir*, 2002, **18**, 1374–1379.
- P. Calvert and S. Mann, *Nature*, 1997, **386**, 127–129.
- V. M. Kaganer, H. Möhwald and P. Dutta, *Rev. Mod. Phys.*, 1999, **71**, 779–820.

Growth of Calcite Single Crystals Underneath Monolayers of 5,11,17,23-Tetra-*t*-butyl-25,26,27,28-tetrakis(carboxymethoxy)calix[4]arene

Dirk Volkmer* and Marc Fricke

Bielefeld, Fakultät für Chemie der Universität

Received July 21st, 2003.

Dedicated to Professor Bernt Krebs on the Occasion of his 65th Birthday

Abstract. The amphiphilic 5,11,17,23-tetra-*t*-butyl-25,26,27,28-tetrakis(carboxymethoxy)calix[4]arene (**1**) forms stable monolayers at the air-water interface which serve as template to induce growth of CaCO₃ (calcite) single crystals. The nucleation density and the preferred orientation(s) of calcite single crystals depend on the surface pressure applied to the monolayer. Models of the pressure-dependant aggregation of amphiphiles at the air-water interface are derived from the crystal structures of the novel Ca coordina-

tion compounds [(Ca(C₅₂H₆₀O₁₂))₂Ca(H₂O)₂(CH₃OH)₃Ca(H₂O)₂(CH₃OH)₂·12CH₃OH·4H₂O (**2**) and [Ca(C₅₂H₆₀O₁₂)Ca(H₂O)_{2.5}(MeOH)_{0.5}]·7H₂O·CH₃OH (**3**). Structural data are analyzed in terms of supramolecular packing arrangements and Ca coordination motifs of the constituting amphiphilic macrocycles.

Keywords: Calix[4]arenes; Monolayers; Crystal engineering; Calcite; Biomineralization

Wachstum von Calciteinkristallen unter Monoschichten aus 5,11,17,23-Tetra-*t*-butyl-25,26,27,28-tetrakis(carboxymethoxy)calix[4]aren

Inhaltsübersicht. Das amphiphile 5,11,17,23-Tetra-*t*-butyl-25,26,27,28-tetrakis(carboxymethoxy)calix[4]aren (**1**) bildet an der Wasser-Luft-Grenzfläche stabile Monoschichten, die als Templat für ein gerichtetes Wachstum von CaCO₃ (Calcit) Einkristallen dienen. Die Keimdichte und die Vorzugsorientierung(en) der Calciteinkristalle sind abhängig vom Oberflächendruck in der Monoschicht. Modelle für die druckabhängige Aggregation der Amphiphile in

der Wasser-Luft-Grenzschicht werden aus Kristallstrukturen der neuartigen Ca-Koordinationsverbindungen [(Ca(C₅₂H₆₀O₁₂))₂Ca(H₂O)₂(CH₃OH)₃Ca(H₂O)₂(CH₃OH)₂·12CH₃OH·4H₂O (**2**) und [Ca(C₅₂H₆₀O₁₂)Ca(H₂O)_{2.5}(MeOH)_{0.5}]·7H₂O·CH₃OH (**3**) abgeleitet. Die Strukturdaten werden im Hinblick auf supramolekulare Packungs- und Ca-Koordinationsmotive der am Aufbau beteiligten amphiphilen Makrozyklen analysiert.

Introduction

Crystallization of inorganic solids at self-organized surfaces is an important process in biomineralization and crystal engineering [1, 2]. Nucleation and growth steps taking place at the interface are often specific and result in a particular crystal morphology or polymorph. In recent years Langmuir monolayers [3] and self-assembled monolayers (SAMs) [4] have been employed as 2D crystallization templates which induce epitaxial growth of highly oriented calcium carbonate crystals, the most abundant biomineral in nature. Physical parameters such as interfacial electrostatics, [2, 4, 5] hydrogen bonding [3, 5] and interfacial molecular

recognition events including geometrical lattice matching [2, 3] and stereochemical complementarity [6] were discussed as crucial factors in this context. In order to mimic structural aspects of the interactions between acidic proteins and biogenic calcite in calcified tissues (i. e. mollusk shells) we employ oligoacids based on amphiphilic calix[*n*]arene moieties as biologically inspired supramolecular templates for epitaxial crystal growth [7].

Employing macrocyclic amphiphiles we would like to address the rather fundamental question concerning the putative structure of crystal nucleation sites in calcified tissues. Investigations on the amino acid composition of different natural proteins associated with biomineralization reveal sequence motifs which are particularly rich in aspartic acid and glutamic acid residues, respectively [8]. Unfortunately, none of the acidic proteins extracted from calcified tissues have yet been grown into single crystals suitable for X-ray crystallographic investigations and thus three-dimensional structures are currently not available. However, a representative structural model of a mineral/peptide interface architecture may be derived from the iron storage protein (ferritin) which is regarded as an archetypal biological model for the formation of a nanocrystalline mineral phase within a confined space [9]. Here, the ferritin L-chain subunit bears

* Dr. D. Volkmer

Faculty of Chemistry (AC1)

University of Bielefeld

D-33501 Bielefeld (Germany)

P.O. Box 100 131

Telephone: (+49) 521-106 6142

Fax: (+49) 521-106 6003

E-mail: dirk.volkmer@uni-bielefeld.de

Supporting information for this article is available on the WWW under <http://www.wiley-vch.de/home/zaac> or from the author

four suitably aligned glutamic acid residues that are necessary for mineral formation. Artificial organic molecules can be designed such as to mimic the confined arrangement of acidic residues in natural proteins. Macrocyclic calix[*n*]arenes such as **1** are especially suited for this purpose since they are synthetically readily available. These molecules form confined arrays of co-aligned carboxylic acid groups, the number and relative positions of which show systematic structural variations depending on the size of the macrocyclic backbone.

Here we present the synthesis and X-ray structure analysis of two novel Ca coordination compounds of the amphiphilic ligand 5,11,17,23-tetra-*t*-butyl-25,26,27,28-tetrakis(carboxymethoxy)calix[4]arene (**1**), namely the compounds [(Ca(C₅₂H₆₀O₁₂))₂Ca(H₂O)₂(CH₃OH)₃Ca(H₂O)₂(CH₃OH)₂]·12CH₃OH·4H₂O (**2**) and [Ca(C₅₂H₆₀O₁₂)Ca(H₂O)_{2.5}(MeOH)_{0.5}]·7H₂O·CH₃OH (**3**). Monolayers of **1** are spread on an aqueous subphase containing Ca ions and the Langmuir isotherms recorded are analyzed in terms of monolayer stability, aggregation behaviour, and average area/molecule. Models of the putative packing arrangements of calix[4]arene molecules at the air-water interface and possible Ca coordination motifs are derived from crystal data of **2** and **3**.

Results and Discussion

X-ray crystallographic investigations

Although there are quite a few crystal structures of *t*-butyl-calix[4]arene derivatives described in literature, a single crystal X-ray structure analysis of a metal complex of the carboxylic acid derivative has not been reported so far. In a previous study [7] we have presented the X-ray structures of 5,11,17,23-tetrakis-(1,1,3,3-tetramethylbutyl)-25,26,27,28-tetra(carboxymethoxy)calix[4]arene (C₆₈H₉₆O₁₂·4.75CH₃OH·0.25H₂O, **5**) and its corresponding calcium complex [Ca(C₆₈H₉₂O₁₂Ca)(DMSO)₂(H₂O)]·2.5DMSO (**6**). In this paper we present the X-ray structural data of two Ca complexes of 5,11,17,23-tetra-*t*-butyl-25,26,27,28-tetrakis(carboxymethoxy)calix[4]arene (**1**).

Crystal structure of **2**.

Single crystals of the compound [(Ca(C₅₂H₆₀O₁₂))₂Ca(H₂O)₂(CH₃OH)₃Ca(H₂O)₂(CH₃OH)₂]·12CH₃OH·4H₂O (C₂₄₂H₄₀₈Ca₈O₉₈, **2**) were obtained from methanol solution containing 5 vol.% of water. Slow evaporation of the solvent at room temperature leads to formation of colorless (highly fragile) crystals of **2**. Single crystals suitable for X-ray crystallographic investigations were hard to obtain, mainly due to the rapid loss of solvent molecules (within seconds) upon exposing the crystals to air. Consequently the structure refinement converged to a relatively high final R value. The crystal structure of **2** in fact shows that a host of solvent molecules are occluded in the crystal lattice. Most of the atomic positions of the lattice solvent mol-

ecules had to be refined with a site occupancy factor below 1.0 which confirms our observation of the rapid aging of the crystals. Furthermore, a fraction of the Ca ions (Ca(4A,B) including their coordinated ligands) are placed at two slightly different crystallographic positions which excluded the possibility of a fully anisotropic refinement).

The X-ray structure analysis shows that **2** consists of an octacalcium coordination compound. The asymmetric unit contains four Ca ions, two of which are strongly sequestered by a calix[4]arene ligand **1**. The unit cell thus contains one formula unit of the complex. The coordination of a single Ca ion to **1** leads to formation of the structurally rigid [Ca(C₅₂H₆₀O₁₂)]²⁻ moiety which in turn serves as bridging unit in compound **2**. Two [Ca(C₅₂H₆₀O₁₂)]²⁻ moieties are coordinated to four Ca ions in a μ₄-bridging mode, while at the same time two of them act as capping ligand in a μ₂-bridging mode (Fig. 1). The four Ca ions Ca(3), Ca(4A), Ca(3)*, and Ca(4A)* span a plane and the distance of Ca(2) (Ca(1), respectively) at normal direction towards this plane amounts to 3.81 Å (1.45 Å).

The coordination environments of Ca(1) and Ca(2) each consist of eight oxygen donors provided by the calix[4]arene ligand **1**. The square planes spanned by the phenolic and the carboxylate oxygen donors of Ca(1), (Ca(2), respectively), are rotated by 33.3° (29.9°) against each other. The

Table 1 X-Ray crystallographic data for compounds **2** and **3**

Compound	2	3
Empirical formula	C ₂₄₂ H ₄₀₈ Ca ₈ O ₉₈	C _{53.5} H ₈₅ Ca ₂ O ₂₃
Formula weight	5206.39 g · mol ⁻¹	1176.38 g · mol ⁻¹
Crystal system	triclinic	orthorhombic
Space group	<i>P</i> 1̄ (no. 2)	<i>Pbcn</i> (no. 60)
Unit cell dimensions	<i>a</i> = 16.526(3) Å <i>b</i> = 21.936(4) Å <i>c</i> = 23.029(5) Å <i>α</i> = 99.36(3)° <i>β</i> = 99.04(3)° <i>γ</i> = 110.13(3)°	<i>a</i> = 49.75(1) Å <i>b</i> = 13.252(3) Å <i>c</i> = 20.068(4) Å
Cell volume	7527(3) Å ³	13231(5) Å ³
Formula units per cell	1	8
Calculated density	1.149 g · cm ⁻³	1.181 g · cm ⁻³
Diffractometer type	SMART 1K (Bruker AXS)	
Temperature	183(2) K	
Radiation (wavelength)	Mo-K _α (0.71073 Å)	
Scan type	ω-scan	
2θ range for data collection	3.18 – 55.74°	6.06 – 52.04°
Index ranges	0 ≤ <i>h</i> ≤ 21 –26 ≤ <i>k</i> ≤ 25 –30 ≤ <i>l</i> ≤ 29	0 ≤ <i>h</i> ≤ 61 0 ≤ <i>k</i> ≤ 16 0 ≤ <i>l</i> ≤ 24
Reflections collected	79513	68146
Independent reflections	31060 [R _{int} = 0.0957]	12527 [R _{int} = 0.0896]
Data / restraints / parameters	31060 / 0 / 1575	12527 / 0 / 733
Structure solution	SHELXS-97	
Refinement Program	SHELXL-97	
Goodness-of-fit	1.561	1.027
Final R indices [I > 2σ(I)]	R _f = 0.1535, wR ₂ = 0.4093	R _f = 0.1003, wR ₂ ^(a) = 0.2823
R indices (all data)	R _f = 0.2279, wR ₂ = 0.4548	R _f = 0.1252, wR ₂ ^(a) = 0.3015
Largest peak and hole	1.350 and –1.003 e Å ⁻³	0.966 and –0.677 e Å ⁻³

^{a)} w = 1/[σ²(F_o²) + (0.1571 · P)2 + 44.09 · P] with P = (F_o² + 2 · F_c²)/3

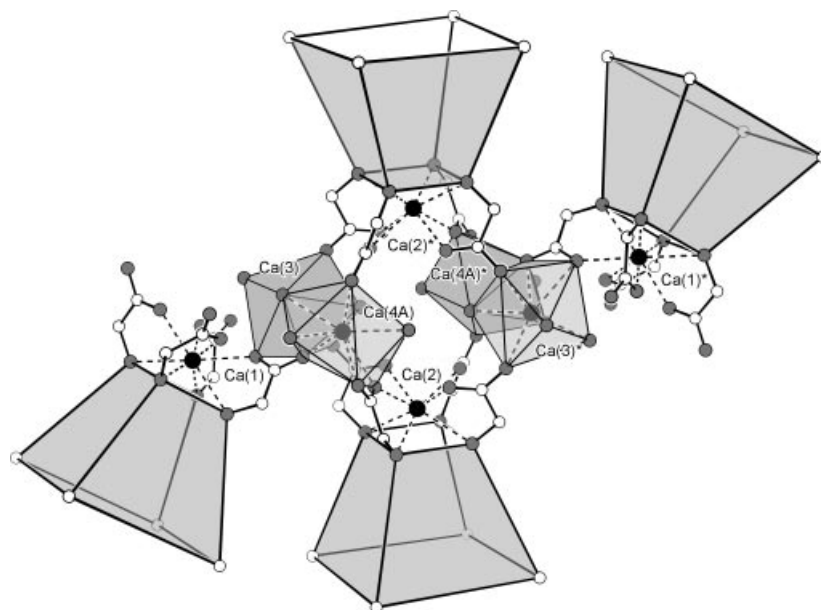


Fig. 1 Simplified representation of the coordination scheme of **2** (coordination polyhedrons are displayed for interconnecting Ca ions only). Selected Ca...Ca non-bonding distances:

Ca(1)...Ca(3): 4.67(7), Ca(1)...Ca(4A): 6.21(6), Ca(3)...Ca(4A): 3.65(7), Ca(2)...Ca(3): 5.91(13), Ca(2)...Ca(4A): 5.44(8), Ca(3)...Ca(4A)*: 7.11(6), Ca(3)...Ca(3)*: 8.99(4) Å.

coordination, therefore, is best described as an intermediate form between a square antiprism and a cube.

The coordination environment of Ca(3) (Ca(4A), respectively) also consists of eight oxygen donors, four of which stem from different calix[4]arene ligands while the other ones belong to coordinated methanol or water ligands. Ca(3) and Ca(4A) form a triply bridged, dinuclear unit with a short Ca...Ca distance of 3.65(7) Å (Fig. 2).

The calix[4]arene molecules adapt a highly symmetrical cone-conformation where the hydrophobic *para-t*-butyl substituents are placed at stereochemically equivalent positions. The pseudo C_{4v} symmetry axis of the μ_4 -bridging ligand is tilted by 25° against the plane normal of the *ab* crystal plane while the corresponding tilt angle of the μ_2 -bridging calix[4]arene amounts to 18°.

Compound **2** forms a lamellar structure where the hydrophilic constituents (carboxylate residues, Ca ions, crystal methanol and water solvate) and the hydrophobic residues segregate into different layers. This supramolecular packing arrangement is reminiscent of the bilayer structural motif of membrane forming biogenic lipids and likewise amphiphilic molecules [10]. The bilayers run parallel to the crystallographic *ab*-plane and layer stacking follows the *c*-direction (Fig. 3). The average surface area occupied by a single calix[4]arene molecule in the *ab*-plane of the crystal structure of **2** amounts to 1.70 nm². This value is considerably higher than the average molecular surface area as determined from the Langmuir isotherms of **1** on an aqueous subphase (see the following section). A closer examination of the crystal structure of **2** indeed shows that the packing arrangement of calix[4]arene residues is interspersed with solvate molecules which leads to holes in the layer structure. The pack-

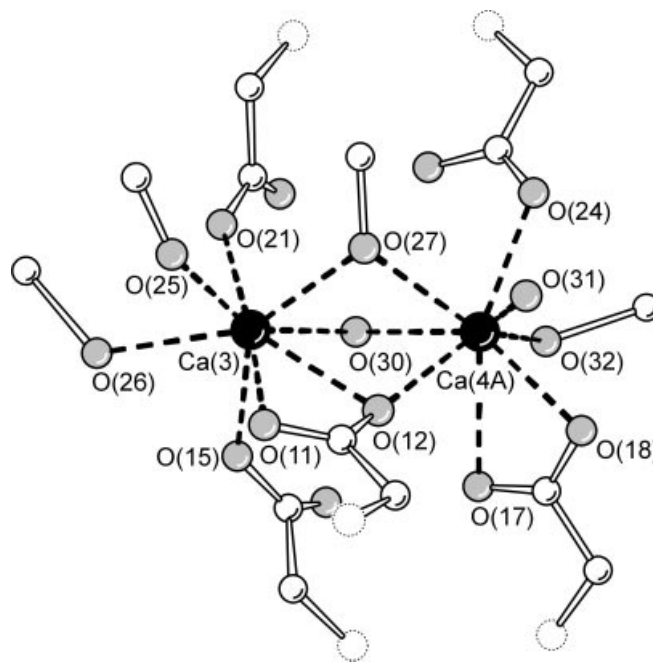


Fig. 2 Ball-and-stick model of the dinuclear Ca centers in the crystal structure of **2**.

(The carboxylate groups shown here are part of different calix[4]arene ligands (**1**), most atoms of which are omitted for clarity). Selected Ca–O bond lengths:

Ca(3)–O(11): 2.62(4), Ca(3)–O(12): 2.55(3), Ca(3)–O(15): 2.33(4), Ca(3)–O(21): 2.29(3), Ca(3)–O(25): 2.40(3), Ca(3)–O(26): 2.52(5), Ca(3)–O(27): 2.53(3), Ca(3)–O(30): 2.43(1), Ca(4A)–O(12): 2.34(6), Ca(4A)–O(17): 2.67(5), Ca(4A)–O(18): 2.26(2), Ca(4A)–O(24): 2.41(7), Ca(4A)–O(27): 2.72(3), Ca(4A)–O(30): 2.47(3), Ca(4A)–O(31): 2.42(2), Ca(4A)–O(32): 2.46(1) Å.

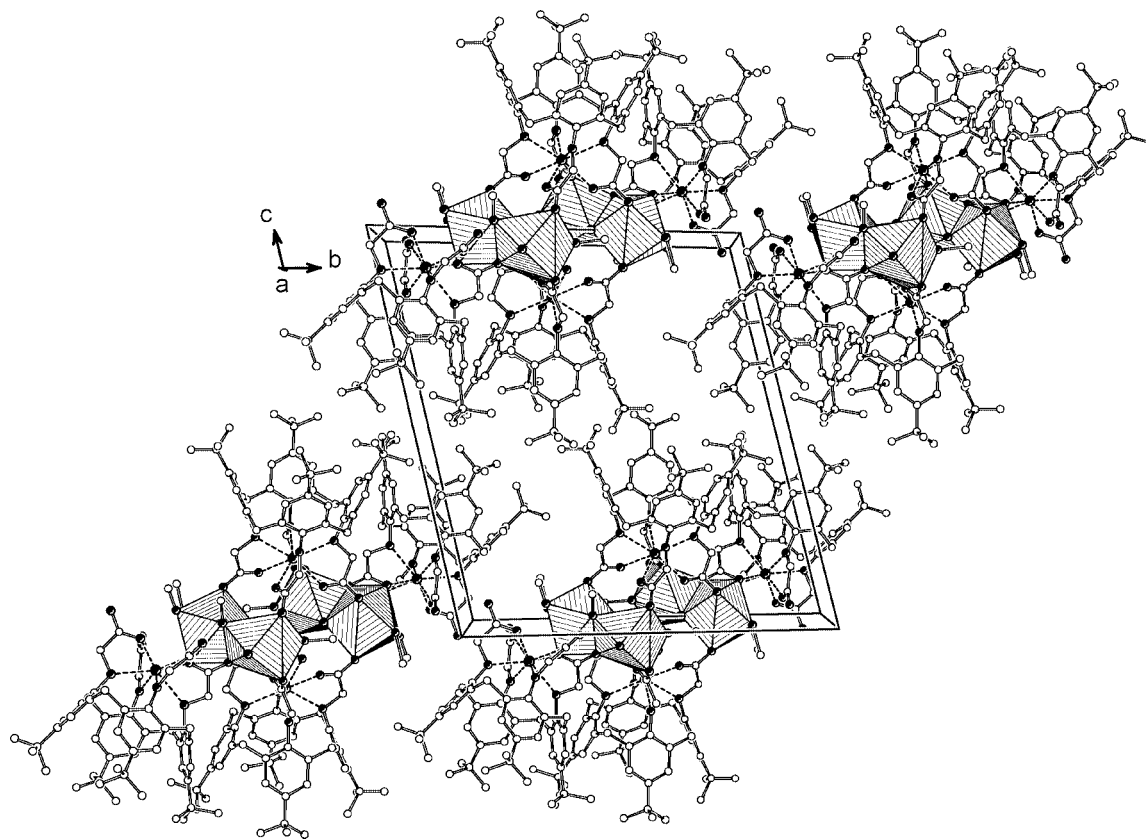


Fig. 3 Ball-and-stick model of the supramolecular packing arrangement of **2** in the crystal lattice. (Hydrogen atoms and non-coordinated solvent molecules are omitted for clarity. Coordination polyhedrons are displayed for interconnecting Ca ions only.)

ing of calix[4]arene ligands in the *ab*-plane of **2** may therefore serve as model for the putative arrangement of $[\text{Ca}(\text{C}_{52}\text{H}_{60}\text{O}_{12})]^{2-}$ moieties at the air-water interface at low surface pressure π .

Crystal structure of **3**

Single crystals of the Ca complex **3** were obtained by slow re-crystallization of the crude product from MeOH/H₂O mixtures (10/1 vol.%) held at 90 °C. The Ca complex may be formally described as a coordination polymer with the sum formula $1/n [\text{Ca}(\text{C}_{52}\text{H}_{60}\text{O}_{12})\text{Ca}(\text{H}_2\text{O})_{2.5}(\text{MeOH})_{0.5}]_n \cdot 7\text{H}_2\text{O} \cdot \text{CH}_3\text{OH}$ ($\text{C}_{53.5}\text{H}_{85}\text{O}_{23}\text{Ca}_2$, **3**).

Apparently, a 1:1 complex of a single Ca ion and the octadentate ligand **1** forms at the beginning, which possesses a two-fold net negative charge under the chosen reaction conditions (excess of $\text{Ca}(\text{OH})_2$). The non-coordinated carboxylic acid oxygen donors of each mononuclear $[\text{Ca}(\text{C}_{52}\text{H}_{60}\text{O}_{12})]^{2-}$ building block can then bind to excess “free” calcium ions in solution to build up a coordination polymer.

The coordination environments of Ca ions in the crystal structure of **3** are quite different: The Ca ion (Ca(1), Fig. 4) sequestered by the calix[4]arene ligand **1** is eight-fold coordinated. As in the crystal structure of **2**, the Ca(1) coordination polyhedron may be described as an intermediate form between a square antiprism and a cube. The square

planes spanned by the phenolic and the carboxylate oxygen donors, respectively, are rotated by 34° against each other. In contrast, the bridging metal ions (Ca(2)) are in a distorted pentagonal-bipyramidal coordination environment; each Ca ion is coordinated by four oxygen donors of three different calix[4]arene ligands and the coordination number is completed by two water ligands and a further oxygen donor of a monodentate MeOH ligand. The Ca(2) ions form doubly bridged, dinuclear units with a short Ca...Ca distance of 3.98(1) Å (Fig. 5). Each $[\text{Ca}(\text{C}_{52}\text{H}_{60}\text{O}_{12})]^{2-}$ building block is coordinated to three different Ca ions (μ_3 -bridging mode).

Due to the stoichiometric (2:1) ratio of Ca ions and (deprotonated) calix[4]arene ligands, electrostatically neutral, one-dimensional coordination polymers form which have a dumb-bell shape in cross-sectional view. The coordination strands run in the *c* direction of the crystal lattice (Fig. 6). There are no coordinative bonds between coordination strands next to each other, which may explain the solubility of the complex in trichloromethane. The voids in the packing of coordination strands are filled with (non-coordinated) H₂O/MeOH molecules. In analogy to the lamellar arrangement of the calix[4]arene moieties in the crystal structure of **2**, compound **3** forms a bilayer structure where the polar functional groups and the hydrophobic residues segregate into different layers. Each bilayer runs parallel to the *bc* crystal plane while distinct bilayers are stacked along

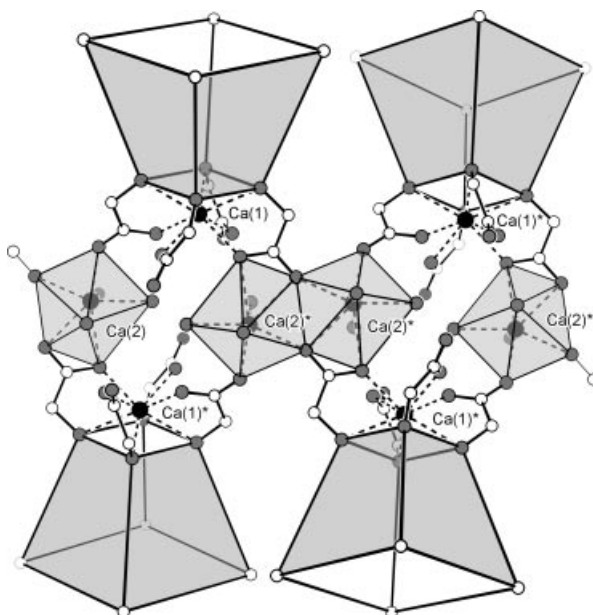


Fig. 4 Simplified representation of the coordination scheme of **3** (coordination polyhedrons are displayed for interconnecting Ca ions only). Selected Ca...Ca non-bonding distances:

Ca(1)...Ca(2): 5.98(1), Ca(1)...Ca(2)*: 4.58(1), Ca(2)...Ca(2)*: 3.98(1), Ca(2)...Ca(2)*: 6.92(1) Å.

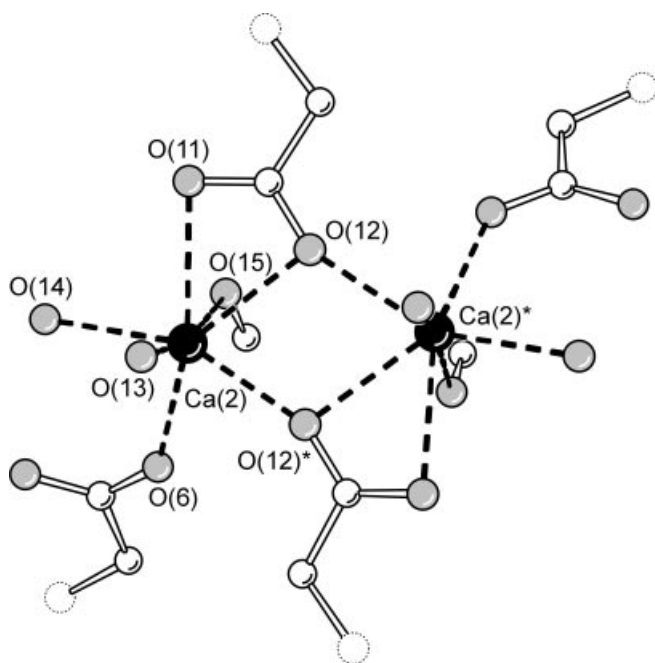


Fig. 5 Ball-and-stick model of the dinuclear Ca centers in the crystal structure of **3**.

(The carboxylate groups shown here are part of different calix[4]arene ligands (**1**), most atoms of which are omitted for clarity). Selected Ca–O bond lengths:

Ca(2)–O(6): 2.31(1) Ca(2)–O(11): 2.57(1), Ca(2)–O(12): 2.50(1),
Ca(2)–O(13): 2.35(1), Ca(2)–O(14): 2.34(1), Ca(2)–O(15): 2.35(1),
Ca(2)–O(12)*: 2.35(1) Å.

the *a* direction. Within the layer, calix[4]arene molecules are close packed with their pseudo C_{4v} symmetry axis tilted by

18° against the *bc*-plane normal. The average surface area occupied by a single calix[4]arene molecule in **3** amounts to 1.33 nm^2 which is considerably lower than the corresponding value calculated from the crystal structure of **2** (Table 2).

A further examination of the arrangement of calix[4]arene ligands in the crystal structure of **3** shows that the packing density of the hydrophobic residues should be close to the maximum reachable value since each *t*-butyl substituent of the ligand is at a van-der-Waals distance to its neighbours. The packing of calix[4]arene ligands in the *bc*-plane of **3** may therefore serve as model for the putative arrangement of $[\text{Ca}(\text{C}_{52}\text{H}_{60}\text{O}_{12})]^{2-}$ moieties at the air-water interface at high surface pressure π . (Packing plots for the in-plane arrangement of calix[4]arene ligands in the crystal structures of **2** and **3**, respectively, are provided as supplementary material).

Monolayer studies

Crystallographic investigations on the solid state structures of Ca salts of **1** are complemented by monolayer studies. Langmuir monolayers were formed on aqueous subphases by spreading compound **1** from trichloromethane solution using a Langmuir trough. The surface pressure–area (π –*A*) isotherms provide information on monolayer stability and phase behaviour. Fig. 7 shows the π –*A* isotherms of compound **1** monolayers spread on an aqueous subphase (Millipore water, or $\text{CaCl}_2/\text{NaHCO}_3$ ($c = 9/18 \text{ mM}$), respectively).

In both cases, relatively stable monolayers form which collapse upon compression at a surface pressure of

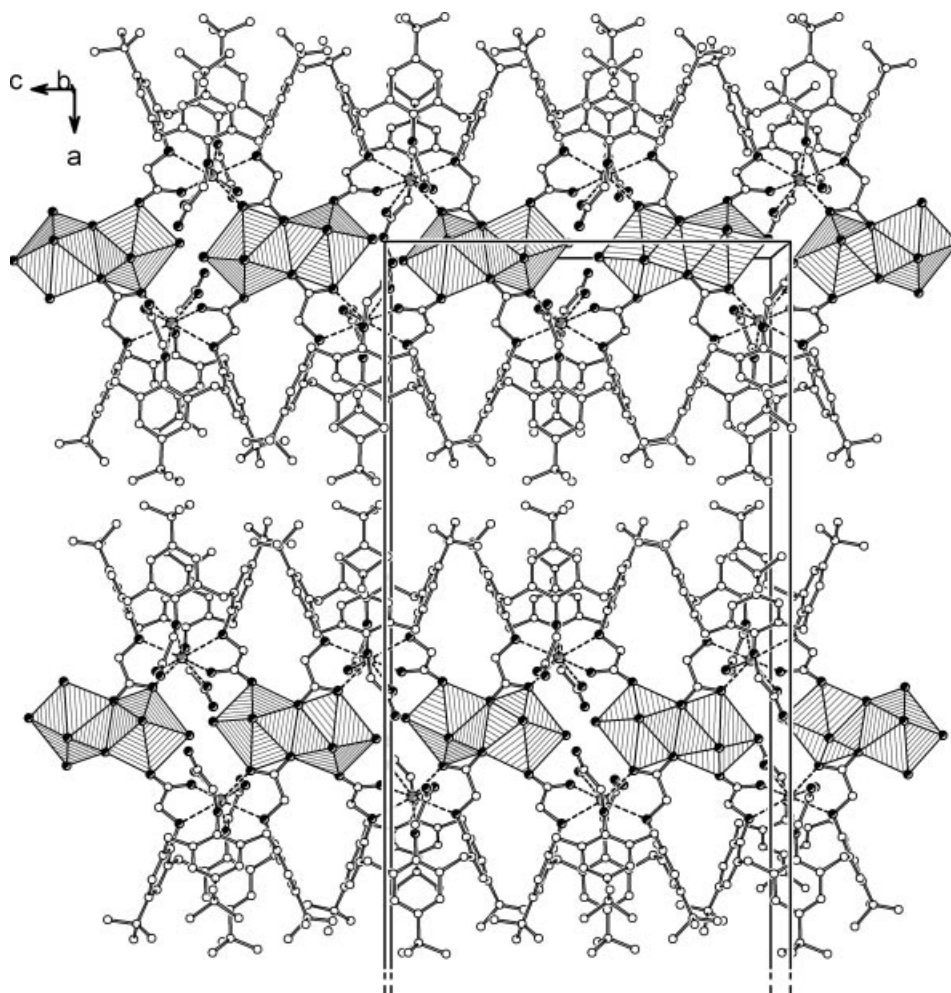


Fig. 6 Ball-and-stick model of the coordination polymer **3** showing the packing arrangement of the one-dimensional polymeric strands in the crystal lattice. (Solvent molecules occluded in the crystal lattice and hydrogen atoms are omitted for clarity. Coordination polyhedrons are displayed for interconnecting Ca ions only.)

Table 2 Area/molecule of calix[4]arene tetraacid derivatives as determined from Langmuir isotherms and from crystal data

Compound	Monolayer (subphase)	Area/molecule/nm ²		Inclination angle/° ^c	Ref.
		Monolayer (subphase)	Crystal data (compound)		
1	1.15–1.20 (H ₂ O) ^a	n.d.	n.d.	n.d.	this work
	1.30–1.40 (Ca(HCO ₃) ₂) ^b	1.70 (2)	25, 18 ^d	this work	
		1.33 (3)	18	this work	
4	1.45–1.50 (H ₂ O) ^a	1.51 (5)	24	[7]	
	1.70–1.75 (Ca(HCO ₃) ₂) ^b	1.70 (6)	34, 24 ^d	[21]	

Compound index: **1**: C₅₂H₆₄O₁₂, **2**: [(Ca(C₅₂H₆₀O₁₂))₂Ca(H₂O)₂(CH₃OH)₃Ca(H₂O)₂(CH₃OH)₂]:12CH₃OH·4H₂O, **3**: [Ca(C₅₂H₆₀O₁₂)Ca(H₂O)_{2.5}(MeOH)_{0.5}]:7H₂O·CH₃OH, **4**: C₆₈H₉₆O₁₂, **5**: C₆₈H₉₆O₁₂·4.75CH₃OH·0.25H₂O, **6**: [Ca(C₆₈H₉₂O₁₂Ca)(DMSO)₂(H₂O)]·2.5DMSO

n.d. = not determined

^a Millipore water, resistance 18.2 MΩ·cm)

^b Aqueous subphase containing CaCl₂/NaHCO₃, c = 9/18 mM

^c Angle between the pseudo C_{4v} symmetry axis of the calix[4]arene molecule and the plane normal of the most densely packed crystal plane

^d Two symmetry-independent calixarene molecules/asymmetric unit

~30 mN/m (pure water) and ~40 mN/m (Ca containing aqueous subphase), respectively. The featureless isotherms suggest fluid properties of the condensed phase in both cases. On water the onset of pressure increase is at ~1.30 nm²/molecule whereas the surface pressure of the Ca containing solution starts to rise at a significantly higher

value (~1.80 nm²/molecule). We assume that this behaviour is due to electrostatic/coordinative interactions of Ca ions which cause the carboxylic acid residues of **1** to become deprotonated. Expansion effects of monolayers spread on metal ion-containing subphases, similar to those observed here, have been reported for several systems [11].

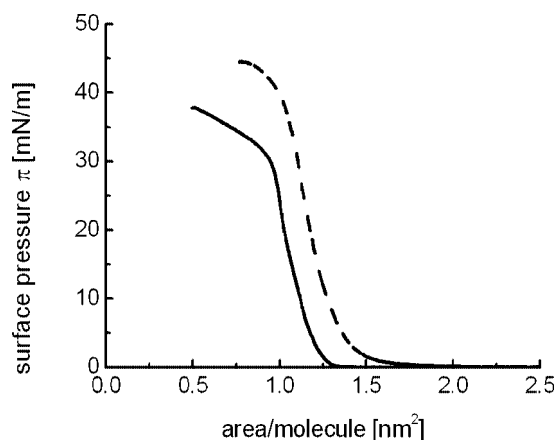


Fig. 7 π -A isotherms of monolayers of **1** at 22 °C on H₂O (solid line), and aqueous CaCl₂/NaHCO₃ ($c = 9/18$ mM, dashed line).

The area per molecule of **1** in the monolayers is estimated from extrapolating the Langmuir isotherms toward zero pressure. The determined area values are listed in Table 2. Monolayer data are in excellent agreement with the surface areas per molecule as determined from crystal structure analysis. The monolayer data show that the packing density of ligand **1** in the monolayer and in the crystal lattices of **2** and **3** are similar. The two-dimensional packing arrangement of **1** in the monolayer at low surface pressure ($\pi \sim 0.5$ mN/m) is presumably determined by the (highly solvated) polar carboxylate residues and the diffuse layer of Ca ions underneath the monolayer. The packing density of **1** in the crystal structure of compound **2** is almost identical to the corresponding value of the monolayer (~ 1.80 nm²/molecule) at the beginning of compression. We, therefore, suggest that *at low surface pressure* the monolayer mainly consists of oligomeric Ca complexes of **1** which rapidly form. These complexes are free-floating at the air–water interface and they can easily rearrange their relative positions in order to adapt to the rising surface pressure. Upon further compression the complexes start to approach each other until the critical van-der-Waals distance to their nearest neighbours is reached. The crystal structure of compound **3** in fact shows that a highly symmetrical, planar, close-packed arrangement of the hydrophobic *t*-butyl groups is feasible, although intuitively one may assume that the conical shape of the calix[4]arene ligand should introduce some curvature in the layer structure. However, the fact that the C_{4v} symmetry axes of the calix[4]arene units in the crystal structure of **3** are tilted by 18° against the plane normal gives us a hint that the packing affords a compromise between the most *symmetrical* and the most *dense* arrangement of conically shaped amphiphiles. Interestingly, the av. area/molecule of 1.33 nm² as calculated from the crystal data of compound **3** corresponds to a surface pressure value of ~ 6 mN/m in the monolayer. Assuming a similar arrangement of calix[4]arene ligands in the crystal structure and the monolayer, this would mean that a relatively high and constant, external pressure is required in order to force the calix[4]arene units into this periodic arrangement.

It should be noted that crystals of compound **3** in fact were grown under “hydrothermal” conditions, i.e. the solution was kept within firmly sealed test tubes and the re-crystallization temperature was allowed to exceed the boiling point of the solvent mixture.

We would like to stress the point that neither the isotherms of **1** monolayers on pure water nor on a Ca containing subphase indicate the formation of a liquid crystalline phase. While the local arrangement of calix[4]arene moieties in the monolayer and crystal structure might be similar, the monolayer phase clearly lacks the long range order of the crystalline material.

However, it is a common observation that crystalline monolayers composed of molecules which are structurally more complex than the most simple amphiphiles (e.g. monofunctional surfactants with a single saturated hydrocarbon chain) are hardly obtained. A possible reason for this might be that, in the present and related cases, the time frame for recording the Langmuir isotherms is insufficient in order to allow nucleation/growth of two-dimensional crystalline patches to proceed in the compressed monolayer.

CaCO₃ crystallization underneath monolayers

Crystallization of calcium carbonate underneath monolayers of **1** leads to formation of uniformly oriented calcite

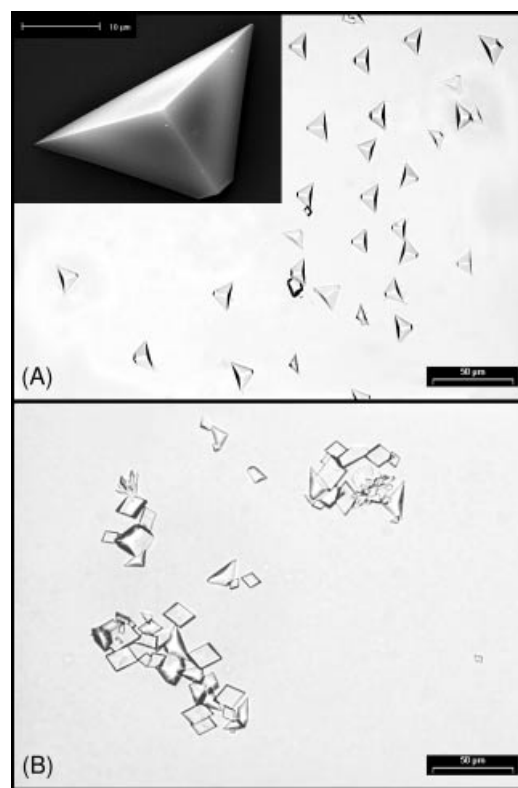


Fig. 8 Optical micrographs of calcite single crystals grown under a monolayer of **1** after 4 h. (A) $\pi = 0.1$ mN/m, CaCl₂/NaHCO₃ ($c = 9/18$ mM). The inset shows a scanning electron micrograph of a (012) oriented calcite single crystal grown under the same conditions. (B) $\pi = 6$ mN/m, CaCl₂/NaHCO₃ ($c = 9/18$ mM).

single crystals at low surface pressure ($\pi = 0.1 - 0.5$ mN/m) and a molecular area of $1.70 - 1.80$ nm². At a higher surface pressure ($\pi = 5 - 12$ mN/m) and a molecular area of $1.25 - 1.35$ nm² the calcite crystals grown underneath the monolayer lack any preferential orientation. Due to insufficient long-term stability of the monolayer at a surface pressure exceeding 20 mN/m, crystallization experiments under these conditions were impracticable.

Crystal growth was observed *in situ* by optical microscopy (Fig. 8). The orientation of calcite crystals was determined by X-ray powder diffraction and geometrical analysis. A more detailed description of the procedure is given elsewhere [7].

The calcite single crystals obtained at low surface pressure display the typical shape of truncated rhombohedrons (Fig. 8A and inset). The truncation occurs parallel to the {01.2} faces of the calcite crystal lattice [4, 12]. In contrast, the crystals which grow underneath the monolayer of **1** at a high surface pressure often possess the highly symmetrical shape of the calcite {10.4} cleavage rhombohedron (Fig. 8B). The nucleation density at high surface pressure is reduced (approximately 1/5) and the spacing between different calcite crystals attached to the monolayer is much less regular as compared to low surface pressure conditions. These observations indicate that at low surface pressure ($\pi = 0.1 - 0.5$ mN/m), the monolayer directs nucleation and growth of the calcite crystals while at higher surface pressure ($\pi = 5 - 12$ mN/m) crystal growth becomes inhibited [18].

Crystallization of (012) oriented calcite crystals has been reported for other self-assembled systems as well. These include polymeric Langmuir-Schaefer films of 10,12-pentacosadiynoic acid, [3d, 13] self-assembled monolayers of carboxylate-terminated alkanethiols supported on silver [4, 14] or Au substrates, [15] as well as hydrogen-bonded molecular ribbons consisting of N,N'-dioctadecyltriazine-2,4,6-triamine and a cyanuric acid derivative [3f]. The templating role of the monolayer has been interpreted in terms of geometrical lattice matching and stereochemical complementarity between the monolayer head groups and the (01.2) crystal plane attached to the monolayer.

We, too, have observed preferential crystallization of (01.2) oriented calcite crystals underneath a variety of structurally dissimilar monolayers. While in all of our investigations we have consistently employed monolayers of tetradentate amphiphilic macrocycles, the molecular structures of the compounds and their crystal packing arrangements differed significantly. Thus, monolayers of amphiphilic calix[4]arene derivatives which possess hydrophobic substituents of varying steric demands [7, this study] as well as amphiphilic resorc[4]arene derivatives (e.g. *rccc*-5,11,17,23-tetracarboxy-4,6,10,12,16,18,22,24-octa-*O*-methyl-2,8,14,20-tetra-(*n*-undecyl)resorc[4]arene, [16] which are structurally complementary to calix[4]arene ligands, uniformly led to the same orientation of calcite crystals. Since furthermore, the oriented growth of calcite single crystals underneath the monolayers always and exclusively

occurred at very low surface pressure, where the monolayers exist in a liquid-expanded state, an epitaxial correlation of the monolayer "lattice" and the {01.2} crystal plane might in fact be ruled out. Our experiments indicate that a low surface pressure is a necessary condition for the growth of uniformly oriented calcite crystals. Under these conditions the amphiphilic molecules in the monolayer may freely rearrange in order to minimize the lattice mismatch with the nucleating crystal face, thereby reducing the interfacial tension of the system [17]. We suggest that non-specific electrostatic effects such as the average charge density or the mean dipole moment of the monolayer determine the orientation of crystals [7, 18]. In fact in all of our investigations, the growth of (01.2) oriented calcite crystals occurred at a surface area corresponding to $1.70 - 1.80$ nm²/molecule which leads to an av. density of $2.22 - 2.35$ carboxylate residues/nm². This hypothesis is further supported by our recent investigations [19] on calcium carbonate growth underneath monolayers of *rccc*-4,6,10,12,16,18,22,24-octa-*O*-(carboxymethyl)-2,8,14,20-tetra-(*n*-undecyl)resorc[4]arene, where a change in the number of coordinating residues per molecule (8 instead of 4) leads to a completely different calcium carbonate growth characteristics (*vide infra*). Efforts are currently undertaken to analyze the particular growth orientation of calcium carbonate crystals in this and likewise systems.

Experimental Section

Melting points were determined with a Electrothermal melting point apparatus and were uncorrected. FT-IR spectra were recorded from KBr pellets on a Shimadzu FTIR-8300 spectrometer. ¹H and ¹³C NMR spectra were recorded on a Bruker DRX 500 spectrometer in DMSO-*d*₆ at room temperature with residual solvent.

Mass spectra were recorded with a Micromass VG Autospec X, Voyager DE spectrometer. Elemental analysis were carried out with a Perkin-Elmer 240 elemental analyzer. All reagents were reagent grade and used without further purification.

5,11,17,23-tetra-*t*-butyl-25,26,27,28-tetrakis-(carboxymethoxy)calix[4]arene (**1**):

The product was prepared according to a slightly modified literature procedure [20]. To a solution of 5,11,17,23-tetra-*t*-butyl-25,26,27,28-tetrakis(ethoxycarbonylmethoxy) calix[4]arene (0.495 g, 0.5 mmol) in tetrahydrofuran (30 mL) was added an aqueous solution of tetramethylammonium hydroxide (25%, 12.8 mL, 35.4 mmol) and the suspension was heated under reflux. After 24 h the suspension was concentrated under reduced pressure, the residue was dissolved in chloroform (20 mL), rinsed with hydrochloric acid (2 × 20 mL) and water (5 × 20 mL). The organic layer was concentrated *in vacuo* and the crude product was re-crystallized from acetonitrile (3 × 100 mL) to give the final product in 70% yield: m.p. 270-272 °C (CH₃CN);

IR (cm⁻¹): $\bar{\nu} = 3412, 2961, 1735, 1480, 1242, 1192, 1129, 1057, 870$.

¹H NMR (DMSO-*d*₆, 500 MHz) $\delta = 6.94$ (s, 8H, ArH), 4.76 (d, 4 H (ArCH₂)), 4.58 (s, 8 H, CH₂COO), 3.22 (d, 4 H, ArCH₂), 1.55 (s, 3 H, CH₃CN), 1.05 (s, 36 H, CH₃).

¹³C-NMR (125 MHz) δ = 171.00 (CH₂COO), 152.36 (ArCO), 145.27 (ArCtBu), 133.45 (ArCH), 125.41 (ArCCH₂), 118.08 (CH₃CN), 71.77 (OCH₂), 33.70 (CH₂Ar), 31.22 (C(CH₃)₃), 30.85 (C(CH₃)₃).

MALDI-MS (matrix 2,5-dihydroxybenzoic acid): m/z = 904 [M⁺ + Na, 100%]; **Elemental analysis** calc. for C₅₂H₆₀O₁₂ · CH₃CN: C 69.95, H 7.42, N 1.54; found: C 69.93, H 7.18, N 1.54%.

[Ca(C₅₂H₆₀O₁₂)₂Ca(H₂O)₂(CH₃OH)₃Ca(H₂O)₂-(CH₃OH)₂·12CH₃OH·4H₂O (2)

5,11,17,23-tetra-*t*-butyl-25,26,27,28-tetrakis(carboxymethoxy)-calix[4]arene (44 mg, 0.05 mmol) and calcium hydroxide (11 mg, 0.15 mmol) were suspended in MeOH abs. (30 mL). The suspension was treated ultrasonically and filtered into a 6 well NUNC multidish with 6 wells. Into each well H₂O (200 μ L) was introduced, the wells were covered with parafilm, and the parafilm was punctured by a needle. The multidish was placed in a sealed desiccator containing a beaker filled with H₂O. Single crystals of **2** grew within a period of 24h.

[Ca(C₅₂H₆₀O₁₂)Ca(H₂O)_{2.5}(MeOH)_{0.5}_n·7H₂O·CH₃OH (3)

5,11,17,23-tetra-*t*-butyl-25,26,27,28-tetrakis(carboxymethoxy)-calix[4]arene (44 mg, 0.05 mmol) and calcium hydroxide (11 mg, 0.15 mmol) were suspended in H₂O (10 mL). The suspension was treated ultrasonically and centrifuged. The pellet was suspended in H₂O (10 mL), treated ultrasonically and was centrifuged. The wet residue was dissolved in MeOH abs. (6 mL) and crystallized at 90 °C. Colourless crystals were obtained after 5 days.

IR (cm⁻¹): $\tilde{\nu}$ 3414, 2959, 1616, 1475, 1425, 1333, 1242, 1192, 1126, 1018, 943, 872, 829.

(IR spectra of **2** and **3** are virtually indistinguishable).

X-Ray Structure Analysis

Details of structure refinement and X-ray crystallographic data are provided as supplementary information. Crystallographic data (excluding structure factors) for the structure reported in this paper have been deposited at the Cambridge Crystallographic Data Centre as supplementary publication CCDC no. 216527 (compound **2**) and CCDC no. 216528, (compound **3**), respectively. Copies of the data can be obtained free of charge on application to CCDC, 12 Union Road, Cambridge CB21EZ (Fax: (+44)1223-336-033; e-mail: deposit@ccdc.cam.ac.uk).

Monolayer Investigations

Monolayer experiments were performed with a double-barrier NIMA trough using a compression speed of 15 cm²/min. The surface pressure of the monolayers was measured using a Wilhelmy plate. The surfactant was spread using a chloroform solution (10 μ L, 0.5 mg/mL). Compression was started after 10 min.

CaCO₃ Crystal Growth Experiments

Solutions of calcium bicarbonate were prepared by bubbling carbon dioxide gas through a stirred aqueous (Millipore water, resistance 18.2 M Ω ·cm) solution of CaCl₂/NaHCO₃ (c = 9/18 mM) for a period of 2 h. Compressed films were formed by adding known amounts of surfactant to generate a liquid- or solid-like film at the air-water interface. Crystals were studied after several times either *in situ* by optical microscopy (Olympus IX 70) or on cover slips laid on the film. The cover slips were also mounted on scanning

electron microscope (SEM) specimen tubs. A Phillips XL30 ESEM operating at 30 keV was used. The calcite crystals were sputtered with Au prior to examination.

Bulk samples for X-ray diffraction (XRD) were obtained by collecting the crystals on cover slips laid on the film and removed horizontally. A Philips PW 1050/70 X-ray powder diffractometer was employed (2θ scans, Bragg-Brentano para-focussing geometry) using CuK α radiation (λ = 1.54 Å).

Crystallographic indices are presented in three-index (*hkl*) notation, based on the hexagonal setting of the calcite unit cell ($R\bar{3}c$, a = 4.96 Å, c = 17.002 Å).

Acknowledgements. D.V. thanks the DFG for a Habilitanden fellowship. M.F. thanks the Graduiertenförderung Nordrhein-Westfalen for a graduate fellowship. This work was financially supported by the Deutsche Forschungsgemeinschaft (DFG Schwerpunktprogramm 1117, "Prinzipien der Biomineralisation"; DFG grant Vo829/2-1).

References

- [1] a) H. A. Lowenstam, S. Weiner, *On Biomineralization*, Oxford University Press, Oxford **1989**; b) S. Mann, *Biomineralization. Principles and Concepts in Bioinorganic Materials Chemistry*, Oxford University Press, Oxford, **2001**; c) L. Addadi, S. Weiner, *Angew. Chem., Int. Ed. Engl.* **1992**, *31*, 153–169; d) L. Addadi, S. Weiner, *Proc. Natl. Acad. Sci. U.S.A.* **1985**, *82*, 4110–4114; e) S. Weiner, L. Addadi, *J. Mater. Chem.* **1997**, *7*, 689–702; f) A. M. Belcher, X. H. Wu, R. J. Christensen, P. K. Hansma, G. D. Stucky, D. E. Morse, *Nature* **1996**, *381*, 56–58.
- [2] a) S. Mann, *Biomimetic Materials Chemistry*, VCH, Weinheim **1996**; b) H. Rapaport, I. Kuzmenko, M. Berfeld, K. Kjaer, J. Als-Nielsen, R. Popovitz-Biro, I. Weissbuch, M. Lahav, L. Leiserowitz, *J. Phys. Chem. B* **2000**, *104*, 1399–1424; c) S. Mann, D. D. Archibald, J. M. Didymus, T. Douglas, B. R. Heywood, F. C. Meldrum, N. J. Reeves, *Science* **1993**, *261*, 1286–1292; d) B. R. Heywood, S. Mann, *Adv. Mater.* **1994**, *6*, 9–20; e) E. Dujardin, S. Mann, *Adv. Mater.* **2002**, *14*, 775–788.
- [3] a) S. Mann, B. R. Heywood, S. Rajam, J. D. Birchall, *Nature* **1988**, *334*, 692–695; b) S. Rajam, B. R. Heywood, J. B. A. Walker, S. Mann, R. J. Davey, J. D. Birchall, *J. Chem. Soc., Faraday Trans.* **1991**, *87*, 727–734; c) B. R. Heywood, S. Mann, *Chem. Mater.* **1994**, *6*, 311–318; d) A. Berman, D. J. Ahn, A. Lio, M. Salmeron, A. Reichert, D. Charych, *Science* **1995**, *269*, 515–518; e) G. Xu, N. Yao, I. A. Aksay, J. T. Groves, *J. Am. Chem. Soc.* **1998**, *120*, 11977–11985; f) S. Champ, J. A. Dickinson, P. S. Fallon, B. R. Heywood, M. Mascal, *Angew. Chem. Int. Ed. Engl.* **2000**, *39*, 2716–2719; g) P. J. J. A. Buijnsters, J. J. J. M. Donners, S. J. Hill, B. R. Heywood, R. J. M. Nolte, B. Zwanenburg, N. A. J. M. Sommerdijk, *Langmuir* **2001**, *17*, 3623–3628; h) E. DiMasi, V. M. Patel, M. Sivakumar, M. J. Oltsza, Y. P. Yang, L. Gower, *Langmuir* **2002**, *18*, 8902–8909.
- [4] a) J. Aizenberg, A. J. Black, G. M. Whitesides, *J. Am. Chem. Soc.* **1999**, *121*, 4500–4509; b) J. Küther, G. Nelles, R. Seshadri, M. Schaub, H. J. Butt, W. Tremel, *Chem. Eur. J.* **1998**, *4*, 1834–1842; c) D. D. Archibald, S. B. Qadri, B. P. Gaber, *Langmuir* **1996**, *12*, 538–546.
- [5] a) L. Addadi, J. Moradian, E. Shay, N. G. Maroudas, S. Weiner, *Proc. Natl. Acad. Sci. U.S.A.* **1987**, *84*, 2732–2736; b)

- S. R. Letellier, M. J. Lochhead, A. A. Campbell, V. Vogel, *Biochim. Biophys. Acta* **1998**, *1380*, 31–45.
- [6] L. Addadi, S. Weiner, in: *Biomineralization*, S. Mann (ed), VCH, Weinheim **1989**, pp. 133–156.
- [7] D. Volkmer, M. Fricke, D. Vollhardt, S. Siegel, *J. Chem. Soc., Dalton Trans.* **2002**, 4547–4554.
- [8] D. Volkmer in *Encyclopedia of Separation Science*, M. Cooke, C.F. Poole (eds.), Vol. 2 (Crystallization), Academic Press **2000**, pp. 940–950.
- [9] P.M. Harrison, P. Arosio, *Biochim. Biophys. Acta* **1996**, *1275*, 161–203.
- [10] H. Ti Tien, in: *Thin Liquid Films*, I. B. Ivanov (ed), *Surfactant Science Series*, Vol. 29, **1988**, pp. 927–1057.
- [11] a) V. A. Arsentiev and J. Leja, in: *Colloid and Interface Science*, M. Kerker, (ed), Vol. 5, Academic Press, New York **1976**, pp. 251–270; b) G.T. Barnes, in: *Colloid Science*, D.H. Everett (ed), Vol. 2, Chemical Society, London 1975, pp. 173–190.
- [12] S. J. Cooper, R. B. Sessions, S. D. Lubetkin, *J. Am. Chem. Soc.* **1998**, *120*, 2090–2098.
- [13] J. Ahn, A. Berman, D. Charych, *J. Phys. Chem.* **1996**, *100*, 12455–12461.
- [14] J. Aizenberg, Y.-J. Han, *J. Am. Chem. Soc.* **2003**, *125*, 4032–4033.
- [15] A. M. Travaille, J. J. J. M. Donners, J. W. Gerritsen, N. A. J. M. Sommerdijk, R. J. M. Nolte, H. van Kempen, *Adv. Mater.* **2002**, *14*, 492–495.
- [16] D. Volkmer, M. Fricke, C. Agena, J. Mattay, *Cryst. Eng. Commun.* **2002**, *4*, 288–295.
- [17] S. J. Cooper, R. B. Sessions, S. D. Lubetkin, *Langmuir* **1997**, *13*, 7165–7172.
- [18] a) M. J. Lochhead, S. R. Letellier, V. Vogel, *J. Phys. Chem. B* **1997**, *101*, 10821–10827; b) P. Calvert, S. Mann, *Nature* **1997**, *386*, 127–129.
- [19] D. Volkmer, M. Fricke, unpublished results.
- [20] S.-K. Chang, I. Cho, *J. Chem. Soc., Perkin Trans. I* **1986**, 211–214.
- [21] D. Volkmer, M. Fricke, unpublished results.

Submitted as FULL PAPER to *Mater. Sci. Eng. C*

Paper presented at NATO ASI

“Learning From Nature How to Design New Implantable Biomaterials:
From Biomineralization Fundamentals to Biomimetic Materials and Processing Routes”
13th to 24th October 2003, Alvor, Algarve Portugal

**Elucidating the Role of Charge Density on the Growth of CaCO₃ Crystals Underneath
Calix[4]arene Monolayers**

Dirk Volkmer,^{*a} Marc Fricke,^a Michael Gleiche^b and Lifeng Chi^b

* Author for correspondence

^a PD Dr. D. Volkmer, Dipl.-Chem. M. Fricke
Faculty of Chemistry (AC1)
University of Bielefeld
D-33501 Bielefeld (Germany)
P.O. Box 100 131
Telephone: (+49) 521-106 6142
Fax: (+49) 521-106 6003
E-mail: dirk.volkmer@uni-bielefeld.de

^b PD Dr. L. Chi, Dr. M. Gleiche
Faculty of Physics (Interface Physics)
University of Münster

Abstract. The amphiphilic 5,11,17,23-tetrakis-(1,1,3,3-tetramethylbutyl)-25,26,27,28-tetra(2-hydroxyethoxy)calix[4]arene (**1**) forms stable monolayers at the air-water interface. The growth of CaCO₃ crystals underneath monolayers of (**1**) is strongly inhibited, in contrast to the corresponding carboxylic acid derivative 5,11,17,23-tetrakis-(1,1,3,3-tetramethylbutyl)-25,26,27,28-tetra(carboxymethoxy)calix[4]arene (**2**), the monolayers of which lead to growth of preferentially oriented calcite single crystals. The growth morphology of CaCO₃ crystals is correlated with the phase behaviour and surface potential of the monolayers. The investigations demonstrate that the average charge density is the dominant factor for heterogeneous nucleation of CaCO₃ crystals at the calixarene monolayer / solution interface.

Keywords: Calix[4]arenes; Monolayers; Surface Potential; Calcite; Biomineralization

D. Volkmer*, M. Fricke, M. Gleiche and L. Chi

Introduction

Crystallization of inorganic solids at the surfaces of biological tissues is an important step in biomineralization. [1] However, the natural processes that control the formation of a particular crystal polymorph or morphology yet are poorly understood. Artificial matrices such as Langmuir monolayers, [2] self-assembled monolayers (SAMs) [3] and polymer thin films [4] have been employed in order to gain insights into the putative mechanisms of template-directed mineralization. Physicochemical parameters such as interfacial electrostatics, [5] hydrogen bonding [3, 5] and interfacial molecular recognition events including geometrical lattice matching [2, 6] and stereochemical complementarity [3, 7] are considered crucial factors in this context. More recently, kinetic effects were discussed on the basis of *in-situ* grazing incidence X-ray diffraction experiments.[8] However, few studies have attempted to quantify the influence of electrostatic interactions on heterogeneous crystal nucleation employing suitable model systems such as Langmuir monolayers.[9]

In our previous work we have reported on calcite single crystals growing underneath monolayers of tetracarboxy-calix[4]arenes (**2**) [10] and tetracarboxy-resorc[4]arenes (**3**) (Scheme 1). [11] Monolayers of **2** and **3** both lead to formation of the same truncated calcite single crystals with their {01.2} crystal face attaching to the monolayer. Detailed investigations on the structures of **2** and **3** have shown that their supramolecular packing arrangements are quite different and thus a heteroepitaxial correlation between the charged headgroups of the monolayer and the (polar) CaCO₃ crystal face that attaches to the monolayer can be ruled out.

We have therefore suggested that macroscopic monolayer properties such as average charge density or mean dipole moment of the templating monolayer determine the orientation of CaCO₃ crystals. [10,11] In order to gain more insights into the interactions between dipolar monolayers and hydrated calcium and carbonate ions we now employ the non-charged amphiphilic 5,11,17,23-tetrakis-(1,1,3,3-tetramethylbutyl)-25,26,27,28-tetra(2-hydroxyethoxy)calix[4]arene (**1**), the monolayer of which strongly inhibits heterogeneous nucleation of CaCO₃ crystals. Monolayers of **1** and **2** were spread on aqueous subphases of different compositions and the resulting surface pressure–area (π –A) isotherms are analysed in terms of phase behaviour. The simultaneously recorded surface potential–area (ΔV –A)

isotherms reveal insights into the interactions between subphase ions and monolayer molecules. The monolayer structure of compound **1** is furthermore characterized by means of Brewster angle microscopy (BAM). The growth of calcite (CaCO_3) single crystals underneath monolayers of **1** and **2** is monitored *in situ* by optical microscopy.

Results and Discussion

Monolayer studies

Langmuir monolayers were formed on aqueous subphases by spreading compound **1** from trichloromethane/methanol (9:1) and **2** from trichloromethane solution using a Langmuir trough (NIMA 601BAM). The recorded surface pressure–area (π –A) isotherm provides information about monolayer stability and phase behaviour. The surface potential–area (ΔV –A) isotherm characterizes the pressure-dependent electrostatic properties of the monolayers. The measured surface potential attributes to the average orientation of amphiphilic (= dipolar) molecules in the monolayer. For monolayers built up from charged amphiphiles the solvation shell of water molecules, the first adlayer of counter ions, and the concentration gradient of ions perpendicular to the monolayer contribute to the surface potential, too. [12]

Remarkably, the surface potential technique often allows to investigate monolayer properties at a very early stage of compression when the surface pressure still is at 0 mN/m. Figure 1 shows the π –A and ΔV –A isotherms of compounds **1** and **2** spread on different aqueous subphases. Compound **1** forms relatively stable monolayers which collapse upon compression at a surface pressure of ~ 30 mN/m. The π –A isotherms gained from **1** on H_2O , and on 10 mM CaCl_2 , respectively, are almost identical indicating a similar monolayer phase behaviour on both subphases. The onset of the pressure increase starts at a surface value in between 180 and 185 $\text{\AA}^2/\text{molecule}$. The area per molecule of **1** in the monolayers is estimated from extrapolating the Langmuir isotherms toward zero pressure. The determined area values are listed in Table 1. The average area per molecule for compound **1** amounts to 170 – 180 \AA^2 which is significantly (10–15 %) larger than the corresponding value of the tetracarboxy-calix[4]arene **2**. While the area per molecule (145 – 150 \AA^2) of **2** as derived from the isotherm

data have been shown previously to be in excellent agreement with the area value calculated from molecular packing analysis of X-ray structural data, the high surface area of **1** is hard to rationalize. [10] The single crystal X-ray structure analysis reveals a typical structure motif which consists of interdigitated close packed monolayers of **1** extending in the (1 -1 0) crystal plane, in contrast to the bilayer motif frequently reported for other amphiphilic calixarenes. [13] Due to interdigitation of cone shaped calix[4]arenes the molecular surface area in the most densely packed crystal lattice plane is rather small ($144 \text{ \AA}^2/\text{molecule}$). The larger surface area determined from the Langmuir isotherm thus indicates that compound **1** forms a regular monolayer at the air-water interface with the hydrophilic residues uniformly pointing towards the aqueous subphase. A similar behaviour has been observed for monolayers of the octaacid *rccc*-4,6,10,12,16,18,22,24-octakis-*O*-(carboxymethyl)-2,8,14,20-tetra(*n*-undecyl)resorc[4]arene (**4**) and the corresponding alcohol *rccc*-4,6,10,12,16,18,22,24-octa(2-hydroxyethoxy)-2,8,14,20-tetra(*n*-undecyl)resorc[4]arene (**5**). [14]

At a surface pressure of $\sim 5 \text{ mN/m}$ a temperature-dependent phase transition occurs which is reproducible (Figure 1). At temperatures above 30°C the kink disappears and the surface pressure increases linearly (not shown). It should be noted that the average area per molecule (145 \AA^2) at the second kink at $\sim 32 \text{ mN/m}$ is in excellent agreement with the value derived from crystal structure analysis (144 \AA^2) of **1** while the value is sufficiently large to rule out formation of a multilayer. Thus the first broad plateau which is found at a surface pressure $> 32 \text{ mN/m}$ might indicate a second phase transition.

Temperature dependent measurements support this interpretation: The π -A isotherms demonstrate that the surface pressure at which the plateau occurs decreases with increasing temperature. At a surface pressure $> 35 \text{ mN/m}$ a second broad plateau occurs until the surface pressure increases again and the collapse pressure is reached at $\sim 45 \text{ mN/m}$ (not shown). A similar phase behaviour has been reported for monolayers of polyphenyl carboxylic acids.[15] However, a detailed analysis of the monolayer phase diagram of **1** is beyond the scope of this report.

BAM investigations corroborate that there is no difference in phase behaviour for monolayers of **1** spread on different subphases (H_2O and 10 mM CaCl_2). Figure 2 shows a sequence of

typical BAM images on CaCl_2 for selected pressure values. The BAM images show that at zero surface pressure a liquid-expanded phase forms (Figure 2a). At 5 mN/m a liquid-condensed phase can be observed where the film appears homogeneous (BAM image not shown). At ~ 15 mN/m the first bright spots appear which we currently ascribe to the partial crystallization of the monolayer (Figure 2b). Starting from a pressure of ~ 32 mN/m up to a pressure of ~ 35 mN/m the individual areas of the spots grow until they nearly cover the entire subphase at ~ 37 mN/m (Figure 2c).[16]

Surface potential measurements suggest that there are no specific interactions between the hydrophilic headgroup of **1** and the Ca ions in the aqueous subphase. The surface potential on water starts to rise at $\sim 190 - 195 \text{ \AA}^2/\text{molecule}$ and on CaCl_2 at $\sim 185 - 190 \text{ \AA}^2/\text{molecule}$, where the surface pressure still is at zero. The potential curve shows a steep increase finally reaching ΔV_0 values of about 255 mV on water and 270 mV on CaCl_2 .

The potential curve of **1** on H_2O shows a second point of inflection at a surface area of 180 \AA^2 which is coincident with the onset of pressure increase in the Langmuir isotherm thus indicating that a homogeneous monolayer has formed at this point. Thereafter, the increase of the potential curve is less steep until at the collapse pressure a limiting surface potential value is reached ($\Delta V_C = 325 \text{ mV}$ on H_2O and 340 mV on CaCl_2 , respectively).

Previously reported details on the monolayer characteristics of compound **2** are augmented here by surface potential measurements.[10] The π -A isotherm recorded from spreading **2** on a 10mM CaCl_2 subphase (Figure 1, bottom) shows a pronounced expansion effect, i.e. the mean molecular area of **2** is by 12 % larger than the corresponding value from the isotherm data of **2** on pure water. This behaviour is obviously due to electrostatic/coordinative interactions between Ca ions and the deprotonated carboxylic acid residues. Remarkably, the expansion effect is also observed in the supramolecular packing of **2** if the crystal structures of the free acid and its Ca complex are compared with each other (Table 1). [10]

The surface potential of **2** on water starts to rise at $\sim 155 - 160 \text{ \AA}^2/\text{molecule}$ and on CaCl_2 at $\sim 180 \text{ \AA}^2/\text{molecule}$, where the surface pressure still is at zero (Figure 1). The potential curves show a steep increase up to ΔV_0 values of about 200 mV on water and 490 mV on CaCl_2 , respectively. After the first point of inflexion the increase of the potential curve is less steep

until the final potential values are reached ($\Delta V_C = 310$ mV on H_2O and 775 mV on $CaCl_2$) and the Langmuir isotherms indicate that the monolayers collapse.

Two facts deserve special attention if the monolayers are compared to each other. First, it should be noticed that the surface potential curves of **1** and **2** on H_2O are virtually identical. The final surface potential values ΔV_C at the collapse point differ by only 15 mV which is within the experimental error (ca. ± 15 mV) of the surface potential measurements. In contrast, the ΔV_0 value of **1** is about 55 mV higher than that of **2** (H_2O subphase). A similar trend is observed for the monolayer data of the stearyl alcohol and stearic acid, respectively, [17] which demonstrates that at the air-water interface, amphiphilic cone-shaped calix[4]arenes such as **1** and **2** behave similar to simple monofunctional surfactants.

Second, a major difference between monolayers of **1** and **2** arises on aqueous subphases containing Ca ions. While the potential curve of **1** on 10mM $CaCl_2$ indicates no interaction between the monolayer and the ions from the aqueous subphase, the diagram of **2** (Figure 1) shows a huge jump of the surface potential: ΔV_C of **1** is 340 mV (10 mM $CaCl_2$) whereas ΔV_C of **2** amounts to 775 mV (10 mM $CaCl_2$), which is 465 mV higher than ΔV_C on H_2O . For comparison: the surface potential of stearic acid at collapse pressure is 345 mV (10 mM $CaCl_2$), as opposed to 285 mV (H_2O). The huge shift of the ΔV_C value of **2** on a Ca-containing subphase most likely attributes to the strong Ca affinity of **2**. Previous structural investigations have in fact shown that the octadentate ligand **2** readily forms a mononuclear Ca complex. [10] In this regard the amphiphilic calix[4]arene **2** behaves dissimilar to monofunctional surfactants where the low Ca affinity leads to formation of a diffuse adlayer of Ca ions underneath the monolayer. (Recent grazing incidence X-ray diffraction experiments of arachidate monolayers indicate that, on average, only one Ca ion is bound per 4–8 surfactant molecules.[8])

We conclude that formation of a Ca complex of **2** gives rise to a huge increase of surface potential which is not observed for the electrostatically neutral compound **1**. Upon compression the cone-shaped calix[4]arenes **1** and **2** both show an increase in surface potential indicative of a pressure-dependent co-orientation of molecular dipoles at the air–water interface. This behaviour once again is reminiscent to the monolayer properties of simple monofunctional surfactants which shows that amphiphilic calix[4]arenes can be

regarded as stiff molecular dipoles (the vector of the molecular dipole moment coincides with the pseudo C_{4v} symmetry axis of the molecule). The Langmuir isotherms of **1** and **2** furthermore show that, at the onset of pressure, both monolayers are in a liquid-expanded state where the arrangement of molecules is lacking a long-range order. [10] Whereas the monolayers of **2** do not show any indication of a phase transition until film collapse occurs, the phase behaviour of **1** at a pressure > 5 mN/m is more complex and the BAM investigations hint at formation of a highly ordered liquid condensed phase. GIXD investigations are currently underway to prove this assumption.

CaCO₃ crystallization underneath monolayers

Crystal growth was observed *in situ* by optical microscopy (Figure 3). The orientation of calcite crystals was determined by X-ray powder diffraction and geometrical analysis. A more detailed description of the procedure is given elsewhere. [10]

Upon spreading monolayers of **1** on a 9 mM Ca(HCO₃)₂ we observe a marked inhibition of CaCO₃ crystal nucleation. The calcite single crystals which grow underneath monolayers of **1** most often possess the highly symmetrical shape of the calcite {10.4} cleavage rhombohedron. A quantitative analysis of optical micrographs of CaCO₃ crystals grown underneath monolayers of **1**, or at the air-water interface (without monolayer), respectively, reveals a strong inhibition effect: the crystal density observed underneath monolayer of **1** is roughly 0.1 times that of the control experiment. Monolayers of stearyl alcohol or cholesterol show similar inhibition effects.[18] It is conceivable that the octadentate calix[4]arene derivative **1** might sequester a single Ca ion in a fashion similar to the carboxylic acid derivative **2**. Based on the surface potential measurements presented here, however, this assumption can be ruled out.

In contrast to the inhibition effect of **1**, uniformly oriented calcite single crystals form underneath monolayers of **2** at low surface pressure ($\pi = 0.1 - 0.5$ mN/m). The calcite single crystals obtained display the typical shape of truncated rhombohedrons (Figure 3b). The truncation occurs parallel to the {01.2} faces of the calcite crystal lattice. [10] The CaCO₃ crystal density underneath the monolayer of **2** is approximately 20 times that of the density underneath monolayers of **1** under the same experimental conditions and the spacing between

different calcite crystals which attach to the monolayer is highly regular. These observations indicate that monolayers of **2** at low surface pressure ($\pi = 0.1 - 0.5$ mN/m) direct nucleation and growth of calcite crystals while underneath monolayers of **1** crystal growth becomes inhibited. At higher surface pressure ($\pi = 5 - 25$ mN/m) non-truncated calcite rhombohedra form which lack any preferential orientation. The nucleation density at high surface pressure is reduced (approximately 1/5) and the spacing between different calcite crystals attached to the monolayer is much less regular as compared to the monolayer of **2** at low surface pressure.

Concluding Remarks

In this study we have examined electrostatic interactions between monolayers of structurally related amphiphilic calix[4]arene derivatives **1** and **2** and subphase ions by employing surface potential measurements. In the low pressure region ($\pi = 0.0 - 0.5$ mN/m) of the monolayer phase diagram the experimental ΔV_0 values for monolayers of **1** and **2** on H₂O are almost identical. On a Ca containing subphase (10 mM CaCl₂) ΔV_0 shows a significant increase only for monolayers of **2** which clearly demonstrates that calix[4]arene derivative **1** is unable to bind Ca ions by virtue of electrostatic and / or coordinative interactions.

Our experiments furthermore indicate that a low surface pressure ($\pi = 0.1 - 0.5$ mN/m) is a necessary condition for the growth of uniformly oriented calcite crystals.[19] The phase diagram of **2** and previous studies on the monolayer structure [10] show no indication of long range order in the monolayer, that is the x- any y-components of the molecular dipole-moments are laterally uncorrelated.

The templating role of monolayers has frequently been interpreted in terms of a geometrical and stereochemical complementarity between the arrangement of headgroups in the monolayer and the position of Ca ions in the crystal plane which attaches to the monolayer.[2-7, 20]

Our investigations, however, demonstrate that such delicate and complex interactions most likely vanish if structurally mobile template matrices such as monolayers are employed. Most probably non-specific electrostatic effects such as the average charge density or the mean dipole moment of the monolayer determine the orientation of crystals.[5, 21] In fact in all of our investigations conducted so far, the growth of (01.2) oriented calcite crystals occurred at a

surface area corresponding to 1.70 – 1.80 nm²/molecule which leads to an av. density of 2.22 – 2.35 carboxylate residues/nm². [22] This hypothesis is further supported by our recent investigations on calcium carbonate growth underneath monolayers of *rccc*-4,6,10,12,16,18,22,24-octa-*O*-(carboxymethyl)-2,8,14,20-tetra(*n*-undecyl)resorc[4]arene (**4**), where a change in the number of coordinating residues per molecule from four to eight corresponding to 4.71 – 5.00 carboxylate residues/nm² leads to a completely different CaCO₃ growth characteristics (*vide infra*). [23]

Future investigations will focus on crystallization on CaCO₃ underneath mixed monolayers of compounds **1** and **2**. By inserting a nucleation active oligoacid in a matrix of a structurally similar alcohol which inhibits crystal growth, we should be able to explore the lower limit of the charge density which still leads to formation of uniformly oriented calcite single crystals. A further attractive but rather demanding research target concerns the question as to whether or not a *single* molecule of an oligoacid can promote formation of a single CaCO₃ crystal nucleus. Structurally well-defined oligomeric acids such as **2** or **3** might turn out to be valuable model compounds in this regard.

Acknowledgements. D.V. thanks the DFG for a Habilitanden fellowship. M.F. thanks the Graduiertenförderung Nordrhein-Westfalen for a graduate fellowship. This work was financially supported by the Deutsche Forschungsgemeinschaft (DFG Schwerpunktprogramm 1117, “Prinzipien der Biomineralisation”; DFG grant Vo829/2). Donation of the starting material *p*-1,1,3,3-tetramethylbutylphenol by CONDEA Chemie GmbH (Marl, Germany) is gratefully acknowledged.

Experimental

Melting points were determined with a Electrothermal melting point apparatus and were uncorrected. FT-IR spectra were recorded from KBr pellets on a Shimadzu FTIR-8300 spectrometer. ^1H and ^{13}C NMR spectra were recorded on a Bruker DRX 500 spectrometer in CDCl_3 at room temperature with residual solvent. Elemental analysis were carried out with a Perkin-Elmer 240 elemental analyzer. All reagents were reagent grade and used without further purification.

5,11,17,23-Tetrakis-(1,1,3,3-tetramethylbutyl)-25,26,27,28-tetra(2-hydroxyethoxy)-calix[4]arene (1)

The product was prepared according to a slightly modified procedure.[24] To a stirred suspension of LiAlH_4 (1.3 molar excess with respect to the corresponding stoichiometric ratio) in 10 mL of dry THF was added dropwise a solution of 5,11,17,23-tetrakis-(1,1,3,3-tetramethylbutyl)-25,26,27,28-tetra(ethoxycarbonylmethoxy)calix[4]arene (250 mg, 0.21 mmol) in 10 mL dry THF. The reaction mixture was stirred for 12 h under an argon stream. The excess of LiAlH_4 was destroyed by careful addition of water and the solvent was evaporated under reduced pressure. The residue was diluted in chloroform and washed with sulphuric acid (3×30 mL, 10 %) and water (3×30 mL). The organic phase was evaporated under reduced pressure and the crude product was recrystallized from ethanol to give the desired product as crystalline solid. Mp. 240°C (ethanol).

IR (cm^{-1}): $\tilde{\nu}$ 3462, 2952, 1601, 1475, 1366, 1250, 1205, 1085, 1047, 866, 806.

^1H NMR (500 MHz, 25°C , TMS): δ = 6.80 (s, 8 H, ArH), 5.10 (s, 4 H, OH), 4.33 (d, $^2J = 12.6$ Hz, 4 H, ArCH₂), 3.97 (m, 8 H, OCH₂CH₂), 3.93 (m, 8 H, OCH₂CH₂) 3.19 (d, $^2J = 12.7$ Hz, 4 H, Ar-CH₂), 1.51 (s, 8 H, CCH₂C), 1.09 (s, 24 H, CH₃), 0.65 (s, 36 H, CH₃). ^{13}C NMR (125 MHz) δ = 152.4 (Ar 25,26,27,28-C), 145.0 (Ar 5,11,17,23-C), 133.2 (Ar 1,3,7,9,13,15,19,21-C), 126.3 (all ArC-H), 77.9 (ArOCH₂CH₂OH), 61.7 (ArOCH₂CH₂OH), 57.3 (CCH₂C), 37.9 (Ar-CCH₂), 32.3 (CH₂C), 31.6 (ArC(CH₃)₂), 31.1 (CH₂C(CH₃)₂), 30.6 (ArCH₂Ar). Elemental analysis calcd. for $\text{C}_{68}\text{H}_{104}\text{O}_8$: C 77.82, H 9.99; found: C 77.11, H 9.33.

5,11,17,23-Tetrakis-(1,1,3,3-tetramethylbutyl)-25,26,27,28-tetra(carboxymethoxy)-calix[4]arene (2):

Compound **2** was synthesized according to the procedure described in a previous paper.[10]

Monolayer Investigations

Monolayer experiments were performed with a double-barrier NIMA trough using a compression speed of 15 cm²/min in order to ensure reproducibility. The surface pressure of the monolayers was measured using a Wilhelmy plate. Langmuir monolayers were formed on aqueous subphases by spreading compound **1** from a trichloromethane/methanol (9:1) solution (50 µl, 0.5 mg/mL) and **2** from a trichloromethane solution (50 µl, 0.5 mg/mL). Compression was started after 10 min. Simultaneously, the surface potential was recorded using a vibrating plate located at ca. 2 mm above the water surface. The reference electrode, made from stainless steel, was placed in the aqueous subphase. Each isotherm was measured at least three times. Brewster angle microscopy were performed with a NIMA Langmuir trough (NIMA 601BAM) using a BAM-2 (NFT, Göttingen).

CaCO₃ Crystal Growth Experiments

Solutions of calcium bicarbonate were prepared by bubbling carbon dioxide gas through a stirred aqueous (double de-ionized H₂O, resistance 18.2 MΩ·cm) solution of CaCl₂/NaHCO₃ (c = 9/18 mM) for a period of 2 h. Compressed films were formed by spreading the solutions of surfactants in order to generate liquid-like films at the air-water interface. Crystals were studied after several times either *in situ* by optical microscopy (PZO Biolar upright microscope) or on cover slips laid on the film (Olympus IX70). Crystal growth experiments were repeated at least five times.

Crystallographic indices are presented in three-index (*hkl*) notation, based on the hexagonal setting of the calcite unit cell ($R\bar{3}c$, $a = 4.96 \text{ \AA}$, $c = 17.002 \text{ \AA}$).

Table 1 Area/molecule of calix[4]arene derivatives as determined from Langmuir isotherms and from crystal data

Compound	Area/molecule [nm ²]		Ref.
	Monolayer (subphase)	Crystal data (compound)	
1	1.70–1.75 (H ₂ O) ^a	1.44	this work, [13]
	1.70–1.75 (CaCl ₂) ^b	n.d.	this work
2	1.45–1.50 ^a	1.51 (4)	[10]
	1.65–1.70 ^b	1.70 (5)	[10]
3	1.65–1.70 ^a	1.60 (6)	[11]
	1.75–1.80 ^b	1.83 (7)	[11]

Compound index: **1**: C₆₈H₁₀₄O₈, **2**: C₆₈H₉₆O₁₂, **3**: C₆₈H₉₆O₁₂, **4**: C₆₈H₉₆O₁₂·4.75CH₃OH·0.25H₂O, **5**: [Ca(C₆₈H₉₂O₁₂Ca)(DMSO)₂(H₂O)]·2.5DMSO, **6**: C₈₄H₁₂₈O₁₆·(CH₃CN)_{1/8}, **7**: [Ca(C₈₄H₁₂₆O₁₆)(DMSO)₂(H₂O)₂]·(DMSO)·(H₂O)₄

n.d. = not determined

^a Double de-ionized water, resistance 18.2 MΩ·cm

^b Aqueous subphase containing CaCl₂, c = 10 mM

Figure Captions

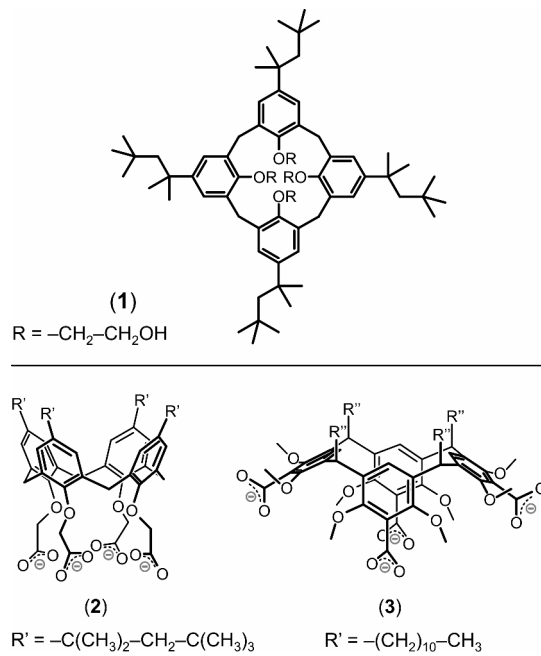
Scheme 1. Amphiphilic compounds used in the present and in previous investigations: 5,11,17,23-tetrakis-(1,1,3,3-tetramethylbutyl)-25,26,27,28-tetra(2-hydroxyethoxy)calix[4]arene (**1**), 5,11,17,23-tetrakis-(1,1,3,3-tetramethylbutyl)-25,26,27,28-tetra(carboxymethoxy)calix[4]arene (**2**), and *rccc*-5,11,17,23-tetracarboxy-4,6,10,12,16,18,22,24-octa-*O*-methyl-2,8,14,20-tetra(*n*-undecyl)resorc[4]arene (**3**).

Figure 1 From top row left to bottom row right: Surface pressure–area, π –A (dashed line) and surface potential–area, ΔV –A (solid line) isotherms of **1** on H₂O (22°C), **1** on CaCl₂ (c = 10 mM, 22°C; Point markers a–c refer to the corresponding BAM images in Figure 2), **2** on H₂O (22°C), and **2** on CaCl₂ (c = 10 mM, 22°C).

Figure 2 BAM micrographs of monolayers of **1** on 10 mM CaCl₂ at 22°C. Monolayer domains appear as light regions. Image (a) was recorded at zero surface pressure, image (b) at 32 mN/m, and image (c) at 37 mN/m. Size: 430 × 320 μm^2 .

Figure 3 Optical micrographs of calcite single crystals grown under a monolayer of **1** and **2** on CaCl₂/NaHCO₃ (c = 9/18 mM) after 6 h ($\pi = 0.1$ mN/m).

Figures



Scheme 1 (as to appear in the manuscript, width: 7.0 cm)

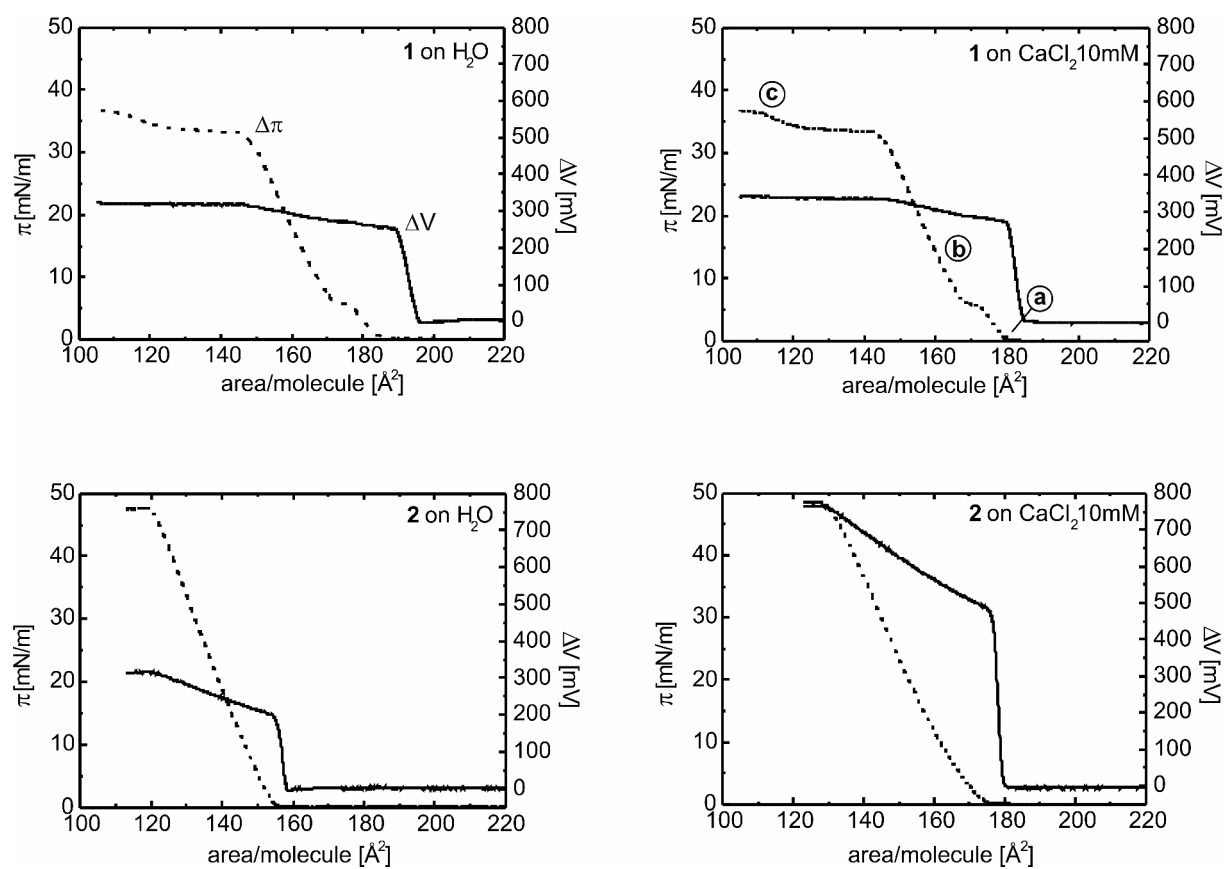


Figure 1 (as to appear in the manuscript, width: 16.0 cm)

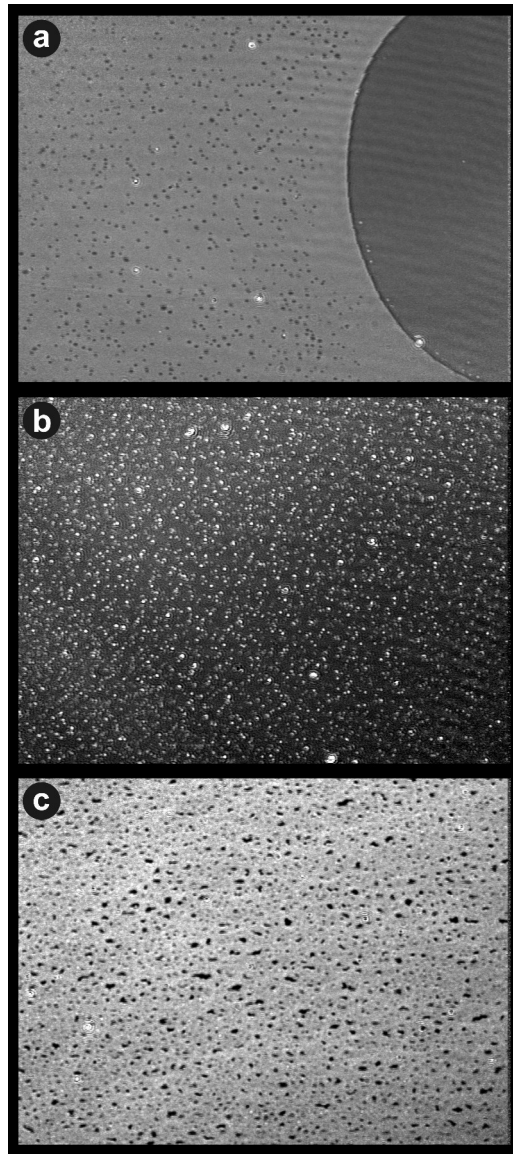


Figure 2 (as to appear in the manuscript, width: 6.8 cm)

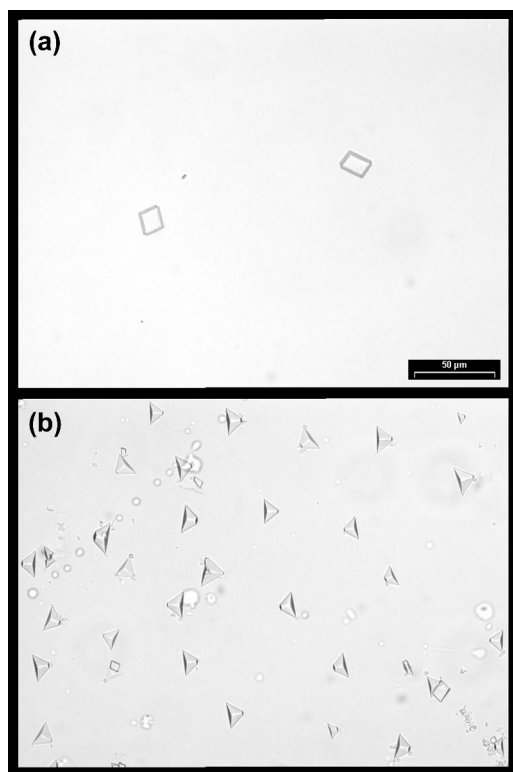


Figure 3 (as to appear in the manuscript, width: 6.8 cm)

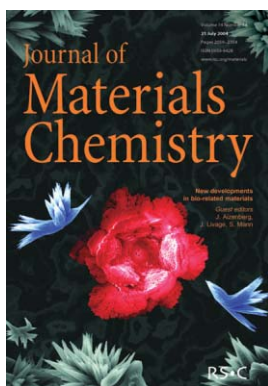
References

- [1] a) H. A. Lowenstam, S. Weiner, *On Biomineralization*, Oxford University Press, Oxford 1989; b) S. Mann, *Biomineralization. Principles and Concepts in Bioinorganic Materials Chemistry*, Oxford University Press, Oxford, 2001.
- [2] a) S. Mann, B. R. Heywood, S. Rajam, J. D. Birchall, *Nature* 334 (1988) 692; b) S. Champ, J. A. Dickinson, P. S. Fallon, B. R. Heywood, M. Mascal, *Angew. Chem. Int. Ed. Engl.* 39 (2000) 2716; c) P. J. J. A. Buijnsters, J. J. J. M. Donners, S. J. Hill, B. R. Heywood, R. J. M. Nolte, B. Zwanenburg, N. A. J. M. Sommerdijk, *Langmuir* 17 (2001) 3623.
- [3] a) J. Aizenberg, A. J. Black, G. M. Whitesides, *Nature* 398 (1999) 495; b) J. Küther, G. Nelles, R. Seshadri, M. Schaub, H. J. Butt, W. Tremel, *Chem. Eur. J.* 4 (1998) 1834; c) D. D. Archibald, S. B. Qadri, B. P. Gaber, *Langmuir* 12 (1996) 538.
- [4] a) A. Berman, D. J. Ahn, A. Lio, M. Salmeron, A. Reichert, D. Charych, *Science* 269 (1995) 515; b) H. Cölfen, M. Antonietti, *Langmuir* 14 (1998) 582.
- [5] a) L. Addadi, J. Moradian, E. Shay, N. G. Maroudas, S. Weiner, *Proc. Natl. Acad. Sci. U.S.A.* 84 (1987) 2732; b) S. R. Letellier, M. J. Lochhead, A. A. Campbell, V. Vogel, *Biochim. Biophys. Acta* 1380 (1998) 31.
- [6] S. Mann, D. D. Archibald, J. M. Didymus, T. Douglas, B. R. Heywood, F. C. Meldrum, N. J. Reeves, *Science* 261 (1993) 1286.
- [7] a) L. Addadi, S. Weiner, in: *Biomineralization*, S. Mann (ed), VCH, Weinheim 1989, pp. 133–156; b) J. Aizenberg, A. J. Black, G. M. Whitesides, *J. Am. Chem. Soc.* 121 (1999) 4500.
- [8] E. DiMasi, M. J. Oltsza, V. M. Patel, L. Gower, *CrystEngComm* 5 (2003) 346.
- [9] M. J. Lochhead, S. R. Letellier, V. Vogel, *J. Phys. Chem. B* 101 (1997) 10821.
- [10] D. Volkmer, M. Fricke, D. Vollhardt, S. Siegel, *J. Chem. Soc., Dalton Trans.* (2002) 4547.
- [11] D. Volkmer, M. Fricke, C. Agena, J. Mattay, *CrystEngComm* 4 (2002) 288.
- [12] a) D. M. Taylor, *Adv. Colloid. Interface. Sci.* (87) 2000 183; (b) P. Dynarowicz-Latka, A. Dhanabalan, O. N. Oliveira, Jr., *Adv. Colloid Interface Sci.* 91 (2001) 221.
- [13] Crystal data of **1**: monoclinic, space group $C2/c$; $Z = 4$, $a = 25.8237(13)$, $b = 12.2123(6)$, $c = 21.1292(10)$ Å; $\beta = 108.715(1)^\circ$. Details on the crystal structure will be reported elsewhere.

-
- [14] K. Ichimura, M. Fujimaki, Y. Matsuzawa, Y. Hayashi, M. Nakagawa, *Mater. Sci. Eng. C* 8-9 (1999) 353.
- [15] P. Dynarowicz-Latka, A. Dhanabalan, A. Cavalli, O. N. Oliveira, Jr., *J. Phys. Chem.* 104 (2000) 1701.
- [16] W. He, D. Vollhardt, R. Rudert, L. Zhu, J. Li, *Langmuir* 19 (2003) 385.
- [17] The ΔV_C value of a stearyl alcohol monolayer on H₂O (400 mV) is 115 mV higher than that of a stearic acid monolayer (285 mV). a) O. N. Oliveira, Jr., C. Bonardi, *Langmuir* 13 (1997) 5920; b) V. Vogel, *Struktur und Dynamische Eigenschaften von Monomolekularen Lipidfilmen*, PhD Thesis, Johann Wolfgang Goethe Universität, Frankfurt, 1987.
- [18] S. Rajam, B. R. Heywood, J. B. A. Walker, S. Mann, R. J. Davey, J. D. Birchall, *J. Chem. Soc., Faraday Trans.* 87 (1991) 727.
- [19] S. J. Cooper, R. B. Sessions, S. D. Lubetkin, *J. Am. Chem. Soc.* 120 (1998) 2090.
- [20] a) B. R. Heywood, S. Mann, *Chem. Mater.* 6 (1994) 311; b) I. Weissbuch, M. Lahav, L. Leiserowitz, *Crystal Growth Design* 3 (2003) 125.
- [21] P. Calvert, S. Mann, *Nature* 386 (1997) 127.
- [22] D. Volkmer, M. Fricke, *Z. Anorg. Allg. Chem.* 626 (2003) 2381.
- [23] D. Volkmer, M. Fricke, C. Agena, J. Mattay, *J. Mater. Chem.*, in press.
- [24] S. E. Matthews, P. Schmitt, V. Felix, M. G. B. Drew, P. D. Beer, *J. Am. Chem. Soc.* 124 (2002) 1341.

Journal of Materials Chemistry

Take a look!
Hot Articles
www.rsc.org/materials/hot



New developments in bio-related materials Guest editors J. Aizenberg, J. Livage, S. Mann

Cover: See Dirk Volkmer, Marc Fricke, Ceno Agena and Jochen Mattay, pp. 2249–2259. The pictures show polycrystalline CaCO_3 crystals grown underneath monolayers of a resorcinarene octaacid. The red and blue colours of the specimens relate to different luminescence colours that Mn-doped CaCO_3 crystals show upon irradiation with UV light which allows one to distinguish between the different polymorphs. In a broader sense, the image tries to symbolize the narrow ridge between art and science in the flourishing field of bio-inspired materials.
Image reproduced by permission of Dirk Volkmer.
© Dirk Volkmer 2004



contents

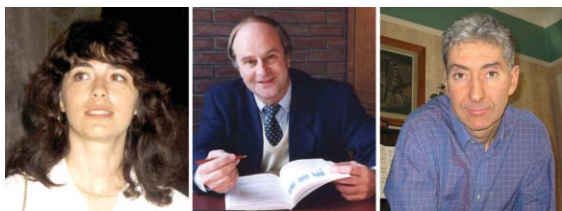
EDITORIAL

E5 E6

New developments in bio-related materials

J. Aizenberg, J. Livage and S. Mann

Guest editors J. Aizenberg, J. Livage and S. Mann give an overview of the second special issue of 2004 in *Journal of Materials Chemistry* on New Developments in Bio-related Materials.



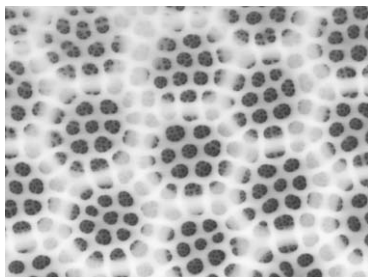
FEATURE ARTICLES

2059 2065

Silica formation in diatoms: the function of long-chain polyamines and silaffins

Manfred Sumper and Nils Kröger

Unique polyamine-modified peptides are involved in formation of the stunning, intricate biosilica structures of diatoms.



Interfacial electrostatics guiding the crystallization of CaCO₃ underneath monolayers of calixarenes and resorcarenes†

Dirk Volkmer,^{*a} Marc Fricke,^a Ceno Agena^b and Jochen Mattay^b

^aFaculty of Chemistry (AC1), University of Bielefeld, P.O. Box 100 131, D-33501 Bielefeld, Germany. E-mail: dirk.volkmer@uni-bielefeld.de

^bFaculty of Chemistry (OC1), University of Bielefeld, P.O. Box 100 131, D-33501 Bielefeld, Germany.

Received 1st March 2004, Accepted 6th April 2004

First published as an Advance Article on the web 27th May 2004

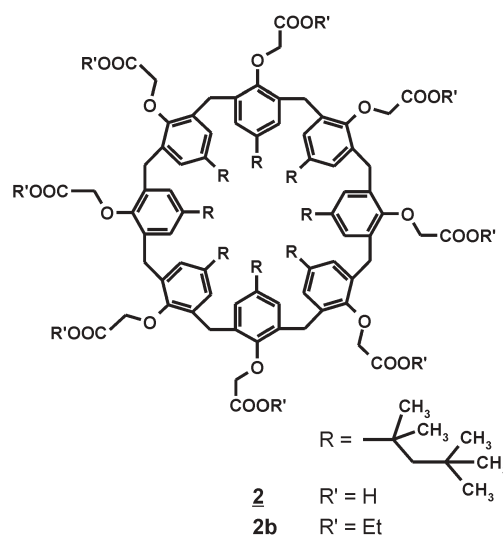
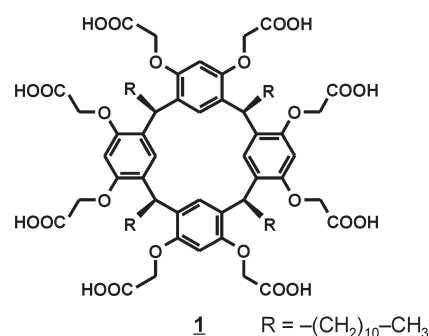
The amphiphilic octaacids *rccc*-4,6,10,12,16,18,22,24-octakis-*O*-(carboxymethyl)-2,8,14,20-tetra(*n*-undecyl)resorc[4]arene (**1**) and 5,11,17,23,29,35,41,47-octakis(1,1,3,3-tetramethylbutyl)-49,50,51,52,53,54,55,56-octa(carboxymethoxy)calix[8]arene (**2**) form stable monolayers at the air–water interface which induce growth of CaCO₃ crystals at the monolayer–solution interface. Uniformly (012) oriented rhombohedral calcite single crystals grow underneath a monolayer of **2**, whereas crystallization under a monolayer of **1** preferentially leads to formation of acicular aggregates of aragonite crystals. While polymorph selection and orientations of the CaCO₃ crystals critically depend on the average charge density of the monolayer, the molecular shape and the particular Ca coordination behaviour of the amphiphiles that form the monolayer are of minor importance. CaCO₃ crystal growth underneath monolayers of macrocyclic amphiphiles is briefly reviewed and the present experimental observations are compared to previous related investigations on “template-induced” biomimetic mineralization.

Introduction

Crystallization of inorganic solids at self-organized surfaces is an important process in biomineralization¹ and crystal engineering.² Nucleation and growth steps taking place at the interface are often specific and result in a particular crystal polymorph or morphology.³ However, the natural processes that control mineral formation are, as yet, poorly understood. Artificial matrices such as Langmuir monolayers,⁴ self-assembled monolayers (SAMs),⁵ and polymers⁶ have been employed in order to gain insights into the putative mechanisms of template-directed mineralization. Physical parameters such as interfacial electrostatics^{2,4,7} hydrogen bonding^{3,5} and interfacial molecular recognition events including geometrical lattice matching^{2,3} and stereochemical complementarity⁸ are considered crucial factors in this context.

Calcium carbonate is the most abundant crystalline biomineral. Three stable CaCO₃ polymorphs—calcite, aragonite and vaterite—exist, all of which occur in calcified tissues. In order to mimic structural aspects of the interactions between acidic proteins and biogenic CaCO₃ in calcified tissues (*e.g.* mollusk shells) we employ Langmuir monolayers of macrocyclic oligoacids as biologically inspired supramolecular templates for crystal growth.

In previous studies we have reported on the growth of uniformly (012) oriented calcite single crystals underneath structurally diverse monolayers of tetracarboxy-calix[4]arenes⁹ and tetracarboxy-resorc[4]arenes.¹⁰ We have suggested that non-specific electrostatic effects such as charge density or mean dipole moment of the monolayer molecules determine the orientation of crystals. In order to further support this hypothesis we present here investigations on the crystallization of CaCO₃ underneath monolayers of two macrocyclic octacarboxylic acids (Scheme 1)



Scheme 1 Structural formulae of *rccc*-4,6,10,12,16,18,22,24-octakis-*O*-(carboxymethyl)-2,8,14,20-tetra(*n*-undecyl)resorc[4]arene (**1**) and 5,11,17,23,29,35,41,47-octakis(1,1,3,3-tetramethylbutyl)-49,50,51,52,53,54,55,56-octa(carboxymethoxy)calix[8]arene (**2**). (Compound **2b** is the ethyl ester derivative of **2**).

† Electronic supplementary information (ESI) available: representative optical and scanning electron micrographs of CaCO₃ crystals grown underneath a monolayer of **1** at low surface pressure; additional crystallographic data including numbering schemes, tables and refinement details. See <http://www.rsc.org/suppdata/jm/b4/b403132f>

with different surface charge densities, namely *rccc*-4,6,10,12,16,18,22,24-octakis-*O*-(carboxymethyl)-2,8,14,20-tetra(*n*-undecyl)resorc[4]arene (**1**) and 5,11,17,23,29,35,41,47-octakis(1,1,3,3-tetramethylbutyl)-49,50,51,52,53,54,55,56-octa(carboxymethoxy)calix[8]arene (**2**). We describe an improved synthesis and the crystal structures of **1** and **2b** [5,11,17,23,29,35,41,47-octakis(1,1,3,3-tetramethylbutyl)-49,50,51,52,53,54,55,56-octa(ethoxycarbonylmethoxy)calix[8]arene, the ethyl ester of **2**. The dynamic macroscopic monolayer structure of **2** is characterized by means of Brewster angle microscopy (BAM). The growth of CaCO₃ crystals underneath monolayers of **1** and **2** is monitored *in situ* by (polarization) optical microscopy. Analysis of CaCO₃ growth morphologies is based on scanning electron microscopy and X-ray diffraction experiments. Using UV excitation, the luminescence of Mn²⁺-doped CaCO₃ crystals is employed as spectroscopic probe in order to distinguish between different CaCO₃ polymorphs in complex crystal aggregates.

Results and discussion

X-Ray crystallographic investigations

Continuing our efforts on analysing typical solid state packing motifs of amphiphilic calixarene derivatives we here present X-ray crystallographic data of *rccc*-4,6,10,12,16,18,22,24-octakis-*O*-(carboxymethyl)-2,8,14,20-tetra(*n*-undecyl)resorc[4]arene (**1**) and 5,11,17,23,29,35,41,47-octakis(1,1,3,3-tetramethylbutyl)-49,50,51,52,53,54,55,56-octa(ethoxycarbonylmethoxy)calix[8]arene (**2b**). We have previously shown that the average area per calixarene molecule in a Langmuir monolayer often is in good agreement with the corresponding value gleaned from its solid state structure provided that the amphiphilic compound forms a layered structure and the overall volume contribution of intercalated solvent molecules is negligible. Numerical differences between these two surface area values, on the other hand, are indicative of unusual packing arrangements of the amphiphiles at the air–water interface. Since large macrocyclic compounds such as resorcarenes and calixarenes can assume a variety of energetically equivalent conformations, the X-ray structures give us a glimpse of what their molecular shapes might look like and how these molecules could interact with their nearest neighbours in a monolayer.

Crystal structure of 1. X-Ray crystallographic investigations on single crystals of *rccc*-4,6,10,12,16,18,22,24-octakis-*O*-(carboxymethyl)-2,8,14,20-tetra(*n*-undecyl)resorc[4]arene (**1**) represent the second example of a *rccc*-resorcarene which contains *n*-undecyl and carboxylic acid residues. The crystal data of **1** may best be compared with those of *rccc*-5,11,17,23-tetracarboxy-4,6,10,12,16,18,22,24-octa-*O*-methyl-2,8,14,20-tetra(*n*-undecyl)resorc[4]arene (**3**) which we have reported previously.¹⁰ Although the numbers and the substitution patterns of carboxylic acid groups are different, these two derivatives share common features in their molecular shapes and the packing in the crystal lattices.

Single crystals of **1** were obtained by crystallization at 90 °C from an acetic acid/H₂O solvent mixture (95/5 vol%). The conformational parameters which determine the resorcarene's molecular geometry are defined in Fig. 1.

The X-ray structure analysis shows that compound **1** adopts a boat conformation which is described by the folding angles $\varphi_{1,2}$ between least squares planes running through atomic positions of opposite benzene rings. In the present crystal structure of **1** φ_1 is 155.3°, while φ_2 amounts to 3.0°; the center-to-center spacing d between opposite benzene rings is 5.15 Å. For comparison: the corresponding values¹¹ from crystal data of **3** are: $\varphi_1 = 168.3^\circ$, $\varphi_2 = 5.2^\circ$, and $d = 4.93$ Å. The high similarity of the conformational parameters of compounds **1** and **3** suggests that the observed boat conformation primarily results from *intramolecular* bonding constrains of

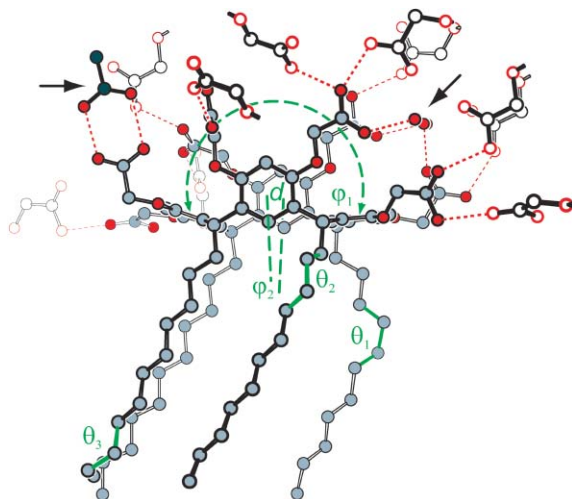


Fig. 1 Ball-and-stick model of the intermolecular hydrogen bonding scheme in the crystal lattice of **1**. Atoms belonging to neighbouring resorcarene molecules are displayed as open circles. Black arrows mark occluded acetic acid and water molecules. (Hydrogen atoms are omitted for clarity.) Definition of geometrical parameters used to describe the molecular structure of resorcarene moieties in the crystal structures of **1**. $\varphi_{1,2}$: folding angles between least squares planes running through atomic positions of opposite benzene rings; d : center-to-center spacing of opposite benzene rings; θ : torsion angle describing *gauche* “defects” occurring at selected atomic positions of the undecyl chains.

the macrocyclic ring system and is not due to specific *intermolecular* interactions between opposite resorcarene moieties in the crystal lattice. This statement gleans further support from the analysis of the hydrogen bonding scheme of carboxylic acid residues found in the crystal structure of **1**. Fig. 1 shows the hydrogen bonding scheme of compound **1** that makes hydrogen bonding contacts to six different nearest neighbours (of which only O–CH₂–COOH fragments are shown). The irregular arrangement of the pendent O–CH₂–COOH groups leads to deviation from ideal *C*_{2v}-symmetry of the boat conformer. Hydrogen bonding occurs intra- as well as inter-molecularly. Based on O···O distance calculations a vast variety of equally strong hydrogen bonds are definable and thus an unequivocal assignment of the most likely positions of acidic protons is impossible. Beside the hydrogen bonding network between resorcarene moieties, some water and acetic acid molecules are found at structurally well-defined positions (black arrow markers in Fig. 1), both leading to a further reduction of the resorcarene's molecular symmetry. Of four undecyl chains only one adopts an energetically favourable all-*trans* conformation (the largest deviation from the ideal torsion angle, $\theta \sim 180^\circ$, being 11.3°), the other ones display a single *gauche* “defect” (av. $\theta \sim 67.7^\circ$) occurring at different atomic positions of the undecyl chains.

The irregular shape of the resorcarene molecules in the crystal lattice leads us to conclude that the supramolecular arrangement is primarily dictated by close-packing principles and not by directional forces between H-bonding donors/acceptors. Compound **1** thus forms a lamellar structure where the hydrophilic constituents (carboxylic acid residues) and the hydrophobic residues (undecyl chains) segregate into different layers. The stacking of layers occurs in *c*-direction of the crystal lattice (Fig. 2). Owing to the fact that each polar headgroup has hydrogen bonding contacts to six different resorcarene neighbours, the lamellae consist of two-dimensional bilayers which extend infinitely in the *ab*-plane of the crystal lattice (Fig. 2 shows an excerpt of a bilayer structure motif highlighted in green). The average surface area occupied by a single resorcarene molecule **1** in the *ab*-plane amounts to 1.71 nm² which corresponds to an average of 4.68 CO₂⁻ per nm². (Table 1 contains a comparative list of experimental monolayer

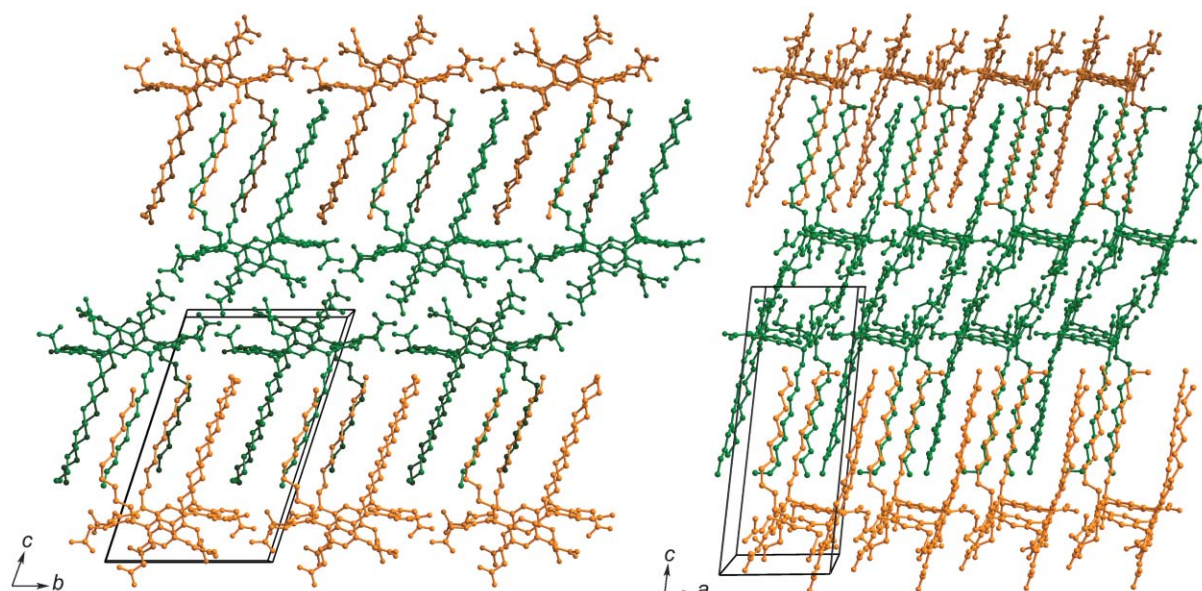


Fig. 2 Packing diagrams showing the interdigitation of bilayers of **1** in the crystal lattice. Resorcarene molecules belonging to the same “inverted” bilayer are represented with identical colors (hydrogen atoms are omitted for clarity).

Table 1 Correlation between area per molecule of amphiphiles used as crystallization templates and the CaCO₃ growth morphologies they induce

Compound	Area per molecule/nm ²			COO [⊖] /nm ²	Polymorph (pref. orientation if any)	Ref.
	Monolayer data	Crystal data	At which CaCO ₃ crystals were grown			
1	1.65–1.70 ^a	1.71				
	1.80–1.85 ^b	n.d.	1.60–1.70	4.71–5.00	Aragonite, vaterite	This work
2	2.70–2.75 ^a	n.d.			Calcite (012)	This work
	2.75–2.80 ^b	n.d.	3.30–3.50	2.29–2.44	Calcite, vaterite	
2b	3.35–3.45 ^a	3.23	n.d.	n.d.	n.d.	This work
3	1.75–1.80 ^b	1.83	2.00–2.10	1.90–2.00	Calcite (012)	10
4	1.70–1.75 ^b	1.70	1.75–1.80	2.22–2.29	Calcite (012)	9a
5	1.30–1.40 ^b	1.70	1.70–1.80	2.35–2.42	Calcite (012)	9b
		1.33	1.25–1.35	3.01	Inhibition	
6	n.p.	0.43	$\pi = 10$ mN/m	4.65	Aragonite, vaterite	27
7	0.50 ^a	n.d.	0.43–0.50	2.00–2.33	Calcite (012)	4b
8					Calcite (012)	6a
9	0.23–0.24 ^b	n.d.	0.22–0.23	4.35–4.44	Calcite (1 $\bar{1}$ 0), vaterite	20

^a H₂O: doubly de-ionized water, resistance 18.2 M Ω cm. ^b Ca(HCO₃)₂: aqueous subphase containing CaCl₂/NaHCO₃, $c = 9/18$ mM. ^c n.d. = not determined; n.p. = not published. ^d Compound index (systematic names for amphiphiles not characterized in this work): **1**: C₈₈H₁₂₈O₂₄; **2**: C₁₃₆H₁₉₂O₂₄; **2b**: C₁₅₂H₂₂₄O₂₄; **3**: C₈₄H₁₂₈O₁₆, *recc*-5,11,17,23-tetracarboxy-4,6,10,12,16,18,22,24-octa-*O*-methyl-2,8,14,20-tetra(*n*-undecyl)-resorc[4]arene; **4**: C₆₈H₉₆O₁₂, 5,11,17,23-tetrakis(1,1,3,3-tetramethylbutyl)-25,26,27,28-tetra(carboxymethoxy)calix[4]arene; **5**: C₅₂H₆₄O₁₂, 5,11,17,23-tetra-*tert*-butyl-25,26,27,28-tetrakis(carboxymethoxy)calix[4]arene; **6**: C₂₄H₃₈O₅, 5-hexadecyloxyisophthalic acid; **7**: N,N'-dioctadecyl-triazine-2,4,6-triamine and a cyanuric acid derivative; **8**: polymeric 10,12-pentacosadiynoic acid; **9**: C₁₈H₃₆O₂, stearic acid.

data for different amphiphiles). Fig. 3 shows a space filling model of the supramolecular packing arrangement of **1** in the crystal lattice. For clarity neighbouring resorcarene molecules

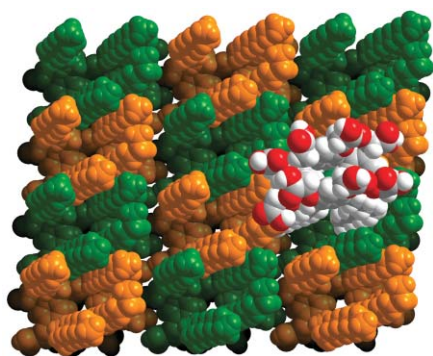


Fig. 3 Space-filling model of the supramolecular packing arrangement of **1** in the crystal lattice.

are distinguished by different colours (orange vs. green). Since the undecyl chains of an isolated bilayer are not bulky enough to fill the space completely (Fig. 3), interdigitation of successive bilayers occurs. The presence of *gauche* “defects” in the conformation of the undecyl chains may represent a further adaptation of the molecules to avoid empty spaces.

Crystal structure of 2b. All attempts to obtain single crystals of calix[8]arene octaacid **2** suitable for X-ray crystal structure investigations so far have failed. However, crystals of the corresponding ethylester derivative were readily available. Single crystals of 5,11,17,23,29,35,41,47-octakis(1,1,3,3-tetramethylbutyl)-49,50,51,52,53,54,55,56-octa(ethoxycarbonylmethoxy)-calix[8]arene (C₁₅₂H₂₂₄O₂₄·C₂H₅OH·H₂O, **2b**) were obtained by recrystallization from an ethanol solution containing 5% water. The X-ray structure analysis shows that the calix[8]-arene molecules adapt a highly symmetrical *flattened cone* conformation (Fig. 4a). Due to crystal packing effects the exact atom positions of the calixarene moiety differ from idealized C₄

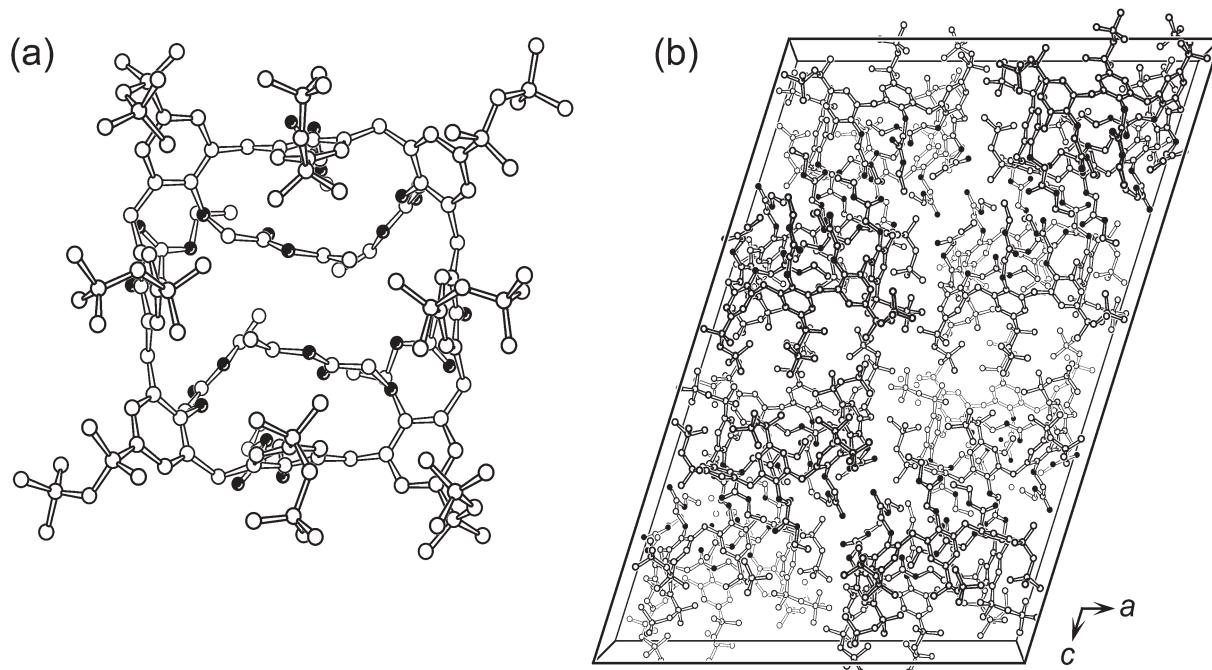


Fig. 4 (a) Ball-and-stick model of the molecular structure of **2b** (C and O atoms represented by open and black circles, respectively. Hydrogen atoms are omitted for clarity). (b) Ball-and-stick model of the supramolecular packing arrangement of **2b** in the crystal lattice (occluded solvent molecules and hydrogen atoms are omitted for clarity).

point symmetry. The ethoxycarbonylmethoxy substituents become irregularly placed such that two of them point inside the huge calix[8]arene cavity, while the neighbouring residues “hang down” from the lower rim which is defined by the circle of phenolic oxygen atoms. As a consequence, no further molecular guests are located within the internal cavities of **2b**, in contrast to host–guest inclusion phenomena frequently observed in conjunction with structurally similar calix[8]arene hosts.¹²

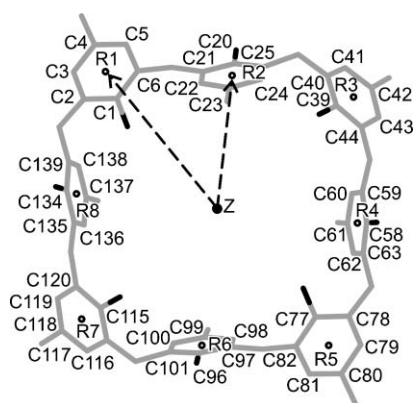
The conformation of the macrocyclic ring system can be defined by a few geometric parameters which are defined in Scheme 2. The midpoints R1–R8 of the benzene rings were calculated and individual distances from their common geometric centre Z are displayed in Table 2. Roughly speaking, the benzene rings show two regularly alternating tilt angles (av. values: 137° and 74°), and the distances Z–R_n assume two different av. values (7.0 Å and 5.5 Å). For comparison: the corresponding geometric parameters of the C₂-symmetric compound 5,11,17,23,29,35,41,47-octakis(1,1,3,3-tetramethylbutyl)-49,50,51,52,53,54,55,56-octakis(2-methoxyethoxy)calix[8]arene¹³—which assumes a *chair* conformation—are 42°,

133°, 68°, 115°, and 7.3 Å, 6.2 Å, 5.0 Å, 6.7 Å, respectively. In both calix[8]arene derivatives the sterically demanding hydrophobic 1,1,3,3-tetramethylbutyl substituents at the upper rim are closely packed.

Compound **2b** forms a lamellar structure where the more hydrophilic constituents (ethoxycarbonylmethoxy substituents, crystal ethanol solvate) and the hydrophobic residues segregate into different layers. The bilayers run parallel to the crystallographic *ab*-plane and layer stacking follows the *c*-direction (Fig. 4b). Within the layer, calixarene molecules are close packed with their pseudo C₄ symmetry axis being tilted by 28° against the *ab*-plane normal. The average surface area occupied by a single calix[8]arene molecule in the *ab*-plane amounts to 3.23 nm².¹⁴

Monolayer studies

Crystallographic investigations on the solid state structures of **1** and **2b** are complemented by monolayer studies of **1** and **2**. Langmuir monolayers were formed on an aqueous subphase by spreading compound **1** from trichloromethane/tetrahydrofuran (4 : 1) and **2** from trichloromethane/methanol (9 : 1) solution using a Langmuir trough. The surface pressure–area (π -*A*) isotherms provide information on monolayer stability and phase behaviour. Fig. 5 shows the π -*A* isotherms of compound **1** and **2** monolayers after having been spread on pure water or



Scheme 2 Definition of geometrical parameters used to describe the molecular structure of the macrocyclic calix[8]arene moiety in the crystal structures of **2b**. R_n denotes the midpoint of the *n*th benzene ring, Z is the geometric centre of R1–R8.

Table 2 Distances between the midpoints of benzene rings (R1–R8) of **2b** and their calculated geometric centre Z (left). Angles between l.s. planes through R1–R8 and l.s. planes through individual benzene rings (right)

Distance/Å	Angle/°		
Z···R1:	7.01	R1–R8/C1–C6:	146.9
Z···R2:	5.33	R1–R8/C20–C25:	73.4
Z···R3:	6.98	R1–R8/C39–C44:	125.2
Z···R4:	5.58	R1–R8/C58–C63:	74.1
Z···R5:	7.01	R1–R8/C77–C82:	147.4
Z···R6:	5.45	R1–R8/C96–C101:	74.2
Z···R7:	6.92	R1–R8/C115–C120:	127.9
Z···R8:	5.61	R1–R8/C134–C139:	74.3

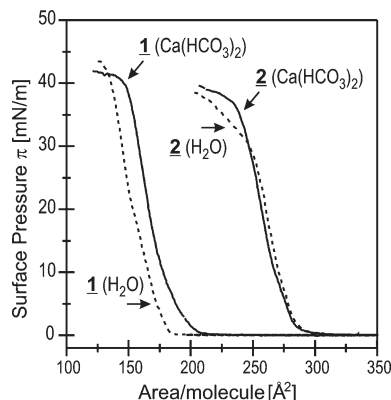


Fig. 5 π - A isotherms of monolayers of **1** and **2** at 22 °C on H₂O (dashed lines), and aqueous CaCl₂/NaHCO₃ ($c = 9/18$ mM, solid lines).

on an aqueous subphase containing CaCl₂/NaHCO₃ ($c = 9/18$ mM).

On both subphases, relatively stable monolayers of **1** form which collapse upon compression at a surface pressure of ~ 40 mN m⁻¹ (pure water *or* Ca containing aqueous subphase). The featureless isotherms suggest fluid properties of the condensed monolayer phase. On pure water the onset of pressure increase is at ~ 190 Å² molecule⁻¹ whereas the surface pressure of the Ca containing solution starts to rise at a significantly higher value (~ 210 Å² molecule⁻¹). We assume that this behaviour is due to electrostatic or coordinative interactions of Ca ions which cause the carboxylic acid residues of **1** to become deprotonated. Expansion effects of monolayers spread on metal ion-containing subphases, similar to those observed here, have been reported for several systems.¹⁵

The area per molecule of **1** in the monolayers is estimated from extrapolating the Langmuir isotherms toward zero pressure. The determined area values are listed in Table 1. Monolayer data are in excellent agreement with the surface area per molecule as determined from crystal structure analysis. The monolayer data indicate that the packing densities of ligand **1** in the monolayer and in the crystal lattice are similar. The two-dimensional packing arrangement of **1** in the monolayer is presumably determined by the (highly solvated) polar carboxylate residues and not by the alkyl chains (for the latter case, a much more complicated monolayer phase behavior should be observed).

BAM images of monolayers of **1** on subphases containing pure water show that already at zero pressure the liquid-condensed monolayer phase forms, which is in agreement with previous reports.¹⁶ The monolayers appear homogeneous within the spatial resolution limit of the BAM. When the collapse pressure is reached and upon further compression, the BAM micrographs display white spots indicating that double-layers are formed (images not shown). CaCO₃ crystallization experiments show that the phase region which appears homogeneously in the BAM (corresponding to a pressure range of $\pi \sim 20$ – 25 mN m⁻¹) provides optimal conditions for the growth of *aragonite* crystals (see below).

The calix[8]arene **2** also forms stable monolayers on pure water or Ca-containing aqueous subphases. On both subphases the pressure increase starts at the same molecular area of ~ 310 Å² molecule⁻¹.¹⁷ The isotherms are almost identical indicating similar phase behaviour. In both cases the mean area per molecule in the monolayer amounts to ~ 280 Å² molecule⁻¹, which is approximately twice the area that we have previously determined for the corresponding tetracarboxy-calix[4]arenes (**4**).⁹ Here, the adsorption layer of Ca ions underneath the monolayer of **2** does not lead to a detectable expansion as opposed to the compression behaviour we have perceived for charged monolayers of calix[4]arenes and resorc[4]arenes.

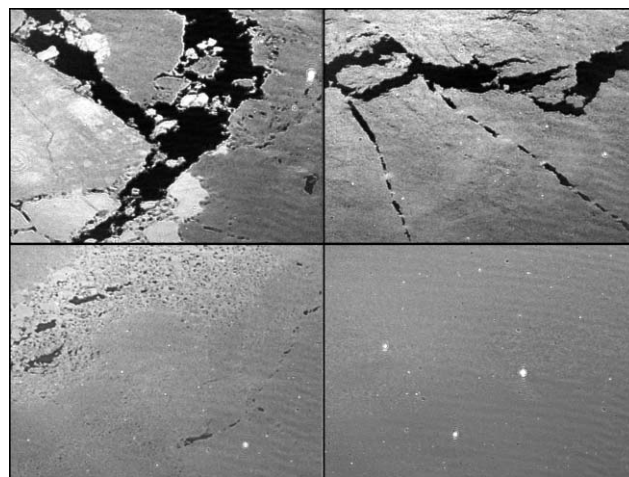


Fig. 6 BAM micrographs of monolayers of **2** at 24 °C on 10 mM CaCl₂. Monolayer domains appear as light regions. All micrographs were recorded at identical surface pressure ($\pi = 0.1$ mN m⁻¹) within a period of 5 minutes. The micrographs show representative morphologies at different sections of the monolayer. Areas of different brightness indicate that liquid-expanded phases coexist with liquid-compressed domains. Imaged area size: 430×320 μm².

Investigations on monolayers of **2** on aqueous subphases containing Cd ions have shown the same effect¹⁸ which has been ascribed to the conformational flexibility of the molecules. Another explanation might be that the packing of **2** in the monolayer is dictated by the bulky 1,1,3,3-tetramethylbutyl substituents attached to the upper rim of the calix[8]arene macrocycle.

BAM investigations corroborate that there is in fact no difference in monolayer phase behaviour of **2** if spread on different subphases (H₂O or 10 mM CaCl₂). Fig. 6 shows a typical sequence of BAM images at near-zero surface pressure. The BAM images demonstrate that already at zero pressure the liquid-expanded (LE) phase coexists with liquid-condensed (LC) domains (areas of different brightness). Since the intensity of the polarized beam reflected from the monolayer shows a delicate dependence on film thickness the observed brightness alterations in the BAM micrographs might be due to different inclination angles of the molecules in the monolayer of **2**. Upon further compression ($\pi > 0.1$ mN m⁻¹) the monolayer appears homogeneous until the collapse pressure is reached when bright dots indicate formation of a multilayer (not shown). The pressure region where the monolayer of **2** displays LE and LC domains ($\pi = 0.0$ – 0.2 mN m⁻¹, ~ 330 – 350 Å² molecule⁻¹) leads to the growth of uniformly oriented *calcite* single crystals (see below). The coexistence of LC domains and a LE phase at near-zero surface pressure might be the reason for a reduced nucleation density of *calcite* single crystals as compared to the corresponding tetracarboxy-calix[4]arene (**4**) the monolayer of which appears more homogeneous in the same pressure range.

CaCO₃ Crystallization underneath monolayers of **1** and **2**

Crystallization of CaCO₃ underneath a compressed monolayer of **1** leads to formation of *aragonite* crystals in the medium surface pressure range ($\pi = 20$ – 25 mN m⁻¹). When the compression is reduced the fraction of *calcite* rhombohedra and *vaterite* florets increases which constitute the predominant crystal species at low surface pressure ($\pi = 0$ – 2 mN m⁻¹). The majority of *calcite* rhombohedra are wedge-shaped crystals with an elevated central region and {104} cleavage planes.¹⁹ Morphologically similar crystals were reported previously.²⁰ Based on electron diffraction from crystals at an early growth stage the authors have concluded that this particular morphology is due to nucleation originating from the {110} crystal face.²¹

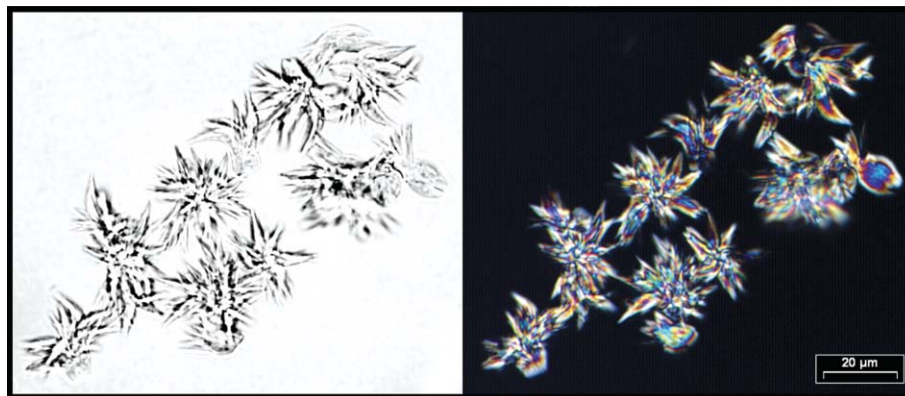


Fig. 7 Left: Brightfield optical micrograph of crystals grown under a monolayer of **1** after 3 h ($\pi = 20 \text{ mN m}^{-1}$, $\text{CaCl}_2/\text{NaHCO}_3$ ($c = 9/18 \text{ mM}$)). Right: Same crystal specimen observed in plane polarized light. (The viewing direction is parallel to the monolayer surface normal, crystals are observed from below the aqueous subphase).

Crystal growth was observed *in situ* by optical microscopy (Fig. 7). Aragonite crystals which grow underneath monolayers of **1** at high surface pressure display the typical acicular morphology of aragonite needles. In addition, varying amounts of vaterite florets form occasionally which are sometimes hardly distinguishable from the aragonite aggregates based on optical micrographs. A closer examination of crystal morphologies by scanning electron micrographs reveals that the aragonite crystal aggregates develop from a central pseudo-hexagonal basal plate which attaches to the monolayer at a central elevation (Fig. 8). This growth process is followed by secondary nucleation of a bunch of needle-type crystallites originating from the central primary crystal nucleus which leads to an over-all “comet-like” appearance of crystal habit.

Owing to the small amounts of crystalline material available through monolayer-directed crystallization and due to the fact that the crystal aggregates which are withdrawn from the water surface lose their original orientations, we were unable to obtain an X-ray diffraction pattern of sufficient quality

employing a standard X-ray powder diffractometer. Instead we inserted a collection of representative crystals into mark capillaries and the X-ray diffraction pattern from the sample was collected by a rotation image using the 1 K CCD area detector of a four circle automated X-ray diffractometer.

Fig. 9 shows a typical X-ray diffraction image of CaCO_3 crystals grown underneath compressed monolayers of **1**. For a quantitative mineral phase analysis the angular diffraction limits were calibrated against a polycrystalline Si reference sample and the intensities of the Debye rings were extracted from the scattering image by integration and normalization of radial brightness profiles. The relative quantities of CaCO_3 polymorphs in the sample were determined by fitting a superposition of theoretical diffraction patterns of calcite, aragonite and vaterite to the experimentally observed pattern. The background originating from diffuse X-ray scattering of the glass capillary and amorphous components of the sample was taken into account by adding intensity values of a 7th order polynomial function to the theoretical curve. Fig. 10a shows the experimental diffraction pattern together with the sum function of the simulated diffraction pattern and the background. The calculated sample composition indicates that aragonite constitutes the major mineral phase (approx. $80(\pm 10)\%$) followed by calcite (approx. $19(\pm 10)\%$). The

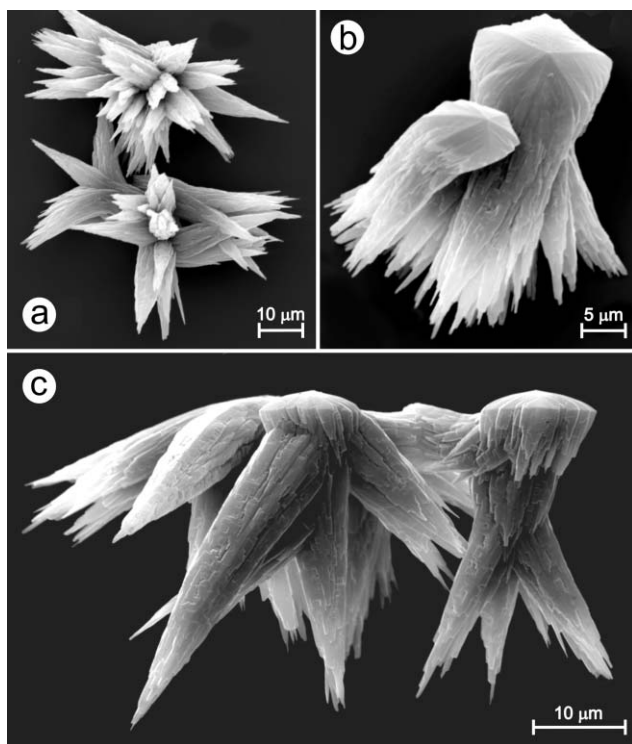


Fig. 8 Scanning electron micrographs (crystals collected after 6 h) of crystals grown under a monolayer of **1** ($\pi = 20 \text{ mN m}^{-1}$, $\text{CaCl}_2/\text{NaHCO}_3$ ($c = 9/18 \text{ mM}$)). Approximate viewing directions are (a) from below, (b) from the top, and (c) from the side of the monolayer.

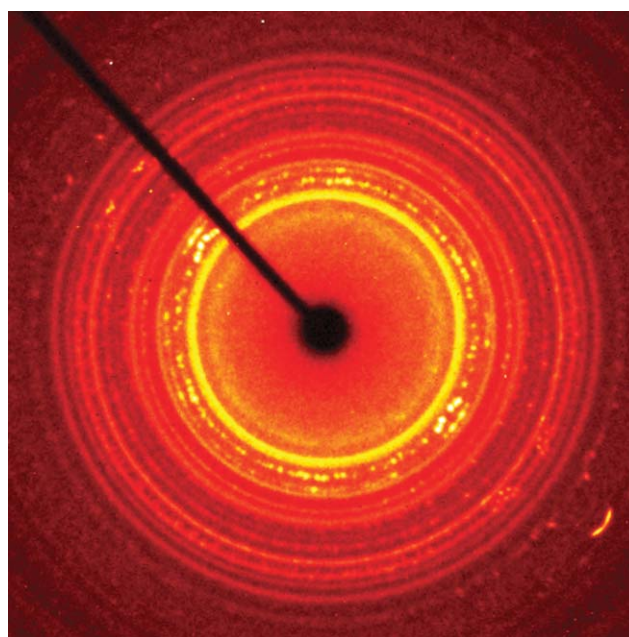


Fig. 9 XRD image from CaCO_3 crystals grown underneath a monolayer of **1**. (Rotation image, Mo- $K\alpha$ X-ray beam).

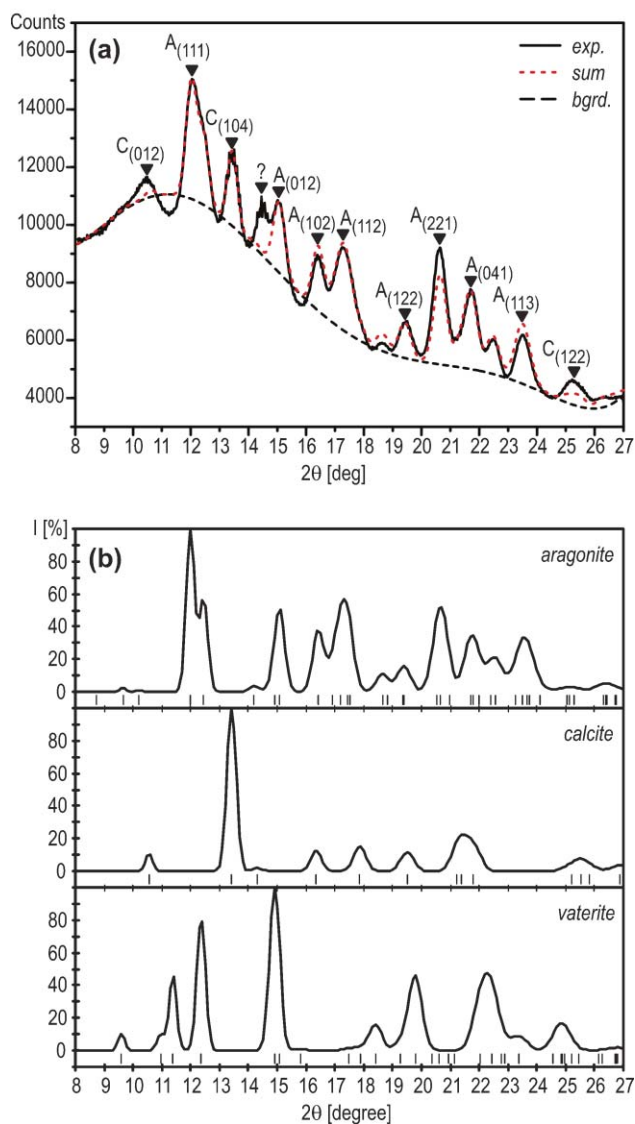


Fig. 10 (a) XRD pattern (solid line) from CaCO_3 crystals grown underneath a monolayer of **1** extracted from the rotation image. The simulated XRD pattern (red small dashes) of a mixture of aragonite/calcite/vaterite (81/18/1 vol%) and the calculated background (dashes). Crystallographic indices are presented in three-index (hkl) notation, based on the hexagonal setting of the calcite unit cell ($R\bar{3}c$, $a = 4.96 \text{ \AA}$, $c = 17.002 \text{ \AA}$) and the conventional setting of the orthorhombic unit cell of aragonite ($Pm\bar{c}n$, $a = 4.96 \text{ \AA}$, $b = 7.97 \text{ \AA}$, $c = 5.74 \text{ \AA}$). (b) Simulated XRD pattern of different CaCO_3 polymorphs assuming a random orientation of crystal specimen. (Simulation parameters: $\lambda = 0.71073 \text{ nm}$, Debye–Scherrer geometry, Gaussian peak profiles with empirically determined full width at half maximum values ($\text{FWHM} = f(u, v, w)$)).

vaterite content of the sample is vanishing small ($< 1\%$) which is somewhat surprising since the characteristic vaterite florets were ubiquitous in all samples. However, owing to the inherent broadness of the experimental diffraction peaks (Fig. 9) the accuracy of the phase analysis is somewhat limited and the exact composition values are slightly dependent on the refinement model.

Based on the results of quantitative phase analysis we therefore assume that the acicular crystal aggregates are composed of aragonite crystals. However, the observation of calcite diffraction peaks led us to explore the abundance of this CaCO_3 polymorph in more detail. From optical micrographs of CaCO_3 crystals grown underneath a compressed monolayer of **1** it becomes readily apparent that a small fraction of crystals consist of (non-truncated) calcite rhombohedra which spontaneously crystallize at the air–water interface regardless of the

surface pressure employed. However, as a second option we considered the possibility that the primary nucleus of the acicular crystal aggregates might consist of calcite instead of aragonite. In order to obtain spatially resolved information of the mineral phase composition we employed fluorescence microscopy. The luminescence of CaCO_3 minerals is a well-documented feature which occurs commonly in CaCO_3 samples of geological and/or biological origin.²² The weak luminescence is due to trace impurities of metal cations that replace Ca ions in the crystal lattice. Especially the presence of Mn^{2+} ions leads to intense luminescence of CaCO_3 crystals under various activation conditions (cathodoluminescence,²³ thermoluminescence²⁴). Preliminary investigations have shown us that differentiation of CaCO_3 polymorphs should be feasible based on the characteristic luminescence of Mn^{2+} ions with the particular crystal fields of the host lattices leading to different wavelengths and decay times of the stimulated emission of photons. While a detailed analysis of the underlying physical principles is clearly beyond this work we note the experimental observation that morphologically distinct CaCO_3 crystals show clearly distinguishable emission colors if the sample is irradiated with intense UV light.

Fig. 11 shows the luminescence micrographs of representative crystal specimen grown underneath compressed monolayers of **1**. It is clearly seen that luminescence of the acicular crystal aggregates leads to a blue glow whereas the luminescence of the vaterite florets and rhombohedral calcite crystals (not shown) shows a significantly red-shifted (red–orange) glow. Furthermore, the luminescence of the acicular crystal aggregates appears homogeneous and we could not detect any regions showing different emission properties. Based on this experiment we conclude that the acicular crystal aggregates are uniformly composed of aragonite.

In contrast to **1**, monolayers of **2** lead to formation of uniformly oriented calcite single crystals at near-zero surface pressure ($\pi = 0.0\text{--}0.2 \text{ mN m}^{-1}$). At a higher surface pressure ($\pi = 0.5\text{--}25 \text{ mN m}^{-1}$) calcite rhombohedra form which lack any preferential orientation. The main orientation of calcite crystals grown underneath monolayers of **2** was determined by X-ray powder diffraction and geometrical analysis. A more detailed description of the procedure is given elsewhere.⁹ The calcite single crystals obtained at low surface pressure underneath monolayers of **2** display the typical shape of truncated rhombohedra. The truncation occurs parallel to the $\{01.2\}$ faces of the calcite crystal lattice. We have previously reported the identical growth behaviour for calcite crystals grown underneath monolayers of resorc[4]arenes and calix[4]arenes (Table 1). At high surface pressure non-truncated calcite $\{10.4\}$ cleavage rhombohedra are observed. This indicates that at zero surface pressure the monolayer directs nucleation and growth of uniformly oriented calcite crystals while at higher surface pressure crystal growth becomes non-specific.²⁵

Summary and conclusion

While in previous investigations we have employed monolayers of tetradentate amphiphilic macrocycles, we here report on the growth of CaCO_3 underneath monolayers of octadentate carboxylic acids. Compounds **1** and **2** were chosen for these investigations since they differ largely in the molecular surface area that each molecule can occupy in a monolayer. It is thus possible to adjust surface charge density underneath the monolayer by the appropriate selection of amphiphiles.

The molecular structures of all compounds investigated so far and their crystal packing arrangements differ significantly. Monolayers of amphiphilic calix[4]arene derivatives which possess hydrophobic substituents of varying steric demands have been employed⁹ as well as amphiphilic resorc[4]arene derivatives¹⁰ which are structurally complementary to the

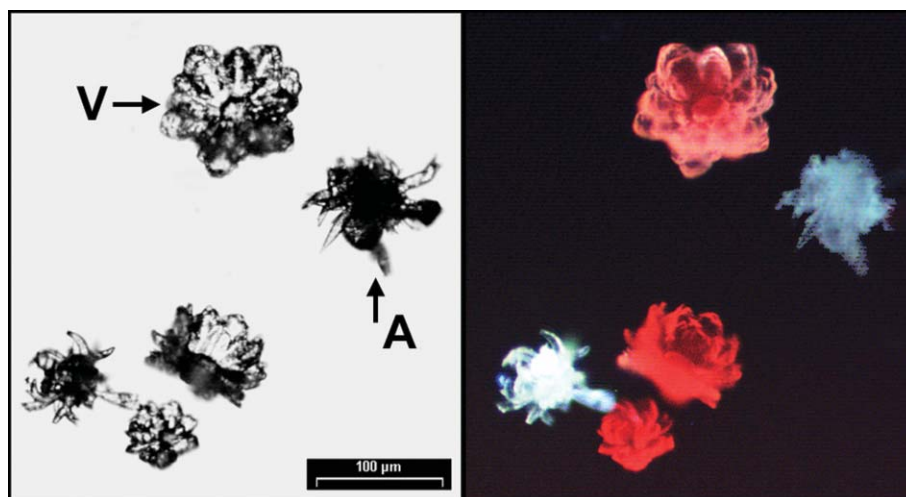


Fig. 11 Left: Brightfield optical micrograph of crystals grown under a monolayer of **1** after 14 h ($\pi = 20 \text{ mN m}^{-1}$, $\text{MnCl}_2/\text{CaCl}_2/\text{NaHCO}_3$ ($c = 0.04/9/18 \text{ mM}$)). Right: Same crystal specimen observed under UV light irradiation.

calix[4]arene ligands and show completely different Ca-coordination motifs.

Despite their structural and functional differences we observe the same orientation of calcite crystals which uniformly grow with their {01.2} crystal face attaching to the monolayers. In particular, the oriented growth of truncated calcite single crystals always and exclusively occurs at very low surface pressure, where the monolayers exist in a liquid-expanded state, an epitaxial correlation of the putative monolayer “lattice” and the {01.2} calcite crystal face can therefore be ruled out.

The templating role of monolayers has frequently (and perhaps without justification) been interpreted in terms of a geometrical and stereochemical complementarity between the arrangement of headgroups in the monolayer and the position of Ca ions in the crystal plane which attaches to the monolayer. Our investigations, however, clearly demonstrate that such delicate and complex interactions most likely vanish if structurally mobile template matrices such as monolayers are employed. Most probably non-specific electrostatic effects such as the average charge density or the mean dipole moment of the monolayer determine the orientation of crystals.²⁶

In fact, for monolayers of **2** and many other (structurally different) amphiphiles the growth of (01.2) oriented calcite crystals occurs at a surface pressure where the average density of carboxylate residues at the air–water interface is about $2.00\text{--}2.44 \text{ COO}^- \text{ nm}^{-2}$ (Table 1).

It is therefore noteworthy that CaCO_3 crystallization underneath monolayers of **1** as reported in this work shows completely different characteristics, namely the formation of acicular aragonite crystal aggregates at high surface pressure and at an ionic composition of the aqueous subphase that would normally yield the thermodynamically more stable calcite. A similar behaviour has been reported earlier for a monolayer of 5-hexadecyloxyisophthalic acid.²⁷ The average charge density as derived from X-ray structure analysis of this compound amounts to $4.65 \text{ COO}^- \text{ nm}^{-2}$.²⁸ Interestingly, crystallization of aragonite underneath monolayers of **1** occurs at a surface pressure where the charge density assumes a similar value ($4.65\text{--}5.00 \text{ COO}^- \text{ nm}^{-2}$, Table 1) which adds further support to our hypothesis that non-directional interfacial electrostatics is the dominant effect in template-directed crystal growth of CaCO_3 under Langmuir monolayers. Crystallization of aragonite from an aqueous subphase lacking soluble (organic) additives has been achieved quite a few times.²⁹ Experimental evidence as described here together with previous literature notes indicate that monolayer molecules possessing a high charge density are able to induce and stabilize metastable crystal phases at the air–water interface. The formation of

aragonite and vaterite in this and related cases is obviously under kinetic control.³⁰ More recently, kinetic effects were discussed in this context on the basis of *in-situ* grazing incidence X-ray diffraction experiments.³¹

We are currently investigating CaCO_3 growth underneath monolayers of 5,11,17,23-tetra-*tert*-butyl-25,27-dicarbonyl-methoxy-26,28-dihydroxycalix[4]arene where the reduced number of carboxylic acid residues per molecule (two instead of four or eight) leads to completely different calcium carbonate growth characteristics. Future investigations will focus on crystallization on CaCO_3 underneath mixed monolayers of macrocyclic oligoacids such as compound **1** or **4** and their corresponding oligoalcohols such as *recc*-4,6,10,12,16,18,22,24-octa(2-hydroxyethoxy)-2,8,14,20-tetra(*n*-undecyl)resorc[4]arene or 5,11,17,23-tetrakis(1,1,3,3-tetramethylbutyl)-25,26,27,28-tetra(2-hydroxyethoxy)calix[4]arene which are strong CaCO_3 crystallization inhibitors.³² By inserting a nucleation active oligocarboxylic acid into a matrix of molecules which inhibits crystal growth we hope to achieve nucleation by single molecules.

Experimental

Synthesis

All solvents used were in p.a. quality or purified by distillation. Melting points were determined on a Büchi B-540 apparatus and are uncorrected. NMR spectra were measured on a Bruker DRX 500 ($^1\text{H-NMR}$: 500.13 MHz; $^{13}\text{C-NMR}$: 125.77 MHz) instrument using 7.24 ppm/77.0 ppm for CHCl_3 . IR spectra were recorded on a Perkin-Elmer 841 infrared spectrophotometer. ESI mass spectra were recorded using an Esquire 3000 ion trap mass spectrometer (Bruker Daltonik GmbH, Bremen, Germany) equipped with a standard ESI source. Samples were introduced by direct infusion with a spring pump. Nitrogen served both as the nebulizer gas and the dry gas. Helium served as cooling gas for the ion trap. Elemental analysis was carried out with a Perkin-Elmer 240 elemental analyzer.

***recc*-4,6,10,12,16,18,22,24-Octakis-*O*-(isopropoxy(oxo)ethyl)-2,8,14,20-tetra(*n*-undecyl)resorc[4]arene.** To a suspension of *recc*-2,8,14,20-tetra(*n*-undecyl)resorc[4]arene³³ (3.00 g, 2.71 mmol) and anhydrous potassium carbonate (7.50 g, 54.3 mmol) in dry acetonitrile (250 mL) was added isopropyl bromoacetate (12.3 g, 8.80 mL, 67.8 mmol) within 5 min. The mixture was heated under reflux for 16 h and concentrated *in vacuo*, followed by dilution in a mixture of diethyl ether and water to separate the organic layer. The water layer was extracted with diethyl ether (3 ×) and the

combined organic layers were washed with water, brine and dried over magnesium sulfate. The solvent was removed *in vacuo* and the crude product was recrystallized twice from acetonitrile. After drying *in vacuo* the product (2.67 g, 1.40 mmol, 52%) was obtained as colourless crystals, mp 61 °C. ¹H-NMR (500 MHz, CDCl₃): δ = 0.84 (t, ³J = 7.0 Hz, 12 H, CH₃-CH₂), 1.20 (d, ³J = 6.2 Hz, 24 H, CH₃-CH), 1.235 (d, ³J = 6.3 Hz, 24 H, CH-CH₃), 1.15–1.35 (m, 72 H, CH₂), 1.82 (m, 8 H, CH-CH₂), 4.20 (d, ²J = 16.1 Hz, 8 H, OCH₂-COO), 4.22 (d, ²J = 16.1 Hz, 8 H, OCH₂-COO), 4.56 (t, ³J = 7.4 Hz, 4 H, Ar-CH-Ar), 5.05 (qq, ³J = 6.3 Hz, ³J = 6.3 Hz, 8 H, CH₃-CH-CH₃), 6.186 (s, 4 H, Ar-H), 6.57 (s, 4 H, Ar-H); MS (ESI) *m/z* 1928.5 ((M + Na)⁺, 100); Elemental analysis calc. for C₁₁₂H₁₇₆O₂₄: C 70.56; H 9.30; found: C 70.57; H 9.27%.

recc-4,6,10,12,16,18,22,24-Octakis-O-(carboxymethyl)-2,8,14,20-tetra(*n*-undecyl)-resorc[4]arene (1). The product was prepared according to a slightly modified literature procedure.³⁴ *recc-4,6,10,12,16,18,22,24-Octakis-O-(isopropoxy(oxo)ethyl)-2,8,14,20-tetra(*n*-undecyl)-resorc[4]arene* (1.00 g, 524 μmol) was dissolved in ethanol (100 mL) and lime potash (50 mL, 20%) and potassium hydroxide (10.0 g, 179 mmol) was added under argon. The mixture was heated under reflux for 10 d and concentrated under reduced pressure. The alkaline solution was rinsed with diluted hydrochloric acid, and the suspension was extracted with ethyl acetate (4 × 500 mL). The combined organic layers were washed with diluted hydrochloric acid and dried over sodium sulfate. The solvent was removed *in vacuo* and the crude product was recrystallized from methanol/water. After drying *in vacuo* the product (798 mg, 508 μmol, 97%) was obtained as white solid, mp 220 °C. Colourless crystals of **1** were obtained by recrystallization from an acetic acid/H₂O solvent mixture (95/5 vol%). ¹H-NMR (500 MHz, CDCl₃): δ = 0.92 (t, ³J = 7.1 Hz, 12 H, CH₃-CH₂), 1.25–1.45 (m, 72 H, CH₂), 1.89 (m, 8 H, CH-CH₂), 4.30 (d, ²J = 16.4 Hz, 8 H, OCH₂-COOH), 4.42 (d, ²J = 16.4 Hz, 8 H, OCH₂-COOH), 4.71 (t, ³J = 7.3 Hz, 4 H, Ar-CH-Ar), 6.438 (s, 4 H, Ar-H), 6.706 (s, 4 H, Ar-H); MS (ESI) *m/z* 1586.9 ((M + NH₄)⁺, 100); Elemental analysis calc. for C₈₈H₁₂₈O₂₄·CH₃COOH·(H₂O)₂: C 64.88; H 8.23; found: C 65.09; H 8.22%.

5,11,17,23,29,35,41,47-Octakis(1,1,3,3-tetramethylbutyl)-49,50,51,52,53,54,55,56-octa(ethoxycarbonylmethoxy)calix[8]arene (2b). The product was synthesized as described for the *tert*-butyl-derivative requiring additional recrystallization steps to give a crystalline product,³⁵ mp 120 °C (ethanol). ¹H NMR (500 MHz, CDCl₃) δ = 6.88 (s, 16 H, ArH), 4.02–4.17 (m, 32 H, OCH₂COO, Ar-CH₂-Ar), 1.56 (s, 16 H, CCH₂C), 1.08 (s, 48 H, CH₃), 0.68 (s, 72 H, CH₃); IR (KBr) 1757 cm⁻¹; MS (ESI) *m/z* 2457.4 ((M + K)⁺, 100); Elemental analysis calc. for C₁₅₂H₂₂₄O₂₄: C 74.96; H 9.27; found: C 74.90; H 9.30%.

5,11,17,23,29,35,41,47-Octakis(1,1,3,3-tetramethylbutyl)-49,50,51,52,53,54,55,56-octa(carboxymethoxy)calix[8]arene (2). The product was prepared according to a slightly modified literature procedure.³⁶ To a solution of 5,11,17,23,29,35,41,47-octakis(1,1,3,3-tetramethylbutyl)-49,50,51,52,53,54,55,56-octa(ethoxycarbonylmethoxy)calix[8]arene (0.70 g, 0.5 mmol) in tetrahydrofuran (30 mL) was added an aqueous solution of tetramethylammonium hydroxide (25%, 12 mL, 33 mmol). The suspension was heated under reflux. After 24 h the suspension was acidified with hydrochloric acid and chloroform was added. The organic layer was concentrated *in vacuo*, redissolved in chloroform, acidified with hydrochloric acid and washed with brine. After drying the organic layer over sodium sulfate and removing the solvent *in vacuo*, the crude product was suspended in acetonitrile to give the final product as white solid, mp > 265 °C (decomp.). ¹H-NMR (500 MHz, CDCl₃, 50 °C): δ = 6.95 (s, 16 H, ArH), 4.19 (s, 16 H, OCH₂COO), 3.96 (s, 16 H, Ar-CH₂-Ar), 1.60 (s, 16 H, CCH₂C), 1.19 (s,

48 H, CH₃), 0.69 (s, 72 H, CH₃); MS (ESI) *m/z* 2247.3 ((M + K)⁺, 100); Elemental analysis calc. for C₁₃₆H₁₉₂O₂₄: C 73.88; H 8.75; found: C 73.60; H 8.96%.

X-Ray structure analysis

Details of structure refinement and X-ray crystallographic data are provided as ESI with key data summarised in Table 3.

CCDC reference numbers 232971 (compound **1**) and 232972 (compound **2b**).

See <http://www.rsc.org/suppdata/jm/b4/b403132f/> for crystallographic data in CIF or other electronic format.

Monolayer investigations

Monolayer experiments were performed with a double-barrier NIMA trough using a compression speed of 15 cm² min⁻¹. The surface pressure of the monolayers was measured using a Wilhelmy plate. Langmuir monolayers were formed on an aqueous subphase by spreading compound **1** from a trichloromethane/tetrahydrofuran (4 : 1) solution (30 μL, 0.1 mg mL⁻¹) and **2** from a 0.23 mM trichloromethane/methanol (9 : 1) solution (10 μL, 0.5 mg mL⁻¹). Compression was started after 10 min. Brewster angle microscopy were performed with a NIMA Langmuir trough (NIMA 601BAM) using a BAM-2 (NFT, Göttingen).

CaCO₃ crystal growth experiments

Solutions of calcium bicarbonate were prepared by bubbling carbon dioxide gas through a stirred aqueous (double deionized water, resistance 18.2 MΩ cm) solution of CaCl₂/NaHCO₃ (*c* = 9/18 mM) for a period of 2 h. Compressed films were formed by spreading the solutions of surfactants in order to generate a liquid-expanded or liquid-condensed film at the air–water interface. Crystals were studied after several times either *in situ* by optical microscopy (PZO Biolar upright microscope) or on cover slips laid on the film (Olympus IX70). The cover slips were also mounted on scanning electron microscope (SEM) specimen tubs. A Phillips XL30 ESEM operating at 30 keV was used. The calcite crystals were sputtered with Au prior to examination.

X-Ray diffraction and CaCO₃ mineral phase analysis

CaCO₃ crystals grown underneath monolayers of **2** were obtained by collecting crystals on glass cover slips laid on the film and removed horizontally. A Philips PW 1050/70 X-ray powder diffractometer was employed (2θ scans, Bragg–Brentano para-focussing geometry) using Cu-Kα radiation (λ = 1.54 Å).

CaCO₃ crystals grown underneath monolayers of **1** were obtained similarly. Due to the irregular crystal habits and the occurrence of three different CaCO₃ polymorphs the intensity of the experimental diffraction pattern was insufficient. Therefore, crystals were filled in a mark capillary with 0.2 mm diameter. A Bruker Nonius 1 K CCD diffractometer was employed using Mo-Kα radiation (λ = 0.71073 Å). The reflections were measured in rotation at a detector distance of 5 cm (2θ < 27°). The intensity was integrated using the program GADDS V3.317. Quantitative mineral phase analysis was performed with the software PowderCell V2.3.³⁷

Luminescence experiments

To a solution of CaCl₂/NaHCO₃ (*c* = 9/18 mM) was added MnCl₂ (*c* = 0.04 mM). Compressed monolayers were formed as described above. After 14 h the crystals were transferred onto cover slips and sorted by hand. Selected specimens were examined by fluorescence microscopy using an inverted stage microscope (Olympus IX 70). The sample was illuminated with a 100 W high-pressure mercury lamp using a U-MWU2 mirror unit (wideband UV excitation at 330–385 nm, 420 nm emission

Table 3 X-Ray crystallographic data for compounds **1** and **2b**

Compound	1	2b
Formula	C ₈₈ H ₁₂₈ O ₂₄ ·CH ₃ COOH·(H ₂ O) ₂	C ₁₅₂ H ₂₂₄ O ₂₄ ·C ₂ H ₅ OH·H ₂ O
<i>M_r</i> /g mol ⁻¹	1665.99	2499.40
<i>T</i> /K	188(2)	183(2)
<i>λ</i> /Å	0.71073	0.71073
Crystal system	Triclinic	Monoclinic
Space group	<i>P</i> $\bar{1}$	<i>C2/c</i>
<i>a</i> /Å	9.9409(7)	34.9691(15)
<i>b</i> /Å	17.2656(11)	18.4700(8)
<i>c</i> /Å	27.3161(18)	49.942(2)
<i>α</i> /°	71.909(1)	90
<i>β</i> /°	83.817(1)	108.521(1)
<i>γ</i> /°	84.922(1)	90
<i>V</i> /Å ³	4423.2(5)	30586(2)
<i>Z</i>	2	8
<i>ρ</i> _{calc} /g m ⁻³	1.251	1.086
<i>μ</i> (Mo-Kα)/mm ⁻¹	0.092	0.072
<i>F</i> (000)	1800	10912
Crystal size/mm	0.80 × 0.15 × 0.06	0.44 × 0.36 × 0.24
<i>θ</i> range/°	1.24–25.02	1.39–25.02
Index ranges	−11 ≤ <i>h</i> ≤ 11, −20 ≤ <i>k</i> ≤ 20, −32 ≤ <i>l</i> ≤ 32	−38 ≤ <i>h</i> ≤ 41, −21 ≤ <i>k</i> ≤ 21, −59 ≤ <i>l</i> ≤ 52
Reflections collected	39701	77537
<i>R</i> (int)	0.0511	0.0448
Independent reflections	15548	26912
Data/restraints/parameters	15548/6/1093	26912/0/1665
GoF	1.326	1.034
<i>R</i> values [<i>I</i> > 2σ(<i>I</i>)] ^a	<i>R</i> ₁ = 0.1129, <i>wR</i> ₂ = 0.3395	<i>R</i> ₁ = 0.0834, <i>wR</i> ₂ = 0.2259
<i>R</i> values (all data) ^a	<i>R</i> ₁ = 0.1704, <i>wR</i> ₂ = 0.3800	<i>R</i> ₁ = 0.1249, <i>wR</i> ₂ = 0.2601
Weighting scheme, <i>w</i> ^{-1b}	[<i>s</i> ² (<i>F</i> _o ²) + (0.2000· <i>P</i>) ²]	[<i>s</i> ² (<i>F</i> _o ²) + (0.1316 <i>P</i>) ² + 74.16 <i>P</i>]
Largest diff. peak/hole/e Å ⁻³	1.335/−0.568	1.256/−1.173

^a *R*₁ = Σ||*F*_o − |*F*_c||/Σ|*F*_o|; *wR*₂ = [Σ*w*(*F*_o² − *F*_c²)²/Σ*w*(*F*_o²)²]^{1/2}. ^b *P* = (*F*_o² + 2*F*_c²)/3.

filter, 400 nm dichromatic mirror). Luminescence optical micrographs were recorded with a Hitachi HV-C20A 3-CCD RGB camera at a resolution of 3 × 768 × 576 pixels.

Acknowledgements

D. V. thanks the DFG for a Habilitanden fellowship. M. F. thanks the Graduiertenförderung Nordrhein-Westfalen for a graduate fellowship. We thank L. Chi and M. Gleiche of the faculty of interface physics (University of Münster) for providing access to BAM instruments. We thank M. Schmidtman (University of Bielefeld, AC1) for XRD measurements. Donation of the starting material *p*-1,1,3,3-tetramethylbutylphenol by CONDEA Chemie GmbH (Marl, Germany) is gratefully acknowledged. This work was financially supported by the Deutsche Forschungsgemeinschaft (DFG Schwerpunktprogramm 1117, “Prinzipien der Biomineralisation”; DFG grant Vo829/2-1) and by the Fonds der Chemischen Industrie.

References and notes

- (a) H. A. Lowenstam and S. Weiner, *On Biomineralization*, Oxford University Press, Oxford, 1989; (b) S. Mann, *Biomineralization. Principles and Concepts in Bioinorganic Materials Chemistry*, Oxford University Press, Oxford, 2001; (c) L. Addadi and S. Weiner, *Angew. Chem., Int. Ed. Engl.*, 1992, **31**, 153–169.
- (a) S. Mann, *Biomimetic Materials Chemistry*, VCH, Weinheim, 1996; (b) S. Mann, D. D. Archibald, J. M. Didymus, T. Douglas, B. R. Heywood, F. C. Meldrum and N. J. Reeves, *Science*, 1993, **261**, 1286–1292.
- (a) A. M. Belcher, X. H. Wu, R. J. Christensen, P. K. Hansma, G. D. Stucky and D. E. Morse, *Nature*, 1996, **381**, 56–58; (b) Y. Levi, S. Albeck, A. Brack, S. Weiner and L. Addadi, *Chem. Eur. J.*, 1998, **4**, 389–396.
- (a) S. Mann, B. R. Heywood, S. Rajam and J. D. Birchall, *Nature*, 1988, **334**, 692–695; (b) S. Champ, J. A. Dickinson, P. S. Fallon, B. R. Heywood and M. Mascal, *Angew. Chem., Int. Ed.*, 2000, **39**, 2716–2719; (c) P. J. A. Buijnsters, J. J. M. Donners, S. J. Hill, B. R. Heywood, R. J. M. Nolte, B. Zwanenburg and N. A. J. M. Sommerdijk, *Langmuir*, 2001, **17**, 3623–3628.
- (a) J. Aizenberg, A. J. Black and G. M. Whitesides, *Nature*, 1999, **398**, 495–498; (b) J. Küther, G. Nelles, R. Seshadri, M. Schaub, H. J. Butt and W. Tremel, *Chem. Eur. J.*, 1998, **4**, 1834–1842; (c) D. D. Archibald, S. B. Qadri and B. P. Gaber, *Langmuir*, 1996, **12**, 538–546.
- (a) A. Berman, D. J. Ahn, A. Lio, M. Salmeron, A. Reichert and D. Charych, *Science*, 1995, **269**, 515–518; (b) H. Cölfen and M. Antonietti, *Langmuir*, 1998, **14**, 582–589; (c) A. Becker, W. Becker, J. C. Marxen and M. Eppele, *Z. Anorg. Allg. Chem.*, 2003, **626**, 2305–2311.
- (a) L. Addadi, J. Moradian, E. Shay, N. G. Maroudas and S. Weiner, *Proc. Natl. Acad. Sci. U. S. A.*, 1987, **84**, 2732–2736; (b) S. R. Letellier, M. J. Lochhead, A. A. Campbell and V. Vogel, *Biochim. Biophys. Acta*, 1998, **1380**, 31–45.
- (a) L. Addadi and S. Weiner, in *Biomineralization*, S. Mann, ed., VCH, Weinheim, 1989, pp. 133–156; (b) J. Aizenberg, A. J. Black and G. M. Whitesides, *J. Am. Chem. Soc.*, 1999, **121**, 4500–4509.
- (a) D. Volkmer, M. Fricke, D. Vollhardt and S. Siegel, *J. Chem. Soc., Dalton Trans.*, 2002, 4547–4554; (b) D. Volkmer and M. Fricke, *Z. Anorg. Allg. Chem.*, 2003, **629**, 2381–2390.
- D. Volkmer, M. Fricke, C. Agena and J. Mattay, *CrystEngComm.*, 2002, **4**, 288–295.
- Average values are calculated from crystallographic independent parameters of two molecules in the asymmetric unit of compound **3** (CCDC reference number 183961).
- C. D. Gutsche, *Calixarenes, Monographs in Supramolecular Chemistry*, J. F. Stoddart, ed., The Royal Society of Chemistry, Cambridge, 1989, pp. 149–185.
- R. Ungaro, A. Pochini, G. D. Andreotti and F. Ugozzoli, *J. Inclusion Phenom. Macro. Chem.*, 1985, **3**, 409–420. CCDC structure code DIZVEN.
- The compound 5,11,17,23,29,35,41,47-octakis(1,1,3,3-tetramethylbutyl)-49,50,51,52,53,54,55,56-octakis(2-methoxyethoxy)calix(8)-arene (CCDC structure code DIZVEN) forms close packed layers in the {101} crystal plane. The calculated surface area/molecule here amounts to 3.03 nm² which is roughly 7% less than the average surface area of **2b**.
- (a) V. A. Arsentiev and J. Leja, in *Colloid and Interface Science*, M. Kerker, ed., vol. 5, Academic Press, New York, 1976, pp. 251–270; (b) G. T. Barnes, in *Colloid Science*, D. H. Everett, ed., vol. 2, Chemical Society, London, 1975, pp. 173–190.
- Y. Matsuzawa, S. Takahiro and K. Ichimura, *J. Inclusion Phenom. Macro. Chem.*, 1999, **35**, 199–210.
- T. Richardson, M. B. Greenwood, F. Davis and C. J. M. Stirling, *Langmuir*, 1995, **11**, 4623–4625.

- 18 A. V. Nabok, T. Richardson, F. Davis and C. J. M. Stirling, *Langmuir*, 1997, **13**, 3198–3201.
- 19 Crystallization of CaCO₃ underneath monolayers of stearic acid yield crystals displaying the same morphology: S. Mann, B. R. Heywood, S. Rajam and J. B. A. Walker, *J. Phys. D: Appl. Phys.*, 1991, **24**, 154–164.
- 20 S. Rajam, B. R. Heywood, J. B. A. Walker, S. Mann, R. J. Davey and J. D. Birchall, *J. Chem. Soc., Faraday Trans.*, 1991, **87**, 727–734.
- 21 Representative optical and scanning electron micrographs of CaCO₃ crystals grown underneath a monolayer of **1** at low surface pressure are provided as ESI. The micrographs show calcite crystals possessing different orientations. There is currently no experimental evidence for CaCO₃ nucleation originating from the {110} crystal faces.
- 22 (a) A. S. Marfunin, in *Spectroscopy, luminescence and radiation centers in minerals*, Springer-Verlag, Berlin, 1979, ch. 5, pp. 141–220; (b) M. R. Krbetschek, J. Götze, A. Dietrich and T. Trautmann, *Radiat. Meas.*, 1997, **27**, 695–748.
- 23 G. M. Walkden and J. R. Berry, *Nature*, 1984, **308**, 525–527.
- 24 T. Calderón, P. D. Townsend, P. Beneitez, J. Garcia-Guinea, A. Millán, H. M. Rendell, A. Tookey, M. Urbina and R. A. Wood, *Radiat. Meas.*, 1996, **26**, 719–731.
- 25 S. J. Cooper, R. B. Sessions and S. D. Lubetkin, *J. Am. Chem. Soc.*, 1998, **120**, 2090–2098.
- 26 (a) M. J. Lochhead, S. R. Letellier and V. Vogel, *J. Phys. Chem. B*, 1997, **101**, 10821–10827; (b) P. Calvert and S. Mann, *Nature*, 1997, **386**, 127–129.
- 27 A. L. Litvin, S. Valiyaveetil, D. L. Kaplan and S. Mann, *Adv. Mater.*, 1997, **9**, 124–127.
- 28 S. Valiyaveetil, V. Enkelmann and K. Müllen, *J. Chem. Soc., Chem. Commun.*, 1994, 2097–2098.
- 29 B. R. Heywood and S. Mann, *Chem. Mater.*, 1994, **6**, 311–318.
- 30 (a) G. Falini, S. Fermani, M. Gazzano and A. Ripamonti, *Chem. Eur. J.*, 1998, **4**, 1048–1052; (b) K. Naka, D.-K. Keum, Y. Tanaka and Y. Chujo, *Chem. Commun.*, 2000, 1537–1538.
- 31 E. DiMasi, M. J. Oltsza, V. M. Patel and L. Gower, *CrystEngComm*, 2003, **5**, 346–350.
- 32 D. Volkmer, M. Fricke, M. Gleiche and L. Chi, *Mater. Sci. Eng. C*, accepted.
- 33 The starting compound *rccc*-2,8,14,20-tetra(n-undecyl)resorc[4]-arene was prepared according to a slightly modified literature procedure: L. M. Tunstad, J. A. Tucker, E. Dalcanele, J. Weiser, J. A. Byrant, J. C. Sherman, R. C. Helgeson, C. B. Knobler and D. J. Cram, *J. Org. Chem.*, 1989, **54**, 1305–1312.
- 34 E. Kurita, N. Fukushima, M. Fujimaki, Y. Matsuzawa, K. Kudo and K. Ichimura, *J. Mater. Chem.*, 1998, **8**, 397–403.
- 35 F. Arnaud-Neu, E. M. Collins, M. Deasy, G. Ferguson, S. J. Harris, B. Kaitner, A. J. Lough, M. A. McKervey, E. Marques, B. L. Ruhl, M. M. J. Schwing-Weill and E. M. Seward, *J. Am. Chem. Soc.*, 1989, **111**, 8681–8691.
- 36 S.-K. Chang and I. Cho, *J. Chem. Soc., Perkin Trans. 1*, 1986, 211–214.
- 37 PowderCell 2.3 for Windows. Copyright W. Kraus, G. Nolze, Federal Institute for Materials Research and Testing (Berlin, Germany). The software can be downloaded free of charge from ftp://ftp.bam.de/Powder_Cell/ or from the current link via the CCP14 homepage http://www.ccp14.ac.uk/ccp/ccp14/ftp-mirror/powdcell/Powder_Cell/.

Acidic peptides acting as growth modifiers of calcite crystals†

Dirk Volkmer,^{*a} Marc Fricke,^a Thomas Huber^b and Norbert Sewald^b^a Faculty of Chemistry (AC 1), University of Bielefeld, PO Box 100 131, 33501 Bielefeld, Germany.
E-mail: dirk.volkmer@uni-bielefeld.de; Fax: +49 (0)521 106-6003; Tel: +49 (0)521 106-6142^b Faculty of Chemistry (OC 3), University of Bielefeld, PO Box 100 131, 33501 Bielefeld, Germany.
E-mail: norbert.sewald@uni-bielefeld.de; Fax: +49 (0)521 106-8094; Tel: +49 (0)521 106-2051

Received (in Cambridge, UK) 15th April 2004, Accepted 2nd June 2004

First published as an Advance Article on the web 5th July 2004

Small acidic peptides comprising a repeating Phe–Asp sequence motif exert control, *in vitro*, on the morphology of calcite crystals similar to natural proteins from calcified tissues.

Crystallization of inorganic solids in the presence of organic molecules is an important step in biomineralization¹ and crystal engineering.² Investigations into the amino acid composition of natural proteins which are associated with CaCO₃ biomineralized tissues reveal characteristic sequence motifs which are particularly rich in aspartic and glutamic acid residues.³ It has been suggested that mollusc shell acidic proteins may act as CaCO₃ crystal nucleation promoters. These proteins, upon adsorption onto a framework of water-insoluble macromolecules, might adopt a β -pleated sheet structure, where the carboxylate groups are placed exclusively on one side of the β -sheet.⁴ The structure model implies that the ordered arrangement of carboxylate residues could act as a two-dimensional template for the formation of a CaCO₃ crystal nucleus. Other acidic proteins extracted from different calcified tissues were shown to exert vast control on polymorph selection, texture and morphology of CaCO₃ crystals.⁵ However, up to now only a few artificial oligopeptides have been designed and tested for specific interactions with CaCO₃ single crystals *in vitro*.⁶

Amphiphilic peptides comprising alternating hydrophilic (Asp) and hydrophobic (Phe) amino acid residues, for instance, in fact tend to adopt β -sheet arrangements if spread as a monolayer at the air–water interface.⁷ In this communication we describe the properties of two such acidic peptides (Scheme 1) designed to imitate the epitopes of acidic proteins from calcified tissues.

The amphiphilic peptides H–(Phe–Asp)₂–OH (**1**) and H–(Phe–Asp)₄–OH (**2**) specifically interact with distinct crystal faces of calcite. The morphological features of calcite crystals grown in the presence of **1** or **2** are very similar to calcite crystals grown from solutions containing natural acidic proteins. The peptides were synthesized according to the Fmoc/*t*-butyl strategy on a 2-chloro-

trityl resin (see Electronic Supplementary Information).† Crystallization of CaCO₃ was performed within a sealed desiccator by slow vapor diffusion of CO₂ and ammonia into a solution containing calcium chloride and peptide.⁸ The resulting crystals were harvested at different stages and examined by light and scanning electron microscopy. IR spectroscopy and powder X-ray diffraction of the resulting crystals show that in all cases calcite has formed exclusively (see ESI).† In addition to the normal {10.4} faces, the calcite crystals grown in the presence of **1**, at a concentration of 1 mM, or in the presence of **2**, at a concentration of 50 μ M, respectively, develop a set of stepped diamond-shaped {01.2} crystal faces (Fig. 1). These are clearly distinguishable from the set of prismatic {11.0} faces which are also expressed. In contrast, CaCO₃ crystals grown in the presence of monomeric aspartic acid (3 mM) were indistinguishable from control experiments lacking additives.⁹

The newly formed crystal faces were identified by stereological analysis of scanning electron micrographs taken from crystal specimens at different viewing directions. The assignment of {11.0} and {01.2} faces was derived from measuring the characteristic interfacial angles of the appropriately oriented crystal specimen and comparing the results to computer models of truncated calcite rhombohedra (Fig. 1).¹⁰

The appearance of polar faces on biogenic calcite crystals belonging to index class {01.*l*} with *l* = 1–2 has been reported frequently. Calcite crystals grown in the presence of proteins isolated from sea urchin spicules, sponge spicules, and mollusc shells have been shown to induce the formation of {01.*l*} faces with *l* = 1–1.5.¹¹ Macromolecules extracted from the calcitic layer of

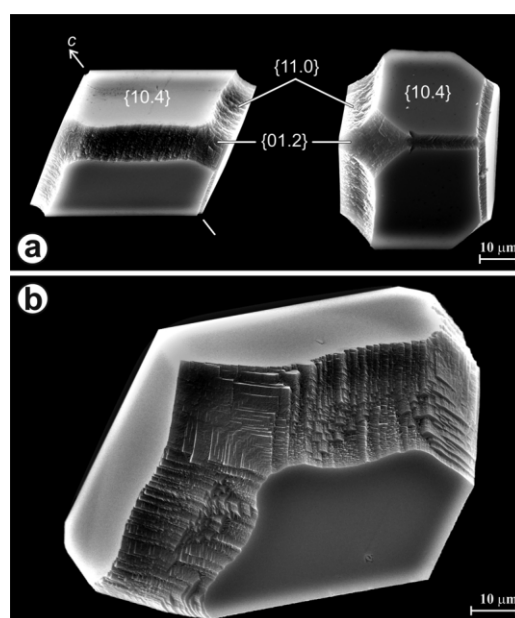
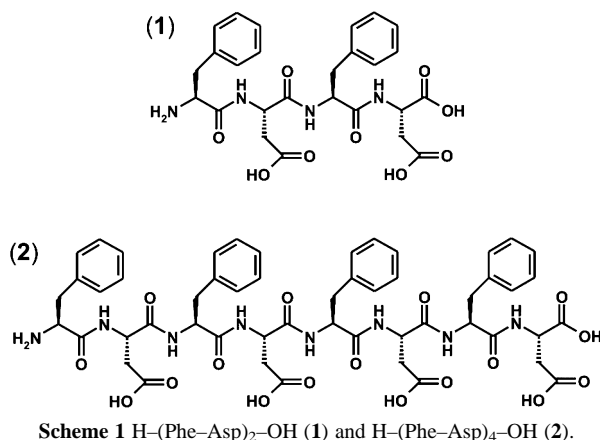


Fig. 1 Scanning electron micrographs of calcite crystals grown in the presence of **2** (ratio of **2** : Ca = 1 : 180). (a) Crystals isolated after 5 h, (b) crystal isolated after 18 h. (Photomontage showing selected crystal specimen).

† Electronic Supplementary Information (ESI) available: full analytical characterization of **1** and **2** as well as experimental details on CaCO₃ crystal growth and crystallographic analysis of the calcite crystal morphology. See <http://www.rsc.org/suppdata/cc/b4/b405613b/>

tunic spicules of ascidians induce exactly the same calcite crystal habit morphology with well-developed stepped faces, indexed as {01.1} ($l = 1.5$).¹² Inhibition of {01.2} crystal faces seems to play an important role in controlling the texture and crystal shape of calcitic sponge spicules.¹³

The {11.0} crystal faces of calcite are less abundant in biological samples but it has been suggested that nucleation of the R-units of *Emiliania huxleyi* coccoliths originates from this particular crystal face.^{14,15}

It should be noted that the {01.2} and {11.0} calcite crystal cleavage planes bear few common features with regard to their symmetry and electrostatic properties (Fig. 2). Surface models show that carbonate ions emerge almost perpendicular to the crystal faces, and it has been argued that this orientation should be favourable for interaction with acidic macromolecules containing Asp- or Glu-rich domains by virtue of stereochemical and geometrical recognition.¹⁶ However, it is still an open question if epitaxial or stereochemical correlations which are implicit in many literature schemes showing an adsorbate layer of organic molecules sticking to a particular crystal cleavage plane represent a physically realistic model of the interface.¹⁷ CaCO₃ crystals grown underneath monolayers of amphiphilic oligoacids such as calixarenes,¹⁸ or resorcarenes,¹⁹ for instance, often expose a single {01.2} crystal plane facing the monolayer. There is sound experimental evidence that this particular crystal orientation is caused by non-directional forces such as average charge density or mean dipole moment of the monolayer (the crystal growth plane, respectively). Since the peptide molecules we are using are very flexible, a template or epitaxy mechanism is currently ruled out although it would certainly be possible to construct foldamers of **1** and **2** which possess a spacing of the carboxylic acid residues that is commensurate with the positions of Ca ions in the inhibited crystal planes.

The expression of {01.2} and {11.0} faces of calcite induced by synthetic peptides containing a repeating Phe-Asp sequence motif bears novel insights into the crystallization of CaCO₃ under biological control. Thus, amphiphilic peptides such as **1** or **2** and similar peptides containing glutamic acid residues are ideal candidates for imitating epitopes of acidic proteins which are abundant in calcified tissues. To the best of our knowledge this is the first example where artificial peptides exert the same influence on the growth habit of calcite crystals as has been reported for natural acidic proteins isolated from skeletal elements of various organisms. Moreover, this is the first example where a single peptide selectively interacts with two different faces of calcite which might indicate that the peptide possesses distinct, energetically favourable conformations. In order to elucidate the predominant structure of the peptides in solution 2D-NMR investigations are currently under way.

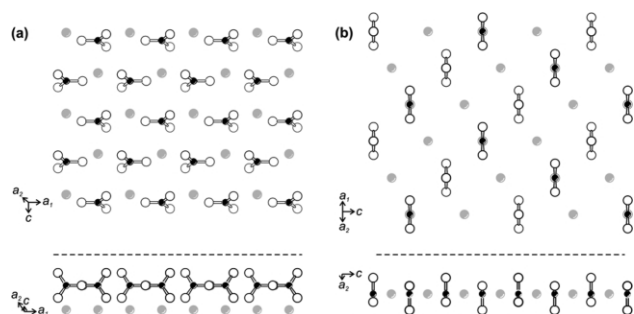


Fig. 2 Calcite surface layers of (a) the {01.2} cleavage plane and (b) the {11.0} cleavage plane.

This work was financially supported by the Deutsche Forschungsgemeinschaft (DFG Schwerpunktprogramm 1117, "Prinzipien der Biomineralisation"; DFG grant Vo829/2-1).

Notes and references

- H. A. Lowenstam and S. Weiner, *On Biomineralization*, Oxford University Press, Oxford, 1989.
- D. Braga, *Angew. Chem.*, 2003, **115**, 5702 (*Angew. Chem., Int. Ed.*, 2003, **42**, 5544).
- D. Volkmer, Biomineralization, in *Encyclopedia of Separation Science*, ed. M. Cooke and C. F. Poole, Academic Press, 2000, **vol. 2**, p. 940.
- (a) S. Weiner and W. Traub, *FEBS Lett.*, 1980, **111**, 311; (b) S. Mann, *Biomineralization. Principles and Concepts in Bioinorganic Materials Chemistry*, Oxford University Press, Oxford, 2001.
- (a) A. M. Belcher, X. H. Wu, R. J. Christensen, P. K. Hansma, G. D. Stucky and D. E. Morse, *Nature*, 1996, **381**, 56; (b) G. Falini, S. Albeck, S. Weiner and L. Addadi, *Science*, 1996, **271**, 67.
- (a) D. B. DeOliveira and R. A. Laursen, *J. Am. Chem. Soc.*, 1997, **119**, 10627; (b) C. Li, G. D. Botsaris and D. L. Kaplan, *Cryst. Growth Des.*, 2002, **5**, 387; (c) L. A. Estroff, C. D. Incarvito and A. D. Hamilton, *J. Am. Chem. Soc.*, 2004, **126**, 2.
- H. Rapaport, K. Kjaer, T. R. Jensen, L. Leiserowitz and D. A. Tirrell, *J. Am. Chem. Soc.*, 2000, **122**, 12523.
- L. Addadi and S. Weiner, *Proc. Natl. Acad. Sci. USA*, 1985, **82**, 4110.
- Control experiments containing 3.0 mM Asp solely showed rhombohedral calcite crystals with {10.4} faces. In contrast to our observations inhibition of calcite {1-1.0} faces in the presence of Asp (0.5 mM) has been reported under slightly different experimental conditions. S. Mann, J. M. Didymus, N. P. Sanderson, B. R. Heywood and E. J. A. Samper, *J. Chem. Soc., Faraday Trans.*, 1990, **86**, 1873.
- Truncated calcite rhombohedra were modeled with SHAPE V7.1, ©2002 by Shape Software, Kingsport (USA).
- J. Aizenberg, S. Albeck, L. Addadi and S. Weiner, *J. Cryst. Growth*, 1994, **142**, 156; S. Albeck, S. Weiner and L. Addadi, *Chem.-Eur. J.*, 1996, **2**, 278; J. Aizenberg, J. Hanson, T. F. Koetzle, S. Weiner and L. Addadi, *J. Am. Chem. Soc.*, 1997, **119**, 881.
- J. Aizenberg, G. Lambert, S. Weiner and L. Addadi, *J. Am. Chem. Soc.*, 2002, **124**, 32.
- J. Aizenberg, J. Hanson, T. F. Koetzle, L. Leiserowitz, S. Weiner and L. Addadi, *Chem.-Eur. J.*, 1995, **1**, 414.
- S. Mann and N. H. C. Sparks, *Proc. R. Soc. London, Ser. B*, 1988, **234**, 441.
- We could retrieve only one literature example where a water soluble additive was shown to interact specifically with the {11.0} crystal faces of calcite. This was observed in a crystallisation assay containing nitrilotriacetic acid at a concentration of 62.5 μ M. D. D. Archibald, S. B. Qadri and B. P. Gaber, *Langmuir*, 1996, **12**, 538.
- (a) L. Addadi, J. Moradian, E. Shay, N. G. Maroudas and S. Weiner, *Proc. Natl. Acad. Sci. USA*, 1987, **84**, 2732; (b) S. Mann, *Nature*, 1988, **332**, 119.
- Recent work has suggested a precise match between the spatial orientation of the terminal carboxylate moieties of self-assembled 1- ω carboxyalkanethiol monolayers on Au substrates and the corresponding specifically nucleated CaCO₃ crystal planes. However, the formation of a rigid, smooth and uniform template surface is a necessary precondition and it seems unlikely that the surface of biological tissues adopts a similar degree of structural perfection. (a) J. Aizenberg, A. J. Black and G. M. Whitesides, *J. Am. Chem. Soc.*, 1999, **121**, 4500; (b) J. J. M. Donners, R. J. M. Nolte and N. A. J. M. Sommerdijk, *J. Am. Chem. Soc.*, 2002, **124**, 9700.
- (a) D. Volkmer, M. Fricke, D. Vollhardt and S. Siegel, *J. Chem. Soc., Dalton Trans.*, 2002, 4547; (b) D. Volkmer and M. Fricke, *Z. Anorg. Allg. Chem.*, 2003, **629**, 2381.
- (a) D. Volkmer, M. Fricke, C. Agena and J. Mattay, *CrystEngComm*, 2002, **4**, 288; (b) D. Volkmer, M. Fricke, C. Agena and J. Mattay, *J. Mater. Chem.*, 2004, **14**, in press, DOI: 10.1039/b403132f.

6. Publikationen, Auszeichnungen, Vorträge und Posterpräsentationen

6.1 Publikationen

- [1] D. Volkmer, M. Fricke, C. Agena, J. Mattay, *CrystEngComm.* **2002**, 4, 288–295.
- [2] D. Volkmer, M. Fricke, D. Vollhardt, S. Siegel, *J. Chem. Soc., Dalton Trans.* **2002**, 4547–4554 (Titelbild).
- [3] D. Volkmer, M. Fricke, *Z. Anorg. Allg. Chem.* **2003**, 626, 2381–2390.
- [4] D. Volkmer, M. Fricke, M. Gleiche, L. Chi, *Mater. Sci. Eng. C*, im Druck.
- [5] D. Volkmer, M. Fricke, C. Agena, J. Mattay, *J. Mater. Chem.* **2004**, 14, 2249–2259 (Titelbild).
- [6] D. Volkmer, M. Fricke, T. Huber, N. Sewald, *Chem. Commun.* **2004**, 1872–1873.
- [7] D. Vollhardt, V. B. Fainerman, A. Roth, M. Fricke, D. Volkmer, *J. Phys. Chem. B*, im Druck.
- [8] D. Volkmer, M. Fricke, B. Decker, J. Mattay, *CrystEngComm.*, in Vorbereitung.
- [9] D. Volkmer, M. Fricke, T. Huber, N. Sewald, *Chem. Eur. J.*, in Vorbereitung.

6.2 Auszeichnungen

- [1] Tagungsstipendium GDCh Jahrestagung in Würzburg, 23.-29.09.2001.
- [2] Tagungsstipendium 6th *International Conference on Inorganic Chemistry* in München, 07.04.-10.04.2002.
- [3] Tagungsstipendium 35th *International Conference on Coordination Chemistry* in Heidelberg, 21.07.-26.07.2002.
- [4] *Young Investigator Award: Biomineralization Gordon Research Conference* in New London, NH (USA), 11.-16.8.2002.
- [5] Tagungsstipendium NATO/ASI *Learning from nature how to design new implantable biomaterials: from biomineralization fundamentals to biomimetic materials and processing routes* in Alvor (Portugal), 13.10.-24.10.2003.
- [6] Abschlußstipendium der Graduiertenförderung des Landes Nordrhein-Westfalen, 01.12.2002-30.11.2003.

6.3 Vorträge

- [1] Seminar „Moderne Aspekte der Biophysik“ an der Fakultät für Physik in Bielefeld, 12.06.2001.
- [2] GDCh JCF Euroregionale in Aachen, 14.02.2002.
- [3] 2nd Workshop der Graduate School of Chemistry and Biochemistry in Bielefeld, 04.07.2002.
- [4] GDCh JCF Euroregionale in Dresden, 01.03.2003.
- [5] 4th Workshop der Graduate School of Chemistry and Biochemistry in Bielefeld, 22.7.2003.
- [6] 1st Joint Workshop on Materials Chemistry in Münster, 08.09.2003.
- [7] Workshop on Investigation of Biomineralization Employing Model Systems in Braunschweig, 23.09.2003.
- [8] NATO/ASI Learning from nature how to design new implantable biomaterials: from biomineralization fundamentals to biomimetic materials and processing routes in Alvor (Portugal), 23.10.2003.
- [9] Seminar “Bautechnik” im Fachbereich Bauingenieurwesen in Kassel, 28.01.2004.

6.4 Posterpräsentationen

- [1] Dalton Discussion 3, Inorganic Crystal Engineering in Bologna (Italien), 09.-11.09.2000.
- [2] GDCh Jungchemikerforum in Hamburg, 20.-22.09.2000.
- [3] GDCh Jungchemikerforum in Leipzig, 18.-20.03.2001.
- [4] GDCh Jahrestagung in Würzburg, 23.-29.09.2001.
- [5] 8th European Conference on Organised Films in Otranto/Lecce (Italien), 03.-07.09.2001.
- [6] GDCh Euroregionale in Aachen, 13.-15.02.2002.
- [7] 6th International Conference on Inorganic Chemistry in München, 07.04.-10.04.2002.
- [8] CrystEngComm Discussion 1, Innovation in Crystal Engineering in Bristol (UK), 29.06.-01.07.2002.
- [9] 2nd Workshop der Graduate School of Chemistry and Biochemistry in Bielefeld, 04.-05.07.2002.
- [10] 35th International Conference on Coordination Chemistry in Heidelberg, 21.07.-26.07.2002.
- [11] Biomineralization Gordon Research Conference in New London, NH (USA), 11.-16.08.2002.
- [12] 3rd Workshop der Graduate School of Chemistry and Biochemistry in Bielefeld, 20.-21.01.2003.

- [13] GDCh Euroregionale in Dresden, 27.02.-01.03.2003.
- [14] *4th Workshop der Graduate School of Chemistry and Biochemistry* in Bielefeld, 21.-22.07.2003.
- [15] *Workshop on Investigation of Biomineralization Employing Model Systems* in Braunschweig, 23.-24.09.2003.
- [16] GDCh Jahrestagung in München, 06.-11.10.2003.
- [17] *Workshop on Molecular Biology and Protein Chemistry in Biomineralization Research* in Bremen, 04.-05.12.2003.
- [18] *5th Workshop der Graduate School of Chemistry and Biochemistry* in Bielefeld, 19.-20.01.2004.

7. Lebenslauf

Name	Marc Fricke
Geburtsdatum	09. 05. 1974
Geburtsort	Bünde
Staatsangehörigkeit	Deutsch
Familienstand	ledig
Anschrift	Voßheide 2, 33619 Bielefeld
Telefon	0521 162779, 0162 5441626
E-mail	fricko@uni.de
seit Dez 2000	Promotionsstudium an der <i>Graduate School of Chemistry and Biochemistry</i> an der Fakultät für Chemie, Universität Bielefeld bei PD Dr. D. Volkmer, AC1
Okt 2000	Diplom in Chemie
Mär 2000 – Okt 2000	Diplomarbeit bei Prof. Dr. Dr. hc mult. A. Müller, AC1
Nov 1999 – Jan 2000	Wissenschaftliche Hilfskraft bei Dr. D. Volkmer, AC1
Jan 1999 – Apr 1999	<i>Visiting Research Fellow</i> am <i>Weizmann Institute of Science</i> in Rehovot/Israel bei Prof. Dr. I. Pecht
Jul 1998 – Sep 1998	Werkstudent am Max-Planck-Institut für Biochemie in Martinsried bei Dr. F. Melchior
Apr 1998 – Jul 1998	Studentische Hilfskraft im Praktikum PC1
Mär 1998 – Apr 1998	Praktikum am Institut für Wasserchemie der TU München bei Prof. R. Nießner
Okt 1996	Diplom-Vorprüfung in Chemie
seit Okt 1994	Chemiestudium an der Fakultät für Chemie, Universität Bielefeld
Aug 1993 – Okt 1994	Zivildienst als Krankenpflegehelfer im Martin-Luther Krankenhaus Schleswig
Aug 1984 – Mai 1993	Gymnasium Lornsenschule Schleswig, Abschluß: Abitur
Aug 1980 – Mai 1984	Grundschule Schuby